Tampere University

MARKUS KARJALAINEN

Utilizing Surgical Smoke to Improve Cancer Surgery

Tampere University Dissertations 784

Tampere University Dissertations 784

MARKUS KARJALAINEN

Utilizing Surgical Smoke to Improve Cancer Surgery

ACADEMIC DISSERTATION
To be presented, with the permission of
the Faculty of Medicine and Health Technology
of Tampere University,
for public discussion in the auditorium TB109
of the Tietotalo building, Korkeakoulunkatu 1, Tampere,
on 5 May 2023, at 12 o'clock.

ACADEMIC DISSERTATION
Tampere University, Faculty of Medicine and Health Technology
Finland

Responsible supervisor and Custos	Associate Professor (tenure track) Antti Vehkaoja Tampere University Finland	
Supervisors	MD, PhD Antti Roine Olfactomics Oy Finland	Professor Niku Oksala Tampere University Finland
Pre-examiners	Assistant Professor Eva Cuypers Maastricht University Netherlands	Docent Markus Metsälä University of Helsinki Finland
Opponent	Professor Zoltan Takats Imperial College London England	

Cover design: Roihu Inc.

ISBN 978-952-03-2859-7 (print)
ISBN 978-952-03-2860-3 (pdf)
ISSN 2489-9860 (print)
ISSN 2490-0028 (pdf)
http://urn.fi/URN:ISBN:978-952-03-2860-3

Carbon dioxide emissions from printing Tampere University dissertations have been compensated.

PunaMusta Oy – Yliopistopaino
Joensuu 2023

PREFACE

Life is full of surprises. Completing this thesis is one of them. Has it been worth the time spent? Answering "yes" would be too short, "no" too dishonest, and "probably" too careful. "I hope so" could be closer to the truth. I hope this thesis will serve as a stepping stone for a new practical method in cancer treatment. Even so, should my hope fade away, my deep gratitude would remain. I'm grateful for the family members, teammates, and friends who walked with me to complete this dissertation.

My gratitude goes to those who know how much I have struggled with writing. Despite the struggles, the thesis is now complete, but it wouldn't be so without your support. My gratitude goes to those who know how much I have struggled with coherence. Thank you for giving me your time and support to bounce through all those dead ends. If you noticed my gifts in engineering, please accept my gratitude for your support. Shared joy is greater than joy alone. Sharing fuels motivation and changes work from tedious labour to passion.

To name a few of the aforementioned supporters, I must include all teammates at Olfactomics. You are the greatest possible coworkers. To add some detail, Niku Oksala poured excitement into the topic. Antti Roine steadfastly pushed the research forward. Osmo Anttalainen explained the DMS technology. Anton Kontunen sharpened the work greatly. Mikko Koskenranta made many parts of the design, and Meri Mäkelä helped in multiple technical issues. Antti Vehkaoja kindly supported the whole thesis and showed me the way of kiteboarding. Finally, I am grateful for my parents, sister and brothers, who eagerly awaited the completion of this project.

However, my greatest discovery and treasure does not stem from engineering, nor from medicine or family and friends, but from something that science cannot fully grasp – the good news about the one who first commanded: "Heal the sick!"

ABSTRACT

A surgical operation is common practice when treating solid cancer tumours. The tumour is removed with a layer of healthy tissue around it to achieve a so-called negative tissue margin. Without the margin or with an incomplete margin, the cancer will likely recur, since some of the leftover cells can regrow into a new tumour. Still, in some tumours, such as brain tumours, minimizing the removal of healthy tissue takes priority over a negative margin to avoid brain damage. It is often difficult to visually recognize the border of the tumour. To decrease bleeding, these operations are performed with an electric knife. The process produces smoke that is harmful to the operating theatre personnel, and the smoke is thus recommended to be removed with a surgical smoke evacuator. During surgical removal, it is possible to distinguish benign from malignant tissue based on the smoke. This makes it possible to detect when the knife hits the tumour and to alert the surgeon, which enables the surgeon to optimize the amount of removed tissue and ensure a sufficient healthy tissue margin. This process should notably decrease the need for reoperations.

In this dissertation, two topics are studied: the structure of surgical smoke as well as the type of risk that operating theatre personnel could be exposed to; and, on the other hand, the possibilities of utilizing the smoke to monitor the tumour resection margin and factors in the analysis equipment affecting its technical performance. More precisely, the studied aspects are the surgical smoke load for the theatre personnel and the classification of tissue types based on surgical smoke.

We studied the utilization of differential mobility spectrometry (DMS) to diagnose brain tumours *ex vivo*. Low-grade glioma (class II) was classified with an accuracy of 94% when compared to control samples. Furthermore, we studied the effect of different tube materials, tube dimensions and temperature on the recovery speed of the measuring system. Delays in the chemical pathway affect the usability of the whole system. Thus, we also studied the chemical signal delays and their effects on system usability.

TIIVISTELMÄ

Leikkaus on yleinen ja vakiintunut kiinteiden syöpäkasvaimien hoitomuoto, jossa kasvain pyritään poistamaan siten, että sen ulkoreunaan jää kaistale tervettä kudosta eli poisto tapahtuu ns. tervekudosmarginaalilla. Mikäli marginaalia ei ole tai se ei ole riittävän leveä, kasvain uusiutuu helposti, sillä on erittäin todennäköistä, että elimistöön jää syöpäsoluja, jotka voivat muodostaa uuden kasvaimen. Kuitenkin esimerkiksi aivokasvaimia leikataan pyrkien minimoimaan tervekudoksen poisto, jottei leikkaus aiheuttaisi aivovauriota. Silmämääräisesti tämän rajan tunnistaminen on haastavaa. Verenvuodon vähentämiseksi leikkauksissa käytetään sähköveistä, joka tuottaa savukaasuja. Savukaasut ovat leikkaussalihenkilöstölle haitallisia, ja siksi ne poistetaan savuimulla. Savuimusta voidaan ottaa näytteitä, jotka sisältävät kemiallista informaatiota leikatusta kudoksesta. Niiden avulla on mahdollista optimoida poistettavan kudoksen määrää ja valvoa kasvaimen tervekudosmarginaalia. Menetelmä voi vähentää uusintaleikkauksien tarvetta merkittävästi. Väitöskirjassa tutkitaan savukaasun koostumusta ja sen mahdollisia vaikutuksia leikkausalueen lähellä työskenteleviin ihmisiin sekä kaasun ominaisuuksien käyttöä tervekudosmarginaalin valvonnassa.

Tarkemmin tarkastelemme eri kudostyyppien kuormittavuuseroja henkilökunnalle. Tutkimme DMS:n käyttökelpoisuutta aivokasvaimia tunnistettaessa *ex vivo*. Matala-asteinen gliooma (luokka II) kyettiin tunnistamaan 94 %:n tarkkuudella verrokkiin nähden. Tutkimme eri putkimateriaalien, lämpötilojen ja mittojen vaikutusta laitteiston kemiallisen signaalin siirtonopeuteen mittausjärjestelmässä. Kemiallisen signaalin viiveet vaikuttavat huomattavasti reaaliaikaisen järjestelmän käytettävyyteen. Siksi tutkimmekin kemiallisen signaalin siirtonopeutta ja siirtonopeuden vaikutusta järjestelmän käytettävyyteen.

CONTENTS

ABBREVIATIONS AND SYMBOLS

APC	argon plasma coagulation
ELPI	electrical low pressure impactor
CA	classification accuracy
CIT	cylindrical ion trap
CCS	collision cross-section
DESI	desorption electrospray ionization
DMS	differential mobility spectrometry
DTIMS	drift tube ion mobility spectrometer
FAIMS	field asymmetric ion mobility spectrometer
FN	false negative
FP	false positive
GBM	glioblastoma multiforme
IDH	isocitrate dehydrogenase
IMS	ion mobility spectrometry
IR	infra-red
MS	mass spectrometry
MTBF	mean time between failures
MTTR	mean time to repair
LIT	linear ion trap
QIT	quadrupole ion trap

REIMS	rapid evaporative ionization mass spectrometry
RF	radio frequency
RFA	radio frequency ablation
RIT	rectilinear ion trap
TISM	trapped ion mobility spectrometry
TN	true negative
TP	true positive
TFD	time to filter detection
TFP	time to filter peak
TFP-SP	time from filter peak to sensor peak
TSD	time to sensor detection
TSP	time to sensor peak
TSR	time to sensor recovery
TWIMS	traveling wave ion mobility spectrometry
UV	ultraviolet
α	rebounce coefficient
Δp	pressure difference
ϵ	depth of potential well
θ	fractional coverage
A	area
C	concentration
D	diffusion
E_a	required kinetic activation energy
E_d	activation energy of desorption

E_p	activation energy
H_s	heat of solution
k	rate contant
k_d	desorption rate constant
$k_{d\infty}$	rate constant at infinite temperature
kDa	kilodalton
M	molecular mass
p	pressure
P	partial pressure
q_s	steady state flow
R	universal gas constant
R_s	rate of bombardment
r_m	distance where potential minimum exist
S	solubility
T	temperature
V	potential energy

LIST OF ORIGINAL PUBLICATIONS

Publication I **Karjalainen M**, Kontunen A, Saari S, et al (2018) The characterization of surgical smoke from various tissues and its implications for occupational safety. PLoS One 13:. doi: 10.1371/journal.pone.0195274

Publication II Haapala I, **Karjalainen M**, Kontunen A, et al (2019) Identifying brain tumours by differential mobility spectrometry analysis of diathermy smoke. J Neurosurg 1:1–7

Publication III **Karjalainen M**, Kontunen A, Mäkelä M, et al (2020) Recovery characteristics of different tube materials in relation to combustion products. Int J Ion Mobil Spectrom 1–8

Publication IV **Karjalainen M**, Kontunen A, Anttalainen A, et al (2022) Characterization of signal kinetics in real time surgical tissue classification system. Sensors Actuators B Chem 131902

In this thesis these articles are referred to as PI, PII, PIII, and PIV.

AUTHOR'S CONTRIBUTION

The author of this thesis was the first author in publications I, III and IV. In publication II, the author was second author. The author's contributions to each publication are described in detail below.

Publication I: **The author** co-planned the test setup, conducted the measurements, participated in data analysis, and led the writing of the manuscript.

Publication II: **The author** was the main person responsible for the technical implementation of the study. The author had the main role of constructing the test setup and participated in all measurements. Haapala contributed to the medical side of the study and was responsible for the sample acquisition process. Both authors contributed to all sections of the article. Haapala led the writing process and had responsibility over the introduction and conclusion sections. The author had the lead responsibility over materials and methods and for the supplementary material. Kontunen was chiefly responsible for the results section.

Publication III: **The author** participated in test planning, contributed to measurements and data analysis, and led the writing and submission of the manuscript as the corresponding author.

Publication IV: **The author** was the main author of the design and building of the testing setup, in addition to participating in test measurements and data analysis and leading the writing of the manuscript.

1 INTRODUCTION

Rapid development in cancer treatment has doubled long-term cancer survival rates in England and Wales in the past 40 years (O'Dowd 2010). Presumably, the trend is also similar elsewhere. Even so, there is room for further development in many aspects of cancer treatment. One of these is surgical margin assessment. The treatment of most solid cancers includes the surgical removal of the abnormal growth before further adjuvant therapies. However, recognizing the tumour border in the operating theatre is difficult and a failure to remove cancerous tissue at the margins increases the risk of recurrence. Additional adjuvant therapies, such as chemotherapy or radiation, are used to reduce the risk of recurrence, but they burden the patient and the health care system. Therefore, many attempts are made to recognize the tumour border efficiently, utilizing various solutions and tactics.

A cancer develops when individual cells mutate and commence abnormal uncontrolled growth. Tumour cells may invade healthy tissues and create new tumours. If cancer cells enter the bloodstream, rapid tumour spreading may occur. The rapid growth of cancerous tumours often involves a so-called Warburg effect (Warburg 1956; Zhang and Du 2012). In the Warburg effect, cancer cells produce energy anaerobically, in contrast to the mostly aerobically functioning healthy cells. Consequently, dysregulated lipid metabolism causes cells to be distinctively different from healthy cells in their structure and metabolism (Ma et al. 2021). This difference can be utilized as information to distinguish healthy and tumour tissue.

In breast cancer surgery, where the best outcomes are obtained by removing the whole cancer with margins, margins are needed to ensure the removal of all cancerous tissue. In contrast, some brain tumours are intentionally removed incompletely due to the negative effects of removing functioning brain tissue. In both cases, the surgical removal is often accomplished with a diathermy knife or bipolar forceps. The knife and forceps heat the tissue to cut or coagulate, where coagulation prevents bleeding. When treated with diathermy, the heat exponentially increases the volatility of molecules, desorbing lipids and other molecules. These molecules carry information regarding their origin.

In combination with a diathermy knife, Schäfer et al. reported in 2009 on a method of surgical margin analysis, in which a mass-spectrometer-based system was combined with a rapid sampling method in order to discriminate chemical information on the cancer and healthy cells (Schäfer et al. 2009). Moreover, many of the surgically treated cancers are identifiable by means of canine olfaction from tissues or body fluids (Pirrone and Albertini 2017; Moser and McCulloch 2010).This indicates that the volatile chemical fingerprint of a cancer is usable in cancer diagnostics.

Surgical smoke consists of gas-phase molecules and particulates. Particulates are mostly formed from condensing gases, since the volatility in a hot diathermy arc is greater than the gas volatility in unheated room air. Cooling gas condenses into particulates, which are harmful to operating theatre personnel (PI) (Limchantra, Fong, and Melstrom 2019). Therefore, it is preferrable to remove the particulates with a surgical smoke evacuation system. A smoke evacuation pencil is a commonly used vacuum method, consisting of a direct vacuum hose connected to a diathermy knife. This system transports gases from the surgical event up to a distance of three metres in one second. Three metres is a suitable distance to transport smoke out of the sterile area, where gas analyser can be safely located (PIV).

Surgical smoke can be analysed with several methods. The optimal method would be compliant with daily use in operating theatres and provide accurate margin evaluation. Furthermore, the device should need only modest maintenance and be reliable in use. Nevertheless, designing such a device is a complex engineering challenge. The central engineering framework for a surgical margin assessment device is detailed in Table 1.

Table 1. Central engineering framework for a surgical margin assessment device

Classification accuracy (CA)	**True predictions divided by all predictions**
Detection speed	Time required for reliable analysis
Reliability	Device reliability as mean time between failures (MTBF) (Elsayed 2012)
Maintainability	Maintainability is classically defined as mean time to repair (MTTR) (Song et al. 2004)
Usability	User experience quality

Classification accuracy (CA) is, firstly, dependent on the information contained in the surgical smoke – i.e. whether the smoke contains the required information. Secondly, the CA depends on the quality of analysis, meaning whether the information is acquired accurately by the device, and, thirdly, on the overall reliability of the device, referring to whether the data acquisition and classification process work as intended. Correct results are produced only if all crucial parts function in unison. The CA of the device specifies how often the device indicates correctly. CA may be the most important technical feature of the device, since margin detection is its primary function. Classification can be tuned for high sensitivity or high specificity according to the cost of false positive or false negative indication. Similarly, detection speed greatly affects usability, and it depends on the analysing method. Maintainability and usability are crucial when adapting a device for daily use, as opposed to use as a research instrument.

Reliability is the result of good system design. However, since designing complete faultless instruments is practically impossible, devices are obligated to have additional technical alarms to indicate faulty events. These alarms indicate when the instrument assumes a technical malfunction. Medical standards define how device failure and other alarms related to the clinical function should be arranged. A surgical margin assessment device has audio feedback to indicate a potential positive margin for the surgeon. The alarm is triggered when the surgeon has cut malignant tissue instead of the intended benign tissue. In contrast, technical alarms indicate internal system malfunctions or a need for maintenance. Although technical alarms improve reliability, they can be harmful when they occur too often or without a proper reason. Such a false or true alarm may be caused by chemical interference (Kumbhani et al. 2017). Repeated alarm signals cause alarm fatigue among medical personnel (Ruskin and Hueske-Kraus 2015), which decreases the usability of medical devices and may cause alarms to be ignored. Therefore, minimizing faults and fault indications is crucial for safe system operation and usability. Because the price of faulty alarms is high, extensive care should be taken to design robust devices, in which a minimum number of technical alarms is needed. Since the number of alarms depends on the technical solutions, a high emphasis when selecting robust devices should be placed on the key aspects of the medical device design.

Medical devices are strictly regulated. They must conform to medical device standards to ensure safe functioning in clinical use. Generally, a device is acceptable if it does not cause unacceptable risk and it functions as intended. This is ensured by following the applicable local and regional laws and regulations, such as the medical device regulation (EU) 2017/745 (Pane et al. 2019). This thesis comprises basic and applied research to develop a clinical method for surgical margin assessment. The thesis includes an overview of some background information for final device development, which unavoidably includes multiple features that are vulnerable to failures (Taghipour, Banjevic, and Jardine 2011).

2 LITERATURE REVIEW AND BACKROUND

This chapter introduces the basics of surgical smoke and related issues. Smoke content is dependent on the type of tissue removed. Therefore, related tissue types are studied to define the reasons behind differences in smoke content. For operating theatre personnel, surgical smoke is a notable health risk. Therefore, some of the health effects of smoke are also reviewed based on the literature.

A robust method for surgical margin assessment would improve the outcome of tumour resections. If the margin detection is based on surgical smoke analysis, it is dependent on the smoke analysis method applied. To obtain a wide understanding of the possible methods, four approaches are reviewed: mass spectrometry, ion mobility, as well as optical sensor and chemical sensor technologies.

2.1 Surgical smoke

Surgical smoke forms when surgical dissection is performed using an energy device. The cauterized tissue is heated rapidly to vaporize liquid and to simultaneously incise tissue. Vaporized tissue then forms surgical smoke. Aerosol physics describe the phenomena related to surgical smoke formation (Hinds 2012). These include particle formation, particle dissolving and adhesion as well as forces that drive particles forward. The composition of surgical smoke is affected by the tissue type and energy instrumentation. Surgical smoke is composed of particles and gas-phase molecules. In PI, we studied smoke particles, and in PII, PIII and PIV, we studied gas-phase molecules.

2.1.1 Tissue structure and types

Human tissues are mostly constructed by water, lipids and proteins (Woodard and White 1986). A typical soft human cell consists of 70% water, 18% proteins, 3% miscellaneous small metabolites, 3% phospholipids, 2% other lipids and 2% polysaccharides (Roberts et al. 2002). In cancer research, commonly studied macromolecules include proteins, lipids and nucleic acids, which take approximately 60%, 15% and 5% of mammalian cell dry mass, respectively. (DeBerardinis and Chandel 2016).

Tissue structures and cancer are studied within many fields of medical biology. Genomics study nucleic acids, focusing on genetic information. Lipidomics entail the study of cellular lipids. Proteomics examine proteins, with a glycoproteomic subbranch specifically focussing on cell surface proteins and their effect on cancer adhesion. Metabolomics entails the study of the unique chemical fingerprints that result from specific cellular processes. Usually, these metabolomic molecules are smaller than 1.5 kDa. Of the cellular components, mostly phospholipids and fatty acids are used in surgical-smoke-based cancer tissue analysis (Azordegan et al. 2013).

Other macromolecules, such as proteins, in human tissue types have some variance. According to RNA analysis, 44% of all proteins are expressed statistically evenly in every tissue type. In contrast, 17% of all proteins are at least five times more enriched in a specific tissue. The rest of the proteins are between these states (Uhlén et al. 2015).

2.1.2 Malignant and healthy tissue

Cancer cell metabolism differs from that of healthy cells. Healthy cells function with aerobic oxidation, but cancer cells mostly extract their energy by anaerobic fermentation (Schwartz, T Supuran, and O Alfarouk 2017). This phenomenon is best known as the Warburg effect, as first described by Otto Warburg (Warburg 1956). These metabolic changes are triggered by mutations in the cells' genome, such as in the p53 tumour suppressor gene (Puzio-Kuter 2011).

Metabolites, such as lactate, glutamate and kynurenine, are increased in most cancerous tissues. In addition, kynurenine levels can indicate cancer progression. Breast cancer has increased levels of certain lipids, carnitines, amino acids and several other metabolites (Reznik et al. 2018). The same biomolecules are partially upregulated in brain tumours. This has been indicated in, for example, a study where a rapid evaporative ionization mass spectrometry (REIMS) method was used to analyse glioblastoma multiforme (GBM), which is an aggressive brain tumour. Twelve lipid metabolites were identified to distinctively accumulate in a GMB tumour and interpreted as biomarkers for GBM (Ma et al. 2021).

Another example of a relevant feature in brain tumour progression is isocitrate dehydrogenase (IDH) protein mutation. IDH is an enzyme that participates in the production of proteins that protect against oxidative stress. A differential mobility spectrometry (DMS) based diagnostic system has been proven to differentiate IDH-mutated and IDH-wild-type tumours (Haapala et al. 2022). Similar results have been obtained with mass spectrometry (MS) (Brown et al. 2021) and with a miniature mass spectrometer (Pu et al. 2019). Diagnosing the IDH mutation status is an important factor when deciding on the extent of resection, since IDH-mutated tumours have a higher probability of a good prognosis. In contrast, IDH wild type generally has a poorer prognosis, and a more conservative resection is therefore preferred (PII).

2.1.3 Tissue vaporization and surgical smoke composition

Energy devices are used extensively in surgical operations, since heating tissue up to the vaporization point cuts precisely and suppresses bleeding. Heating tissue to above 45°C causes irreversible coagulation, cellular vaporization takes place at above 100°C, and at above 200°C, the remaining solid components are reduced to carbon (Munro 2012; Massarweh, Cosgriff, and Slakey 2006).

Commonly used energy devices include monopolar and bipolar electrosurgical devices, ultrasonic devices, laser energy devices, radio frequency ablation (RFA), and argon plasma coagulation (APC) devices. However, RFA and APC are capable of coagulation, but not cutting. (Sankaranarayanan et al. 2013)

Electrosurgery devices cut tissue with high-voltage radio frequency (RF) energy. The high frequency eliminates muscle activation due to the surgical current. In an electrocautery scalpel, the current flow is concentrated onto a small area, where RF energy heats and cuts the tissue. RF pulses include three distinct phases: 1) a constant current through the tissue, 2) tissue vaporization around the electrode, leading to the isolation of the electrode, and 3) the ionization and arching of the vapour around the electrode. (Palanker, Vankov, and Jayaraman 2008)

Monopolar devices resemble a surgical knife, usually having a cutting electrode shaped as a blade. A cutting arc discharge is formed between the electrode and the tissue. The high arching temperature produces plenty of smoke and causes broader tissue damage than other methods. Monopolar devices require a counter-electrode pad, usually placed under the patient. (Sankaranarayanan et al. 2013)

Bipolar devices contain two electrodes, which are shaped like forceps and scissors. This structure is efficient for sealing large blood vessels. It causes less tissue damage and produces less smoke than a monopolar instrument. However, the decreased smoke production hinders the surgical smoke analysis.

Ultrasonic devices produce less heat than other methods, causing less thermal tissue damage and producing no charred tissue smoke. Ultrasonic devices are efficient in sealing small blood vessels of no more than 2 mm in diameter (Dutta and Dutta 2016). Cavitation may cause additional tissue damage with ultrasonic devices (O'Daly et al. 2008).

Laser energy devices yield a precise control of the affected tissue and cause less scarring than other methods. However, laser equipment is expensive. The laser sampling could be used for pathological tissue analysis, where a precise laser beam vaporizes tissue for molecular analysis, enabling precision sampling.

2.1.4 Particle health effects

Energy device surgery spreads smoke particles into the operating theatre. The theatre personnel inhale these toxic particles on a daily basis. Despite the ongoing debate concerning how harmful the smoke is (Limchantra, Fong, and Melstrom 2019), some of the ill effects are evident. In cities, a high exposure over the years to particulates smaller than 2.5 μm in diameter ($PM_{2.5}$) reduces life expectancy by anything from several months to a few years (Brook et al. 2010). Notably, long-term exposure to $PM_{2.5}$ particles is connected to cardiovascular diseases (McGuinn et al. 2019) and pulmonary diseases (Huang et al. 2018).

As regards $PM_{2.5}$ particles, the effect of gravitation is marginal, and the particles rather adhere through inertia, impaction and diffusion. Notably, $PM_{2.5}$ particles can enter deep into an alveolar duct, causing inflammation and other health issues. $PM_{2.5}$ particles have a large surface area and are thereby reactive and able to transport adhered molecules into the alveolar ducts or even alveoli. There is also evidence of the infectivity of surgical smoke. A nurse has been shown to have been infected with the human papillomavirus as a result of inhaling surgical smoke (Calero and Brusis 2003). Small, exhaled particles (< 5 μm) have a threefold effect on infectivity. First, small particles float in the air longer. Secondly, they contain more pathogens. Thirdly, they are inhaled more deeply into the alveolar ducts (Fennelly 2020). Similar behaviour can be expected of surgical smoke.

2.2 Surgical smoke analysis methods for tissue identification

Four possible analysis methods are studied in this literature review. These should be applicable, at least in principle, to surgical smoke analysis for tissue identification. Since cancer tissue differs from healthy tissue, the surgical smoke presumably also varies depending on the source tissue. The following methods of smoke analysis could, in principle, detect these differences. These include optical, mass and mobility spectrometers, as well as chemical sensors.

With optical spectrometers there are studies regarding surgical smoke toxicity (Gianella and Sigrist 2012), (Bratu et al. 2015), but not about tissue identification. However, these studies inform how optical spectrometers function for surgical smoke analysis. Theoretically, chemical sensors should function for surgical smoke analysis to some extent but, no actual studies were found. Presumably, contamination issues would limit the applicability of chemical sensors. Anyhow, all tissue identification studies from surgical smoke are performed with MS or DMS technology. Most of the available studies have been performed with MS and the rest with DMS technology.

2.2.1 Mass spectrometry

Mass spectrometers are the gold standard of molecular analysis. High-resolution mass-to-charge ratio spectrums provide a high information content from the analysed specimens, albeit only providing information on molecular mass and not molecular structure. The information is always acquired from an ionized molecule. The ionization is either from natural processes or, more commonly, executed inside the MS. The analysis occurs in a fraction of a second, which is suitable for rapid tissue analysis. A drawback of MS is that it requires high vacuum power, a complex mechatronic system and plenty of device maintenance (Greaves and Roboz 2014).

Mass spectrometers are powerful tools, but the demand for high vacuum complicates the structural design. Since the cancer margin is a binary question of whether there is tumour tissue or not, and since the chemical fingerprint is clear on a broad spectrum of molecules (St John et al. 2017), a low-performance MS device could potentially perform equally for this binary classification. Therefore, following scope is on a low-resolution MS devices. Recent advances in high-pressure mass spectrometers (HPMS) remove the demand for a high-vacuum pump and enable smaller-sized MS instruments, which could potentially be suitable for margin detection. However, the sample port from atmospheric pressure to vacuum continues to be a challenge (Guo et al. 2018).

A membrane inlet provides a practical means to isolate the vacuum, but it is likely not suitable for rapid smoke analysis. A capillary inlet has a minor drawback in that it requires a high pumping flow. A pulsed sampling is an improvement from a capillary inlet, as pulsing the sampling reduces the required pumping power (Jiao et al. 2021).

The most suitable technologies for HPMS are probably ion trap systems (Figure 1), since they operate in a higher pressure than other MS instruments. In these devices, trapped ions vibrate due to an alternating electric field. Because of the high alternating frequency, the moving direction of the ions changes frequently. This decreases terminal velocity, which further decreases collisions in the vacuum. Ion traps can be disassembled and reassembled without professionals, as opposed to other MS instruments. (Ouyang et al. 2004) Various forms of ion trap structures include a quadrupole ion trap (QIT), a linear ion trap (LIT), and a toroidal ion trap, as well as and their mechanically simplified counterparts, a cylindrical ion trap (CIT), a rectilinear ion trap and a toroidal ion trap with cylindrical electrodes (Tian et al. 2014).

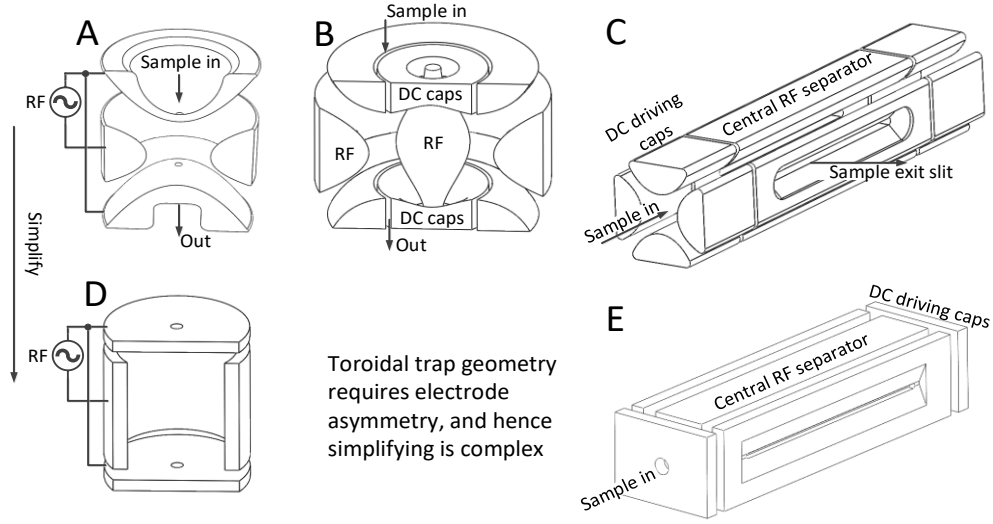

Figure 1. Common ion trap mass spectrometer core configurations. A) Quadrupole ion trap (QIT), B) toroidal ion trap, and C) linear ion trap (LIT), as well as their simplified counterparts D) toroidal ion trap with cylindrical electrodes and E) rectilinear ion trap (RIT); adapted from (Ouyang et al. 2004; Tian et al. 2014).

CIT mass analyser prototypes have been successfully tested in high 1 Torr pressure of ambient air (Blakeman et al. 2017). An increasing RF drive frequency can compensate for peak broadening caused by the increased pressure. Frequencies of up to 9.5 MHz and RF drive voltages of up to 1000 V_{p-p} have been used to drive the MS devices (Blakeman et al. 2016).

Glioma resection was tested on *ex vivo* samples of ten patients to evaluate the intraoperative surgical analysis performance of an ion trap MS device (Pirro et al. 2017). It comprised a desorption electrospray ionization (DESI) source, making it a DESI-MS device. The instrument was a low-resolution, high-pressure linear-ion-trap MS device (LIT-MS), requiring only roughly 30-minute preparation before surgery. There were no challenging calibration issues during a 15-month study. In contrast, Mason et al. used a REIMS device in an *in vivo* study of rectal cancer surgery and claimed that the system has logistical and technical challenges that hinder its use in routine operations. These challenges include the large instrument size and the requirement of technical expertise. The authors suggested that the usability of the technology should improve before adoption to clinical use. (Mason et al. 2020)

2.2.2 Ion mobility spectrometry

Ion mobility spectrometry (IMS) measures the drifting of gas-phase ions under an electric field. IMS can operate in atmospheric pressure or decreased pressure to increase ion separation. Gas-phase molecules can be ionized with many ionization sources, including radiation sources, X-rays, corona discharge and UV photoionization (Eiceman, Karpas, and Hill Jr 2013). Ions are formed mostly through a chemical reaction pathway, where reactant ions are first formed. These are usually hydrated protons in positive polarity: $H^+(H2O)_n$. These then react with analyte molecules, yielding proton-bound monomers by displacing a water molecule, $MH^+ (H_2O)_n + xH_2O$, or dimers by displacing another water molecule. Similarly, in negative polarity, an oxygen anion is first formed: $O_2^-(H_2O)_n$. These then react with an analyte molecule, $MO_2^-(H_2O)_{n-x}$, by displacing a water molecule. (Eiceman, Karpas, and Hill Jr 2013)

These ions tend to react and spread with other molecules and ions, as ions in the gas phase face mutual collisions. This limits the achievable resolution and complicates the IMS spectrums. However, these reactions can be utilized and modified with chemical dopants (Waraksa et al. 2016) and by modifying reaction times. Dopants

can supress the background matrix and reform ion chemistry, which can shift overlapping ion peaks. Ion mobility is measured as ion velocity in a carrier gas. Since there are countless options for how to arrange driving electric fields and a carrier gas, there are various configurations for IMS. However, the six most common IMS configurations are in commercial production (Dodds and Baker 2019; Utriainen, Kärpänoja, and Paakkanen 2003). These are introduced in Table 2 and Figure 2.

Table 2. Common commercial IMS configurations

Drift tube IMS (DTIMS)	Is based on the time-of-flight principle. Measures drifting time under a constant electric field. DTIMS is the most basic IMS configuration. DTIMS has a low sampling cycle compared to the drifting cycle, which decreases sensitivity.
Travelling wave IMS (TWIMS)	Utilizes electric field waves to push ions into a separator, which enables a low operating voltage. Waves also enhance the resolving power and enable long ion channels, but the collision cross-section requires calibration. High sensitivity; nonetheless, operates at low, < 10 mbar pressure.
Trapped IMS (TIMS)	Traps ions with an electric field against a reverse airflow. Can collect and release ions with similar mobility in bursts. Enhanced resolving power, compact structure. Operates at a low, < 10 mbar pressure.
Differential mobility spectrometry (DMS) or field asymmetric IMS (FAIMS)	Separates ions using a high and low electric delustering field and an additional constant compensation electric field. Produces 2-dimensional spectra. Continuous sampling enhances sensitivity. Sensitive to humidity changes. Easy to measure both ion polarities, low resolving power.
Aspiration IMS (AIMS)	Separates ions with a perpendicular airflow and fixed electric field. Has multiple detector electrodes. Low resolving power, but simple structure.
Differential mobility analysers (DMA)	Scans ions with a perpendicular airflow and scanning electric field. Only specific mobility ions exit the slit. Good for large molecules and particles.

The separation principles of common IMS configurations are presented in Figure 2.

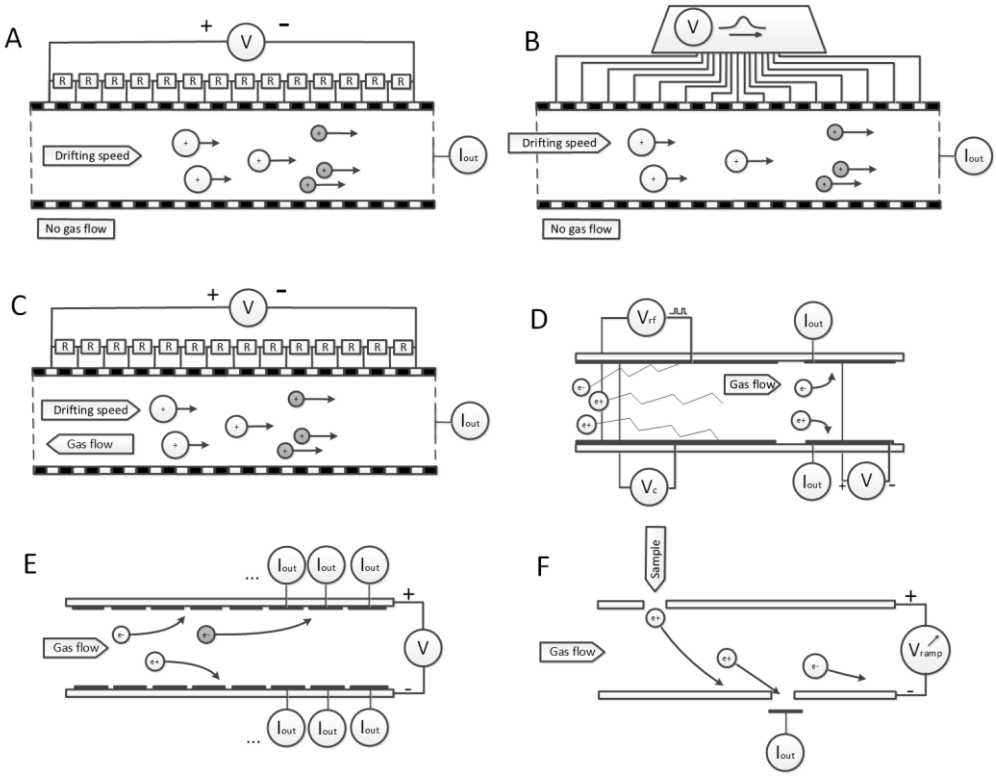

Figure 2. Common IMS configurations. **A) Drift IMS** functions with a time-of-flight principle. Only constant driving and a time-sensitive ion detector are required. **B) Traveling wave IMS** drives ions with voltage pulse waves. The ion channel can be arranged into a circle to enhance the separation length. **C) Trap IMS** has controlled reverse gas flow, which seizes ions at specific places. The electric fields can be complex. **D) DMS** separates with an asymmetric electric field and compensation field. Both ion polarities are measured after the filter region. **E) Aspiration IMS** separates with a constant electric field and constant drift gas flow. Multiple detectors are needed. **F) DMA** operates with constant airflow and a ramping driving voltage. Only ions with specific mobility exit to the ion counter (Intra and Tippayawong 2008).

When considering the most suitable IMS configuration for surgical smoke analysis, multiple parameters must be considered, including sensitivity, resolving power and robustness. Drift tube IMS (DTIMS) is simple and robust. Travelling wave IMS (TWIMS) and trapped IMS (TIMS) have enhanced resolving power but complex structures, and they operate in low pressure instead of atmospheric pressure. Aspiration IMS (AIMS) and differential mobility analysers (DMAs) are simple, with modest resolving power.

Without empirical testing, there is a fair amount of uncertainty about the optimal IMS technology for surgical tissue analysis. However, DMS technology has some clear benefits, such as the fact that the mechanical structure is simple. In contrast, the electronics and spectrum are complex. Moreover, DMS has the specific advantage of providing the possibility to drive energy to the sample. The energy disperses clusters, forming the spectrum according to bond forces. The field energy levels correspond to temperatures of up to a few hundred degrees Celsius (Ieritano et al. 2020; Haack et al. 2019). This declustering works opposite to mutual ion clustering through Brownian motion, electric forces, and Van der Waals forces.

The high electric field opens ion clusters by heating the clusters through collisions (Schneider et al. 2010) and breaking weak intermolecular bonds and hydrogen bonds. Even intramolecular weak covalent or ionic bonds can be broken with high electric fields (Fowler et al. 2020). Since hydrogen bonds are within the operating range, the method is sensitive to water content in the sample, which requires compensation or humidity stabilizing. The DMS measures a spectrum that contains information on the electron and proton affinities of molecules, ion mobilities, properties of the ion clusters, and, in some cases, the internal binding energies of the molecules.

The two-dimensional spectrum has two tuneable electric fields – a high-frequency asymmetric alternating field and a sequentially tuneable constant compensation field – in the axis. The two-dimensional spectrum may be an advantage in pattern recognition, since the data contains additional information on compound structure what is revealed when electric energy disperses the ion clusters. Such a two-dimensional spectrum is illustrated in Figure 3, where the signal feature fingerprint is dependent on the sample matrix. Similar, specific compound-curve relations are presented by Menlyadiev and Eiceman (Menlyadiev and Eiceman 2014).

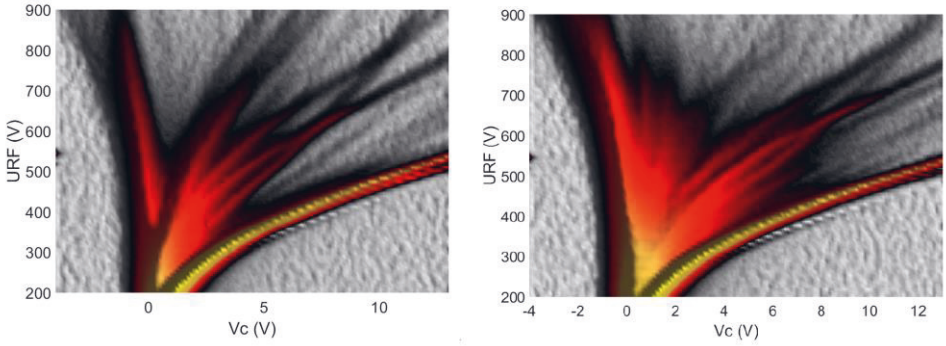

Figure 3. A DMS spectrum where spectral lines curve on a two-dimensional plane, suggesting additional possibilities for feature extraction and object recognition in comparison to a one-dimensional spectrum.

To improve DMS selectivity, a tandem DMS has been proposed, in which two DMS elements are connected in a series. This method is similar to tandem MS. Two DMS elements improve the selectivity for specific compounds by up to 30 times (Menlyadiev and Eiceman 2014). This could improve the classification accuracy (CA) between tissue types, if clear biomarkers could be identified from tissue smoke. In addition, tandem DMS could decrease the sensitivity to external interferents.

2.2.3 Optical spectrometers

Optical spectrometers based on light absorption in gas are modest in complexity in comparison to mass spectrometers but complex when compared to chemical sensors. In terms of device complexity, optical spectrometers are within the same range as standard IMS devices. Therefore, they seem to have a good balance between device complexity and performance as regards optimal methods to be implemented in a surgical smoke analyser. In addition, optical spectrometers are affordable, they can operate with wide dynamic range (Chattopadhyay et al. 2022) and they are robust, as they are capable of self-referencing to some extent (Arevalo-Martinez et al. 2013).

Although there are multiple optical spectroscopy methods, only two have been used to study surgical smoke. These are photoacoustic spectroscopy (PAS) and infrared (IR) spectroscopy. In addition to these methods, the laser sources are relevant, since the optical spectrometer sensitivity typically depends on the laser source used. The light intensity correlates with the signal strength generated from the molecules. Wider-range tunable lasers, such as optical frequency combs (OFC), would increase spectral coverage significantly and thereby increase the amount of molecules simultaneously identified. With conventional light sources, the spectral capability is enough for 1-3 compounds (Henderson et al. 2018).

In IR spectroscopy, the light is absorbed by the molecule at specific wavelengths, depending on molecular bonds. Bond strength correlates with absorptive resonance frequency according to Badger's rule (Badger 1934), which is a crude estimate. A higher bond strength causes higher resonance frequency. Since bonds between atoms have multiple vibrational modes, a single molecule produces multiple absorption lines in the spectrum, which is a characteristic feature of the optical method. Since the optical absorption of sparse gases is weak, the absorption is often amplified by increasing the length of the optical path of the light. These are known as multi-pass cells, where light is reflected multiple times to increase the optical path in the sample gas. Gianella and Sigrist analysed surgical smoke with a Mid-IR (MIR) difference frequency generation (DFG) laser spectrometer and near-IR (NIR) spectrometer (Gianella and Sigrist 2012), demonstrating that IR spectroscopy is suitable for surgical smoke analysis.

Another implemented method for surgical smoke analysis is photoacoustic spectroscopy, which functions on the molecules' photoacoustic response to light. The light heats the molecules, which causes vibrations on an acoustic spectrum. This

method is applicable to trace gas detection (Dumitras et al. 2007). Bratu et al. studied surgical smoke content with laser photoacoustic spectroscopy (LPAS) to evaluate the hazardous volatile compounds of the smoke. LPAS was sensitive and selective for the tested smoke gas components (Bratu et al. 2015).

Some of the optical spectrometers are affected by temperature variations, causing spectral drifting either in the laser source or the optical cavity. Therefore, some compensation methods may be required, such as stabilising device temperature or calibrations (Hodgkinson and Tatam 2012). In addition, humidity variance causes changes in spectral response, which requires compensation. In general, optical methods work well for small molecules but are nonoptimal for large organic molecules (Hodgkinson and Tatam 2012). However, the strength of optical methods lies in the specific, reliable and quantitative measurement of organic gases without the need for frequent calibration (Henderson et al. 2018).

2.2.4 Chemical sensors

Gas-phase chemical sensors are sensitive (Nakhleh et al. 2017), small and simple in structure. Therefore, they have been the first choice in molecular communication (Farsad, Guo, and Eckford 2013) and in many chemical sensing studies (Broza et al. 2019). Regardless of the extensive research, they have not made a breakthrough in medical diagnostics (Nakhleh et al. 2017; Kim et al. 2021). The vast majority of the diagnostic chemical sensors are based on conductive polymers, metal oxides, proteins and, recently, peptides (Broza et al. 2019; Barbosa, Oliveira, and Roque 2018).

Unfortunately, chemical sensors come with unavoidable drawbacks, which require countervailing with opposite characteristics. High sensitivity and selectivity are obtained with strong interaction forces. In contrast, good reversibility is achieved with weak interaction forces, since molecule desorption probability is higher with weak interaction forces. Low selectivity challenges gas sensor utilization because these sensors interfere with other chemicals, making them unreliable in complex chemical environments (de Oliveira et al. 2021). One solution to enhance selectivity is to utilize non-covalent bonds, such as hydrogen bonding, metal–ligand bonding, van der Waals and electrostatic interactions, or hydrophobic forces to construct detailed lock and key structures (de Oliveira et al. 2021). However, there are currently no such chemical gas sensors commercially available.

Designers are thus obliged to balance many design parameters and challenges. For instance, metal oxide sensors (MOS) are sensitive to cross-contaminants and humidity, and while humidity-caused variance in responses could be offset with an additional humidity sensor, humidity sensors are, in turn, cross-sensitive to other cross-contaminants and are usually inaccurate in a high and low humidity. This illustrates the challenges of nonideal measurements and nonideal compensation methods.

In addition, strong interaction forces enable only partial reversibility, which causes poor long-term stability, also referred to as drifting, due to an asymmetric adsorption–desorption cycle and reactive surface alterations. Some similar drifting is caused by alterations in ambient conditions, such as variance in temperature, humidity and pressure (Hierlemann and Gutierrez-Osuna 2008). However, an extensive body of research pushes chemical sensor technology and biosensors to advance, and it is most likely only a matter of time and further research before these types of sensors become suitable for medical diagnostics on a large scale.

2.2.5 Reliability comparison of surgical smoke analysis methods

There is a fundamental challenge in comparing distinctively different detection methods. Specifically, there are no numerical studies to compare surgical smoke analysis performance against different detection methods. However, some characteristics are presented in Table 3, based on the literature survey. The emphasis is placed on reliability and maintainability. Features such as calibration needs, variable compensations, vacuum maintenance, sensitivity to environmental changes and the aging of surfaces and sealings are potential sources of technical faults, affecting system reliability and usability. Similarly, limited resolution or sensitivity increases challenges having to do with environmental disruptions, such as accidental chemical interferents in the operating theatre.

Table 3. Essential factors affecting a surgical smoke analyser's reliability and maintainability

	MS	IMS/DMS	Optical	Chemical sensors
Ambient pressure	0	x	x	0
Ambient humidity	x	xx	x(x)	x
Ambient temperature	x(x)	x	x	x
Sensitivity to sample interferents	x	xx	x	xx
Vacuum	xx	0	0	0
Surface contamination	0	0	x	xx
Component heat drifting	x	x	x	x
Device to device repeatability	x	x	x	x

0: no issue, x: associated challenge, xx: method's characteristic challenge

The characteristic challenge of MS is the demand for high vacuum power, since it complicates the mechanical structure. Additionally, the vacuum inlet fragments the sample molecules, since the rapid pressure drop ejects molecules at a high velocity into the vacuum, breaking the molecular bonds. This distorts the molecular information (Cardoso, Sabin, and Hantao 2022). Repeatability is seen as an issue with MS (Gurdak et al. 2014), although it is certainly also present with all other available operation principles, including DMS (Kontunen et al. 2021). One of the main explanations for repeatability issues could be variation in humidity. Atmospheric plasma ionization sources are sensitive to variances in ambient humidity (Newsome, Ackerman, and Johnson 2014; 2015), especially to low humidity (Feider et al. 2018). Increasing gas temperature decreases the effects of variance in humidity on ionization but increases molecule fragmentation, which, consequently, distorts and decreases information. A better way to compensate for humidity variances is probably to stabilize humidity in the plasma region. Alternatively, there are other ionization options for MS and IMS, such as soft X-rays (O. Anttalainen et al. 2021), although humidity could affect these as well. In contrast to the humidity hypothesis, Jiao et al. discovered that a change in temperature is a major source of variance in mass spectra (Jiao et al. 2021). In addition, open sampling in an operating theatre can cause the intake of samples that include disturbing interferents, such as floor wax (Kumbhani et al. 2017). However, this challenge is likely present with all sensing methods. Lastly, component variances and instrument misalignments (Gamage and Austin 2020) can cause device-to-device variance.

IMS and DMS require compensation for humidity (Safaei et al. 2019) and are sensitive to interferents; however, it is possible to implement technical alarms in the system for the recognition of interferents and environmental risks. Another drawback of IMS and DMS technology is the inherently low resolving power due to the operation in atmospheric pressure and thus the effect of carrier gas molecules on the sample molecules. The optical method has similarly limited resolving power, endangering correct recognition when interferents are present. Lastly, chemical sensors struggle with strong drifting and surface poisoning. Obviously, there is no silver bullet for a perfect surgical smoke analyser.

However, a simple ion trap MS approach, such as the one proposed by Jiao et al. (Jiao et al. 2021), would be a sound option for a smoke analyser, if the design for rapid sampling were constructed and the overall reliability proven to work. In comparison, a DMS-based analyser would work, if the rather black-box approach for chemical responses were accepted, the risks from interferents were on an acceptable level and the clinical accuracy were above the minimum required level. A third option would be a combination of DMS and ion trap MS. This, however, is not preferred, as it would inherently complicate the system and thereby cause new features that are prone to failure. The system would consist a DMS prefilter, providing partially orthogonal separation for MS. In addition, prefiltering would benefit ion trap MS, since it would reduce the space charge effect caused by Coulombic repulsion (Hall et al. 2013). DMS and ion trap MS combine perfectly because DMS filters continuously and an ion trap relies on ion accumulation. Hall et al. discovered a 10-fold increase in trap fill time and, thus, sensitivity for benzoylecgonine from synthetic urine (Hall et al. 2013). For surgical smoke, the improvement should be greater, since the background sample matrix is more complex.

2.2.6 Devices and prototypes for surgical smoke tissue identification

To date, in 2022, there are no surgical smoke tissue analysers approved for clinical use. However, for research purposes, Waters has manufactured a REIMS system, which is based on MS (Tzafetas et al. 2020). There are also a few research prototypes for surgical smoke tissue analysis, such as DESI-LIT-MS (Pirro et al. 2017) and a DMS-based system (PIV).

2.2.7 REIMS and iKnife

The development of margin detection from surgical smoke began after the invention of desorption electrospray ionization (DESI) (Takats et al. 2004), which allowed real-time tissue sampling for MS. Then, in 2009, Schäfer et al. reported on a new method for rapid tissue sampling for MS, entitled rapid evaporative ionization mass spectrometry (REIMS) (Schäfer et al. 2009). This method provided fast, real-time tissue sampling, suitable for distinguishing between healthy and cancerous tissue. Numerous studies have been conducted on the topic ever since (Ogrinc et al. 2021; Balog et al. 2013; St John et al. 2017). REIMS has subsequently also proven to function in *in vivo* research during a rectal cancer operation (Mason et al. 2020).

The commercial system iKnife includes a REIMS source as a spectrometer and sampling system. The spectrometer is connected to normal surgical diathermy equipment. To avoid surgical smoke contamination, REIMS is equipped with inertia-based aerosol filter for large particulates. Smaller particulates are inhaled and driven through a heated collider. (Figure 4.) The heated collision surface declusters and ionizes the sample. Presumably, for ionization, the heated collision surface is less sensitive to variation in humidity than are plasma sources (Newsome, Ackerman, and Johnson 2015). Thereafter, the sample flows to a low-pressure ion separator, StepWave® (K Giles and Gordon 2010). Since only ions are taken to MS sensor, further contamination from neutral molecules is prevented. Jones et al. reported the system working for up to five hours without major contamination (Jones et al. 2019).

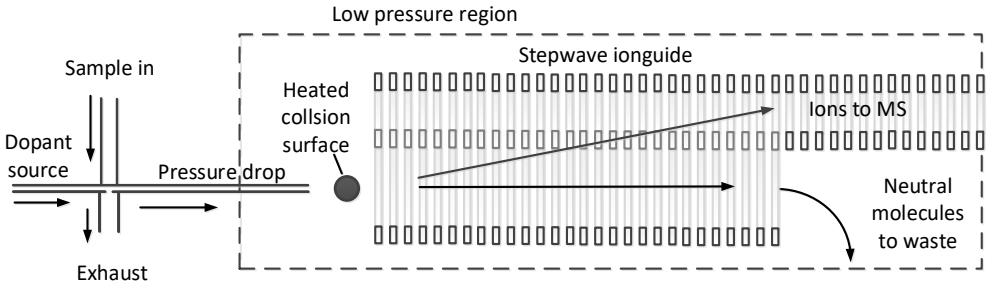

Figure 4. A REIMS source for MS. Inertia pushes large aerosol particles from sample into the exhaust. The dopant source is for isopropanol or equivalent dopants. The heated collision surface separates molecule clusters and ionizes the sample. The stepwave ionguide channels only ions to MS, and uncharged molecules are driven to waste. Adopted from (Jones et al. 2019).

2.3 Characterizing surgical smoke transfer line

System delays include chemical, electrical and data delays. In Figure 5, the illustrated delays consist of: 1) a delay in the surgical evacuation tube, 2) a delay in the particle filter, 3) transport delay from filter to DMS, 4) data transfer delay, and 5) the time it takes to analyse the data and present the result to the operator. Here, we focus on the molecular transport delay, since it is the longest delay and defines the instrument's operation speed. Surgical smoke is transported through a tube, which functions as a transfer line from the scalpel to the spectrometer. Characteristically, molecular signals appear swiftly but disappear slowly. This asymmetry affects the device's design and data analysis. (PIV.)

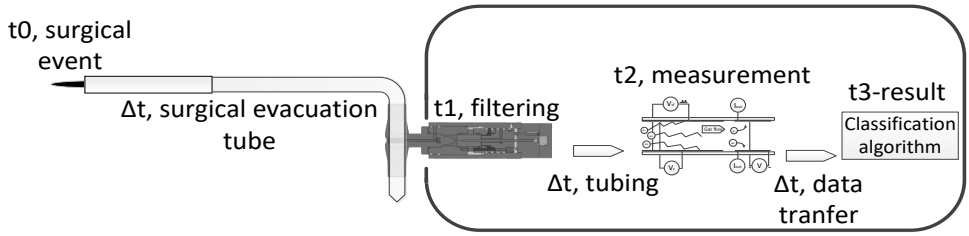

Figure 5. Main delays of the surgical device. These delays consist of smoke transfer from surgical scalpel to filter, the delay from filter to DMS, as well as the DMS measurement, data transfer and data analysis times.

Molecular sorption (attaching and detaching of molecules to surfaces) causes signal delays in the transfer line. Other factors include the flow profile and turbulences. We study the way in which sorption is formed with its subtypes: adsorption, absorption and desorption. Sorption is regulated by molecular forces attaching and detaching molecules.

2.3.1 Sorption

Sorption is a physical and chemical event whereby a molecule attaches to another. The subevents consist of absorption, where a molecule is incorporated into another substance, such as when a gas dissolves into a liquid. In contrast, adsorption occurs on a surface. Desorption, then, is a reverse sorption, whereby molecules detach from one another. Adsorption can be divided into a weaker physisorption with Van der Waals forces and stronger chemisorption with ion or covalent bonds.

Absorption describes the event whereby molecules diffuse into or through the bulk of a material. The general physics behind absoprtion and permeation-related absrption can be estimated in the following manner: the solubility coefficient (S) in (1) defines the absorption capacity or concentration of a solid with Henry's law:

$$C = S \cdot p \tag{1}$$

where C is concentration, S is solubility and p is pressure.

The diffusion coefficient (D) in (2) defines the kinetic property of a permeable membrane. The permeability coefficient (P) defines the rate of the molecular flow. The mutual relation of these coefficients is determined as:

$$P = D \cdot S \tag{2}$$

These coefficients are temperature-dependent in a similar matter to the Arrhenius equation. The temperature coefficients of diffusion, permeation and solubility are described in equations (3), (4) and (5):

$$P = P_0 e^{\left(-\frac{E_P}{RT}\right)} \tag{3}$$

$$D = D_0 e^{\left(-\frac{E_D}{RT}\right)} \tag{4}$$

$$S = S_0 e^{\left(-\frac{H_S}{RT}\right)} \tag{5}$$

where P_0, D_0 and S_0 are base values in a spesific temperature, while E_P and E_D are activation energies. H_S is the heat of the solution, meaning the amount of chemical energy released or absorbed when the solving occurs.

The sample emission rate of an absorbed chemical can be expressed as:

$$q_s = P \cdot A \cdot \frac{\Delta p}{d} \tag{6}$$

where q_s is a steady-state flow of the permeable substance, A is the area, and Δp is the pressure difference across membrane. (Mitchell 2000; Ho, Edmond, and Peacock 2002)

Adsorption describes the bonding of atoms and molecules to a solid surface. The attached compounds are called adsorbates and the solid substrate is the adsorbent. Adsorption is a surface phenomenom, a concequence of a surface-free energy, in which surface atoms posess more free energy than atoms inside the bulk. Threrefore, adsorbed substances minimize the free energy by adhesion to the surface. Adsorption is divided roughly into *physisorption* and *chemisorption*. Physisorption is primarily caused by Van der Waals forces, where the bond energy ranges from approximately 10 to 300 meV. Adsorption caused by ion and covalent bonds is called chemisorption, where the bond energy ranges from roughly 1 to 10 eV.

The *physisorption* force between two molecules can be expressed with attractive Van der Walls forces and the Pauli repulsive force. These are presented in a simplifed manner in the Lennard Jones potential. Therein, the attractive term is in r^6 and repulsive in r^{12}.

$$V_{\mathrm{LJ}} = \epsilon \left[\left(\frac{r_m}{r} \right)^{12} - 2 \left(\frac{r_m}{r} \right)^{6} \right] \tag{7}$$

where ε is the depth of the potential well, r is the distance between particles, and r_m is the distance where the potential minimum exist.

For a more accurate model, the Buckingham potential and other later quantum models exist. Regardless, physisorption to a solid surface can be simplified for a hydrogen atom with an image charge in a conductive surface, which reduces the van der Waals potential from r^6 to r^3 (A in Figure 8). Physisorption potential as energy can be expressed as in the equation in Figure 8.

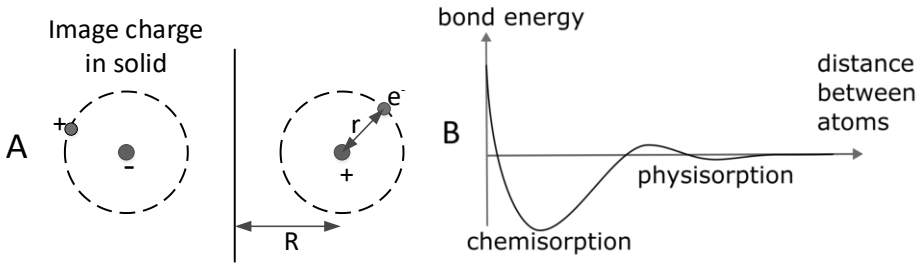

Figure 6. A) Image charge situated inside a solid bulk material, B) a specific case of chemisorption and physisorption as a function of the bond distance, where there is a distinct energy boundary between chemisorption and physisorption.

$$V = \frac{1}{8}\frac{e^2 {r_m}^2}{r^3} \tag{8}$$

where V is potential energy as a function of r, and r_m is the molecule radius. Reduced exponent correlates with reduced bond energy in comparison to chemisorption.

Chemisorption involes a chemical reaction between the surface and the adsorbate. The potential well is described with Morse potential, as opposed to the Lennard-Jones potential in physisorption. Between these potentials, there can exist a potential barrier. Crossing this barrier requires energy to transfer from physisorption to chemisorption (B in Figure 8) (Huber et al. 2019). Physical adsorption and chemical adsorption are compared in Table 4.

Table 4. Table 4. Comparison of physical and chemical adsorption. Adopted from Grinham & Chew, 2017, and Huber et al., 2019. (Grinham and Chew 2017; Huber et al. 2019)

Property	Physical adsorption	Chemical adsorption
Force	Van der Waals, hydrogen bonds	Ion and covalent bonds
Typical bond energy	10–300 meV	1–10 eV
Bond distance from surface	3–10 Å	1–3 Å
Reversibility	Fully reversible	Reversible or irreversible
Specificity of adsorbate–adsorbent reactions	Low	High
Temperature dependency	Negative	Positive in activated adsorption case
Can form multiple layers on the surface	Yes	No

Desorption describes the detaching of the molecules from a surface. Temperature plays a major role in desorption. The Arrhenius equation describes the temperature depency of the reaction rate. Reaction occurs if the kinetic energy exceeds the activation energy E_a. (Do 1998). The rate of desoption is expressed as:

$$k = Ae^{\frac{-E_a}{RT}} \tag{9}$$

where k is rate constant for reaction collision frequency, A is reaction spesific constant, R is universal gas constant, E_a required kinetic activation energy.

Langmuir proposed a kinetic adsorption-desorption equilibrum model for flat homogeneous surfaces, with uniform adsorption sites, which is known as the Langmuir equation (Langmuir 1916). Each site can bind only one molecule. The model consists of a continuous bombardment of gas-phase molecules and a continuous desorption forming equilibrium. The continuous molecule bombardment to a surface can be expressed as:

$$R_s = \frac{P}{\sqrt{2\pi MRT}} \tag{10}$$

where R_s is rate of bombardment, P is partial pressure, M is molecular mass and R is gas constant.

Part of the bombarded molecules bounce back immediately, which can be estimated with coefficient α. The Langmuir model assumes single-layer adsorption, which can be estimated with a fractional coverage θ. Adding these parameters, adsorption rate can be expressed as:

$$R_a = \frac{\alpha P}{\sqrt{2\pi M R_g T}}(1-\theta) \tag{11}$$

where R_a is the adsorption rate, indicating the number of moles adsorbed per unit area per time.

For multilayers Brunauer–Emmett–Teller theory or empirical Freundlich equation is more suitable. In opposite, desorption rate can be described as:

$$R_d = k_d\theta = k_{d\infty}e^{-\frac{E_d}{R_g T}} \tag{12}$$

where k_d is the desorption rate constant, E_d is the activation energy of desorption, which is equal to adsorbed thermal energy in physisorption, and $k_{d\infty}$ is the rate constant for desorption at infinite temperature.

The residence time or adsorption time describes how long molecules are adsorbed on average. It can be estimated with a modified Arrhenius equation, where τ_0 is between 10^{-13} (Wilmoth 1973) to 10^{-12} (Grinham and Chew 2017) seconds.

$$t = \tau_0 e^{\frac{E_a}{RT}} \tag{13}$$

For reference, at room temperature, with $\tau_0 = 10^{-12}$, a 220 meV water–hydrogen bond lasts an average of 23 ns. A 300 meV hydrogen–nitrogen bond lasts 390 ns, while a 1 eV bond lasts nearly 6 hours. For clearance, a typical physisorption residence time ranges from 10^{-13} to 10^{-9} seconds and chemisorption from 10^{-6} to 10^{9} seconds. (Do 1998). Macroscopically, however, the molecules tend to behave with dynamic equilibrium, since after desorption the molecules can be and likely are adsorbed again unto the surface. This slows down the macroscopic time constants compared to the single molecule's time constant.

2.3.2 Particulates in the transfer line

In surgical smoke, most of the evaporated molecules are condensed into particulates. Particulates are formed when the operated tissue is heated rapidly. Some of the tissue is directly torn off as tiny pieces, and the remaining particulates are formed by the cooling gases condensing into particulates. Gas-phase molecules condense into particles, usually from supersaturated vapor and initiation with a nuclei particle. The cooling of hot gases from evaporated tissue cause this gas supersaturation. Most of the condensed particulates are formed from water. When smoke is transported further and diluted, the gas saturation level is decreased, at which point a reverse phenomenon can take place. The particulates evaporate again, returning some of the molecules back to the gas phase. (Hinds 2012)

Coagulation is a process in which the particulates collide and attach to each other, causing them to decrease in number and grow in size. A Brownian motion-based coagulation is known as thermal coagulation and coagulation caused by other forces as kinematic coagulation. When the particle size increases, the relevant physics change. Diffusion plays a relevant role for small, < 1 μm particles, inertia-based phenomena for middle-sized particles, and gravitation for large, > 1 μm particles.

Particles larger than few micrometres are filtrated through gravitation. Particles larger than a few hundred nanometres tend to be filtrated through interception and impaction in fibre filters. Particles smaller than a hundred nanometres tend to be filtrated through diffusion, since Brownian motion is significant in these small particles. The filtering efficiency of a single fibre is illustrated in Figure 7.

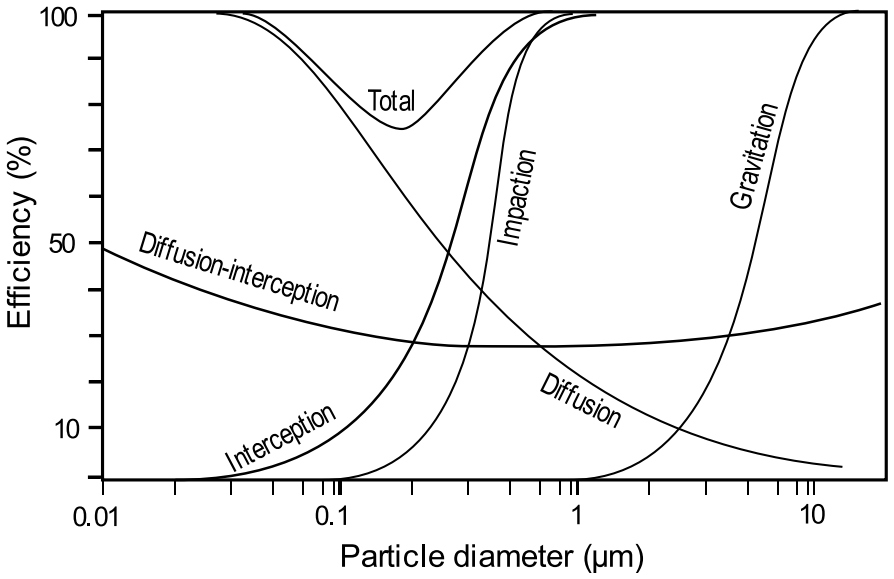

Figure 7. A single fibre's filtering efficiency for particle size distribution, adopted from Hinds, 2012.

2.3.3 Particle filtration

As described earlier, surgical or diathermy smoke contains particulates. In PI, the amounts of emitted particles varied significantly, being in the range of 0.2–9 g/m^3 in the diathermy smoke evacuation system. These concentrations are far above the condensation limit for many VOCs. The particles must be removed or vaporized if the gas is analysed in a gas analyser – otherwise, the smoke particulates would fill and contaminate the sensors and other surfaces and cause carry-over in the analysis when desorbing at a later time. Because the smoke particulates mutually adsorb and desorb molecules, they function as a chemical information buffer. This buffer causes significant carry-over.

A basic particle filter is constructed from a mesh of fibres, forming a porous structure. When particles adhere to the fibre filter, they continue to desorb molecules to the perpendicular flow, which causes significant carry-over. In addition, an unfit filter for a smoke analyser is a cyclone filter which only removes large particles if scaled to applicable dimensions for surgical smoke analyser. A thermophoretic filter is another filter type whose applicability for a surgical smoke analyser remains unproven (Hinds 2012). Giles et al. developed an RF guide to separate particulates (Kevin Giles et al. 2004; K Giles and Gordon 2010) unfortunately, their filter functions in the sub-mbar pressure range, which is unfavourable for non-MS systems. Asbach et al. 2004 reported a method for separating particulates from sample gas utilizing a corona discharge separator (Asbach, Kuhlbusch, and Fissan 2004). The method has been shown to have a filtration efficiency of 96%. A similar principle was utilized by Roine et al. (Roine et al. 2021).

2.3.4 Phoretic effects

Both thermophoresis and turbophoresis are particulate-inertia-based phenomena. A thermophoretic force drives particulates along a temperature gradient. Mainly, particulates tend to move from hot to cold regions spurred on by kinetic energy obtained in a hot region. Similarly, turbophoresis drives particulates from turbulent to laminar flow regions. Since particulates tend to continue the kinetic momentum obtained in a turbulent flow, they end up in less turbulent regions. However, if a particulate has a longer flight relaxation time than it takes to cover the distance to the turbulence minima, the particulate may pass the minima. It is also noteworthy that, since the flow near the tube walls is less turbulent in pipe flow, particulates easily condense onto the walls (Belan, Fouxon, and Falkovich 2014; Hinds 2012). These phoretic effects are significant for particle adhesion and, therefore, for system contamination.

3 AIM AND OBJECTIVES

The aim of this thesis is to study surgical smoke utilization in cancer surgery. The objectives of this thesis are formulated into three research questions.

1. **What is the composition of surgical smoke?** Surgical smoke is studied empirically in publications I and III, in which the particulate distributions of the surgical smoke are characterized and quantified.

2. **How should surgical smoke be analysed in order to obtain accurate tissue recognition?** This question is studied in publications II, III and IV. Additionally, the literature survey has been executed to compare various analysis methods developed for smoke analysis. Answering this research question helps in defining the requirements for the third research question.

3. **How should surgical smoke be transported and modulated in order to obtain optimal tissue analysis?** This question is studied in publications III and IV. Surgical smoke modulation and filtering kinetics are explored. We have investigated how sample smoke should be modulated and transported to achieve optimal analyses from various tissue types. Similarly, we reflect on how these features could be implemented into a medical device.

3.1 Contribution

The scientific contribution of this thesis is twofold. First, this thesis entails a study of surgical smoke composition in relation to occupational health issues in an operating theatre. Secondly, the thesis studies a method for determining the resection margin in real time. The features related to the tissue analysis technology under development have been investigated. The method and features are examined from the perspective of engineering. The literature study emphasizes these factors and expected challenges in safe device operation. The experimental studies cover a DMS-based method for malignant brain tissue detection with *ex vivo* samples, as well as device tubing material choices and the chemical signal kinetics of the studied system.

4 MATERIALS AND METHODS

This thesis contains studies regarding the health impacts of surgical smoke and the development of a real-time surgical margin assessment method. The developmental studies focus on smoke transportation and analysis. All tests were conducted at Tampere University.

4.1 Devices used in surgical smoke analysis

In study PI, the particle size distribution of surgical smoke was analysed with an electrical low-pressure impactor (ELPI, Dekati Oy, Finland). In addition, surgical smoke VOC content was measured with two DMS instruments: Envi-AMC (Environics Oy, Finland) in studies PII and PIII and IonVision (Olfactomics Oy, Finland) in study PIV. These analysing methods provided the basis for the empirical results, supplemented with additional assisting measurands. In addition, different measurement setups were needed to complete these tasks.

4.1.1 Electrical low pressure impactor

The electrical low-pressure impactor (ELPI) is an instrument for characterising particle size distributions based on inertia. It was developed to automize a cascade impactor (Marjamäki et al. 2000). The ELPI has 13 impactor stages and a particle detection range from 30 nm to 10 μm. The impactors collect particles with inertia. If a particle has more inertia than the particular impactor stage cut-off limit allows, the charged particle impacts onto the electrode and releases the electric charge to the detector. The first impactor stage collects particles with the highest inertia and the last impactor stage collects particles with the least inertia. The ELPI has a characteristic limitation with a large concentration. The charged particles repulse each other with a coulomb force, causing some fine particles to collide with the detector intended for large particles. (Virtanen et al. 2001) This may have had some effect on the large particle mass concentrations in study PI.

4.1.2 Envi-AMC

ENVI-AMC® is a DMS developed by Environics Oy, Finland, in 2014. It is sized to fit onto a 19"-rack with a height of 4U. Sample molecules are ionized with Americium 241Am where the sample enters the drift channel. In the channel, an asymmetric electric field can function at a frequency of up to 250 kHz and separation voltages of up to 700 V. Since the electrode gap is 0.25 mm, the separation field reaches up to 3 kV/mm. A detailed description of the sensor can be found in an publication by Anttalainen et al. (O. Anttalainen et al. 2018).

4.1.3 Ionvision and Resect prototype

Olfactomics Oy has developed prototypes for surgical margin analysis aimed for daily clinical use. The prototypes include an industrial design mock-up for studying usability and a conventional engineering prototype to evaluate system performance, both presented in Figure 8. The analysis is based on Ionvision, a DMS device which is essentially an electric-field-tuneable ion filter. It has two electrode channels sized to 6×20×0.25 mm. Data points can be flexibly set up anywhere in the measurement range, containing any pair of separation and compensation fields. The waveform generation is implemented with direct pulsing without resonators, enabling true rectangular pulses. The separation field is limited to 1 kV. The analogue-to-digital converter sampling rate is 333 kHz, and the single data point adjustable averaging is between 20–215 samples. The separation field frequency is adjustable from 250 kHz to 1 MHz.

In study PIV, we used a frequency of 1 MHz in the separation field. To obtain a high temporal resolution, we used eleven pre-selected voltage pairs. The compensation field varied from 0 to 22 V/mm and the separation fields from 800 to 3,668 V/mm. Each time point included eleven data points from the positive and negative ions. We used forward feature selection from a high-resolution scan to select the used voltage pairs.

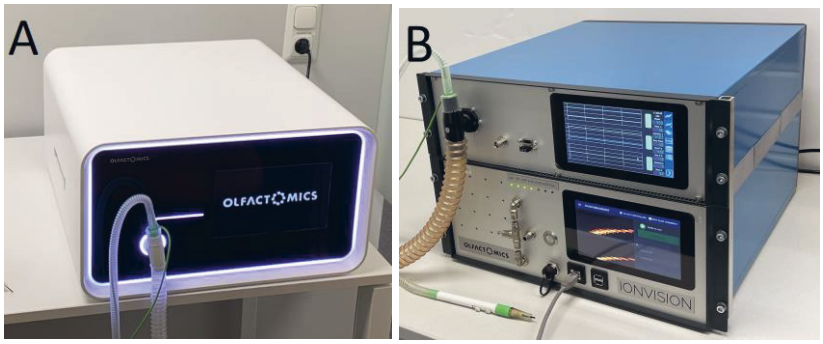

Figure 8. A) A mock-up of a DMS-based surgical margin assessment detection device. B) Engineering prototype.

The engineering prototype has a rapidly changeable particle filter to remove smoke particulates. The system has a weight estimate of 22 kg. The prototype system consists of a high-voltage-driven particle filter to remove particles from the sample stream so that only gas-phase molecules are analysed. Otherwise, these particles (PI) contaminate the spectrometer. To tackle some of the environmental variance, temperature and humidity controllers are implemented. For analysis, the sample is ionized with soft X-rays. The main components of the instrument are presented in Figure 6. The classification algorithm is a crucial part of the system and is a topic of continuous research (A. Anttalainen et al. 2021).

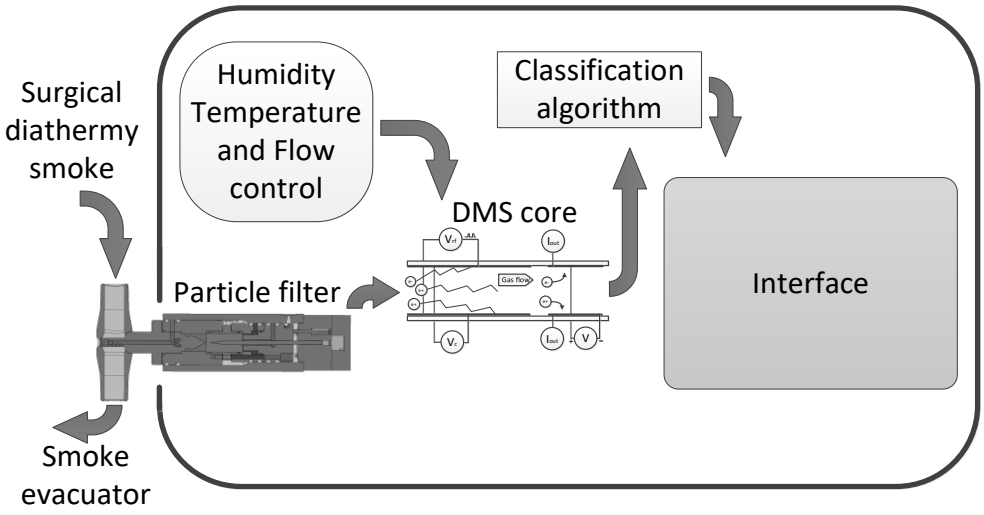

Figure 9. Schematic of a DMS-based surgical smoke analyser. A smoke sample is cleared from particles and analysed in the DMS. The spectrum is classified with a dedicated algorithm. The system has additional humidity, temperature and flow control systems.

4.2 Smoke particle measurements

To quantify surgical smoke particles, we utilized an electrical low-pressure impactor (ELPI, Dekati Inc., Finland), which was used to measure particle number, mass and size distributions. We approximated particle density with standard water density (1 g/cm^3). Samples consisted of ten porcine tissue types: skeletal muscle, liver, fat, renal pelvis, renal cortex, lung, bronchus, skin, as well as grey and white brain matter. Samples were cut with an electrosurgery unit (Itkacut 350MB, Innokas Medical, Finland) set at a nominal power of 120 W. Cuts were automized with a customised 3D-printed stage. We aimed for 4 mm deep and 5 mm long cuts with a 2.4 mm-wide blade. After sample resections, we weighed the sample mass loss with a weight scale (XR205SM-DR, Precisa, Switzerland). We evaluated the hazard to operating theatre personnel caused by inhaling smoke particles. Particulate distribution was estimated with an inverse spherical model (Wang et al. 2015), in which the smoke intensity decreases inversely to the square of the distance from the source. We approximated a general smoke evacuator efficiency of 50% (Wang et al. 2015) and a scalpel-mounted smoke evacuator efficiency of 88% (Pillinger, Delbridge, and Lewis 2003). A general-purpose surgical suction device is commonly a hand-held vacuum used for collecting liquids from the dissection site.

4.3 Smoke analysis methods used for tissue classification

In article PII, we studied brain tumour tissue identification with DMS technology. We utilized samples from 28 patients treated at Tampere University Hospital. These original samples consisted of 6 meningiomas (WHO grade I), 3 pilocytic astrocytomas (grade I), 3 other grade II low-grade gliomas (LGG), 9 glioblastomas (GMB) (grade IV), 5 central nervous system metastases, and 3 control samples. The control samples were haemorrhagic or traumatically damaged brain tissue. The samples were frozen and later cut into samples with a diameter of 3 mm. The samples were analysed with DMS in 9 sessions to obtain 694 measurements, consisting of 121 meningiomas, 154 central nervous system metastases, 35 pilotic astrocytomas, 257 GBMs, 32 LGGs, and 20 control measurements.

The test setup consisted of three parts: 1) An automated tissue sampling unit that was developed to cut standardized incisions, consisting of a modified 3D-printer (RepRap Mendel Prusa i3, Kit Printer 3D), a diathermy system (Itkacut 350 MB, Innokas Medical) and a smoke evacuator (Surtron Evac, LED SpaA); 2) a sample conditioning unit that separated smoke particulates from the sample gas; and 3) the DMS sensor (ENVI-AMC, Environics Oy). In the data analysis, the samples were classified into 2, 5 and 7 classes. These were designed to answer different clinically relevant questions. Seven classes respond to all available individual tissue types with all available data. Five-class classification was performed to remove interference from a tissue preserving agent (Tissue-Tek). Binary classifications were performed for the five most relevant tissue pairs. In many cases, a binary classification is applicable in a surgical operation, when the preliminary conditions, such as tumour type, are known. We used linear discriminant analysis (LDA) as the classifier. To avoid random biases, we applied 10-fold cross-validation for a large dataset and leave-one-out cross-validation for a small sample size.

4.4 Transfer line characteristics

In order to characterize the chemical signal kinetics of surgical smoke, we used an experimental setup illustrated in Figure 10. The setup consisted of the commercial Itkacut 350MB diathermy device (Innokas Medical, Finland); a SafeAir® (Stryker Corp, USA) surgical evacuation unit, equipped with a three-metre surgical evacuation tube with a flow rate of 50 l/min; an Ionvision DMS spectrometer (Olfactomics Oy, Finland); and a custom-made filtration unit for sample conditioning and smoke particle removal. The samples comprised porcine muscle and renal tissue purchased from a local grocery shop. Smoke from the incisions was analysed with the DMS sensor. The filter unit was an in-house-built prototype that removes smoke particulates and compensates for humidity variations. The measurement setup is shown in Figure 10.

Two datasets were collected. One to study delays in the transfer line and one to study the effect of delay on the performance of tissue classification. The first dataset contained 50 one and half second long randomized incisions to porcine renal cortex and skeletal muscle. These incisions were repeated after 20 second clearing time. The second dataset consisted of a second long incisions with 2,3,5, and 11 second clearing times containing 205 incisions in total. (Detailed description in PIV).

The delay estimations between surgical scalpel, filter unit and the spectrometer unit are illustrated in Figure 10.

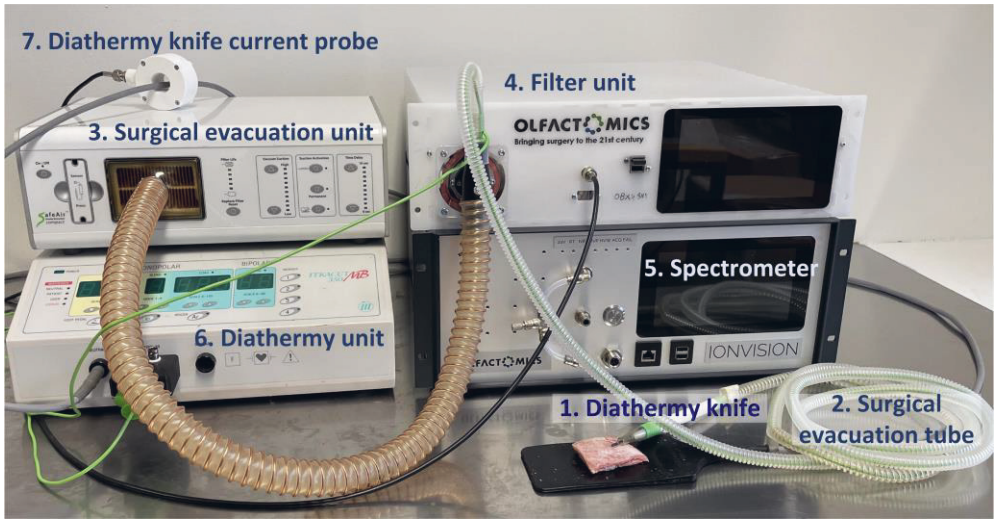

Figure 10. Experimental setup used for an investigation of chemical signal transfer time. The setup consists of a diathermy knife (1), 3-metre surgical evacuation tube (2), commercial surgical smoke evacuation unit with a 50 l/min flow rate (3), smoke filtering and conditioning unit (4), differential mobility spectrometer (5), commercial diathermy unit (6), and a current probe for the diathermy knife (7).

The chemical signal transfer time from diathermy knife to spectrometer is dependent on the construction of the transfer line. In this construction, several parameters have an effect on the performance, such as tube length, flow speed and temperature. Since the system is complex, including smoke particle removal and a commercial surgical smoke evacuator, the transfer time was studied in portions. In Figure 11, the transfer time is presented with six characteristic delay parameters.

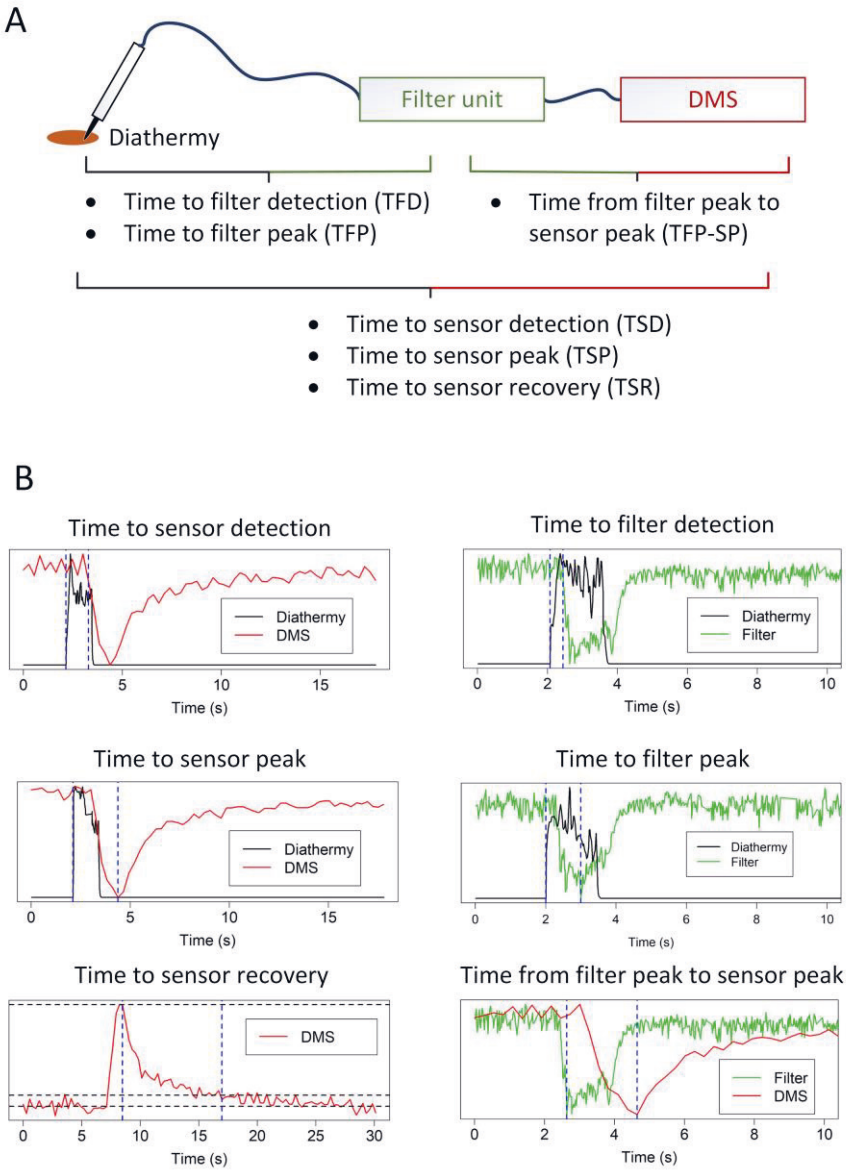

Figure 11. Six delay indicators from the transfer line (A). These illustrate delay behaviour. Figurative illustrations from the delays are illustrated in (B). **Time to sensor detection** indicates the delay from a surgical incision to the first response in a DMS. **Time to filter detection** indicates the time from an incision to the first response in the filter unit, which is roughly the delay in the evacuator tube. **Time to sensor peak** indicates the time from an incision to the peak response in the DMS. **Time to filter peak** indicates the time from an incision to the peak in the filter unit. **Time to sensor recovery** indicates the decay time from the maximum signal to 10%. **Time from filter peak to sensor peak** indicates the delay in the system excluding the surgical tube. Reprinted from PIV.

4.5 Evaluation of transfer tubing recovery

We tested tube material recovery times for surgical smoke. The tube materials were PTFE, PEEK, FEP, Polyetylene, steel, as well as parylene-coated and silconert-covered steel tubes. The exposure was from diathermy knife cuts. The cuts were 3 mm deep and 5 mm long and made on a porcine kidney. The smoke production setup consisted of the same electrosurgical knife as in PII, in PIV with 40 W cutting power. The knife was connected to a XYZ stage modified from a 3D printer (REPRAP Mendel Prusa i3, Kitprinter3d, Spain) and a smoke evacuator (Surtron Evac, Quirumed, Spain). After the smoke exposure, the sample tubes were measured with a DMS instrument. In the measurement phase, the setup consisted only of the individual 30 cm long sample tubes and the DMS device (Envi-AMC, Environics Ltd., Mikkeli, Finland). In contrast, in the contamination phase, there were six tubes parallel to exposure. The second round of tests was performed in a heating cabinet (MICRO, Temperature Applied Sciences [TAS], UK), and the tubes were warmed in 70 °C for 5 minutes before the measurement was started.

The second test setup consisted of a single PFTE tube and a flow rate controller (AS2000, SMC Japan), which were heated to the target temperature in a heating cabinet. The cabinet and the tube were heated in 22, 50, 70 and 100 degrees Celsius before the smoke exposure and measured immediately after the exposure, since no moving of the pipes was required.

5 RESULTS AND DISCUSSION

The core findings and results of the four studies are presented in this chapter. More detailed descriptions are presented in the original publications.

5.1 Surgical smoke particle distribution

Publication I studied the particle distribution in surgical smoke, as well as the health implications of the smoke for operating theatre personnel. Porcine tissues were cut with a surgical diathermy knife to simulate surgical smoke production. During a seven-second incision, the mean weight loss of liver tissue over nine tests was 41 (±12) mg, which yields an evaporation speed of 5.9 (±1.2) mm^3/s. In a 12 l/min surgical evacuation stream, this results in a concentration of 29 g/m^3. The results with the ELPI showed a particle concentration of 9.1 (±4.2) g/m^3, which would indicate a loss or mismatch of 20 (±9.2) g/m^3. This mass is probably mostly spread near the incision area and not vacuumed into the smoke exhaust. The distributions of particulate numbers by tissue type are presented in Figure 12 A, and Figure 12 B shows the mass distributions. The curves are medians derived from ten tests. We identified three tissue type groups: high-particulate-matter (high-PM), medium-PM and low-PM tissue. The majority of the particle mass in the smoke is explained by the large particles. In contrast, the particle number concentration leans towards small particles. Particle distributions indicate at least two particle modes, the first of approximately 10 nm and the second of approximately 100 nm.

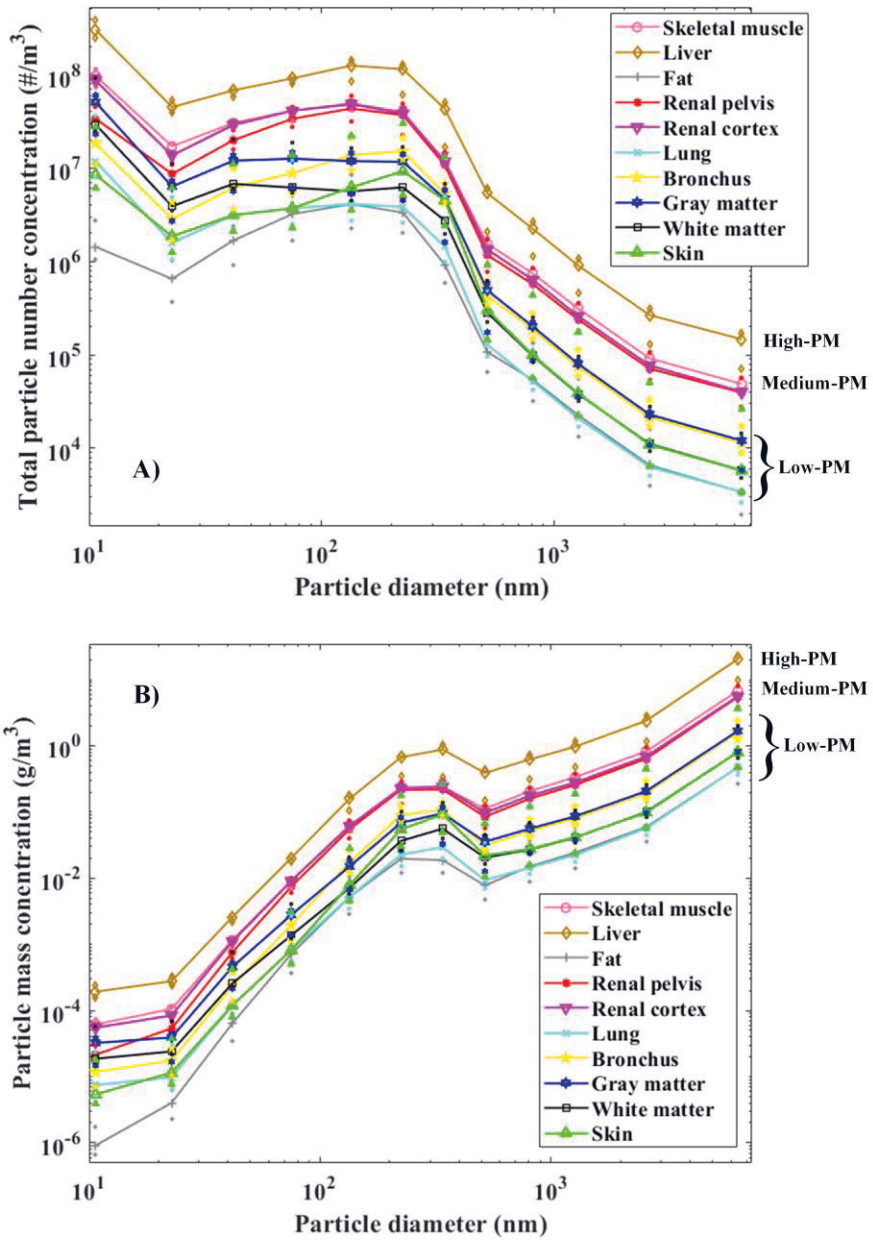

Figure 12. Median particle number (A) and mass (B) concentrations in porcine tissues. Smoke was produced with a diathermy knife. The particle concentrations of the tissue types are grouped into three groups: high-PM, medium-PM and low-PM. Reprinted from PI.

Total particle number concentrations are presented in Figure 13. The variations between tissue types, especially high-PM liver in comparison to other tissues, is clearly visible. We listed liver tissue to high-PM, muscle, renal pelvis and renal cortex to medium-PM and the rest of the tissues to low-PM tissues.

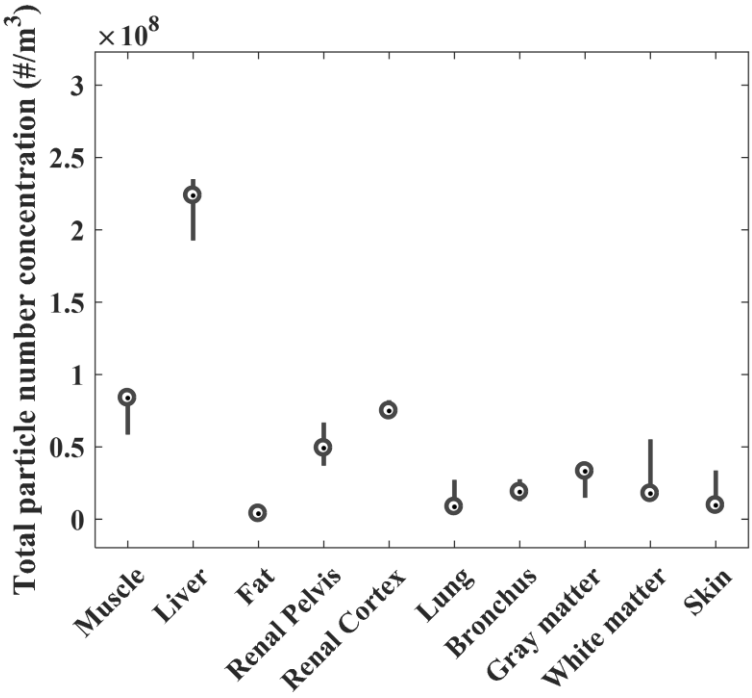

Figure 13. Boxplot graph of the total particle number from each tested tissue types. Medians are marked with dots and quartiles with lines. Reprinted from (PI)

Based on the particle measurements, we estimated the health hazard caused by the surgical smoke to the operating theatre personnel. Based on this, Table 5 presents calculated estimates for the personnel exposures to surgical smoke particles. The table includes three user cases: surgery with no smoke removal, surgery with general-purpose suction and surgery with an integrated smoke evacuator. These concentrations were compared to a common air quality index. We concluded that low-PM tissue did not pose an exposure risk, but medium-PM and high-PM did.

Table 5. Spherical model approximation of particle concentrations from various distances for the tested tissues. Reprinted from PII.

Extrapolated particulate exposures	Distance (cm)	High-PM µg/m3, AQI		Medium-PM µg/m3 AQI		Low-PM µg/m3 AQI	
40 W, with no smoke removal	30	1700	VH	500	VH	86	H
	50	360	VH	110	VH	19	L
	100	46	M	14	VL	2.3	VL
	200	5.6	VL	1.7	VL	0.29	VL
40 W, with general-purpose surgical suction (-50%)	30	870	VH	260	VH	44	M
	50	190	VH	56	VH	9.7	VL
	100	24	L	7.1	VL	1.2	VL
	200	2.9	VL	0.88	VL	0.15	VL
40 W, with integrated smoke evacuator (-88%)	30	200	VH	60	H	10	VL
	50	44	M	13	VL	2.3	VL
	100	5.6	VL	1.7	VL	0.28	VL
	200	0.68	VL	0.21	VL	0.036	VL

VL = very low, L = low, M = medium, H = High, VH = very high

Surgical smoke particles are not only harmful to operating theatre personnel through the respiratory tract, but also a similar stress or overburden occurs in devices exposed to surgical smoke. The diathermy knife collects scarred tissue. Smoke particulates form a layer of tissue material in the smoke evacuation tube and smoke evacuator device. Therefore, these parts have to be replaced frequently. A similar burden is present in measurements connected to surgical smoke. Particulates tend to stick onto tube walls, causing a layer of deposit. In addition, this substance emits volatile compounds, causing chemical interference on a temporal dimension. Notably, we recorded a rough estimate that, in the tubing used in the spectrometer, direct exposure to surgical smoke required an approximately three- to four-fold longer recovery time compared to surgical smoke in which particulates had been removed, (PIII).

5.2 Tissue identification based on surgical smoke

The brain tumour sample classification for the full dataset consisted of seven tissue classes. The CA for these was 50%, where the classification accuracy is the mount of the correct predictions to the total number of predictions. For reference, the mean accuracy of a classifier that assigns a class randomly would be 14% in a seven-class setting. The results are presented in Table 6. When comparing only central nervous system metastases with meningiomas, the cross-validated CA was 74%. When samples with interfering Tissue-Tek tissue preservative were removed, the remaining five-class classification yielded a CA of 83%, demonstrating that Tissue-Tek was a major confounding factor. It penetrates the tissue and preserves it for morphological examination. However, it is likely that Tissue-Tek masks other chemical compounds in the electrosurgical smoke, thereby disturbing the DMS classifier. Notably, a binary classification with ten-fold cross-validation between meningioma and metastasis samples without Tissue-Tek produced a CA of 95%, with 87% sensitivity and 98% specificity. Where, the specificity is the proportion of true negative results to true negative and false positive results. (PII)

Table 6. Classification results and a confusing matrix for all seven tissue classes. Reprinted with permission from PII.

		Assigned class									
		Mening.	No sample	Met	PA	GBM	LGG	Control	Total	Sens.	Spec.
True class	Meningioma	63	0	22	2	33	1	0	121	52%	91%
	No sample	2	72	0	0	1	0	0	75	96%	99%
	Met	18	2	63	6	63	1	1	154	40%	77%
	PA	2	1	11	2	17	1	1	35	6%	98%
	GMB	27	0	75	3	144	5	3	257	56%	68%
	LGG	4	1	10	0	15	2	0	32	6%	99%
	Control	0	0	5	3	11	0	1	20	5%	99%

Met = metastasis; PA = pilocytic astrocytoma. Total classification accuracy was 50%. Mening. = meningioma, Met = metastasis, PA = pilocytic astrocytoma.

In practical clinical applications, the physician often has some assumption regarding the tumour diagnosis even before the surgery, based on imaging, the patient's age,

tumour location and other factors. Narrowing down the diagnostic alternatives improves the possibility of a correct classification result. In general, binary classification yields a significantly higher accuracy than multi-class classification. Table 6 presents the binary classifications of relevant tissue pairs. A particularly promising, 94% CA was obtained with low-grade glioma (LGG) versus control classification. The LGG group may have the greatest impact on survival benefit. Recognizing the LGG tissue border increases the survival expectancy because a more accurate resection and more extensive surgical resection is connected to a longer life expectancy (Sanai and Berger 2008). It is noteworthy to mention that LGG identification from a frozen section is particularly difficult. In Table 7, the positive predictive value (PPV) is the ratio of true positives to all positive results including false positives. Respectively, the negative predictive value (NPV) is the ratio of true negatives to all negative result including false negatives.

Table 7. Classification results of selected relevant binary classifications. Reprinted with permission from PII.

Comparison	N	CA	Sensit.	Specif.	PPV	NPV
Tumour (+) vs control (-)*	40	83%	78%	89%	87%	80%
Meningioma (+) vs met (-)	275	74%	71%	77%	70%	77%
LGG (+) grade vs GBM (-)	64	94%	88%	100%	100%	89%
PA (+) vs diffusively infiltrating glioma (-)	70	70%	77%	63%	68%	73%
LGG (+) vs control (-)	52	94%	97%	90%	94%	95%

Negative predictive value (NPV), positive predictive value (PPV) += positive, -= negative, Sensit. = sensitivity, Specif. = specificity

*five randomly selected tumour samples of every class and five control samples for a balanced set

A major limitation in the study was that samples were collected from only 29 patients, from whom a total of 694 specimens were analysed. However, the classifier performed well with meningiomas, which is in line with the fact that meningiomas are considered to be rather homogenous tumours, as opposed to metastases, gliomas and especially GMBs (Friedmann-Morvinski 2014). Further research is needed in an *in vivo* setting, where bipolar scissors, instead of a diathermy blade, should be used as

the sampling instrument, since they are a routine instrument for neurosurgeons. Also, the detection of the neurosurgical resection margin should be studied.

5.3 Transfer line characteristic

Delays were measured between the diathermy knife, filtration unit and the spectrometer. A total of 50 incisions were performed to obtain statistically stable results. The mean and median as well as the standard deviations of the delays measured in response to a smoke impulse are presented in Table 7. The mean time to sensor detection (TSD), 1.15 seconds, is the minimum time that the device could theoretically function in and the mean time to sensor peak (TSP), 2.35 seconds, is the delay producing the best signal strength. However, some additional delays, such as computational delay, are required for full smoke analysis, and these are fortunately clearly shorter.

Table 8. Numerical indicators of the system impulse response in milliseconds.

(in ms)	TSD	TSP	TSR	TFD	TFP	TFP-SP
mean	1150	2350	8600	380	880	1590
SD	300	370	2320	170	320	680
median	1090	2320	8200	340	820	1500

In this study, the median time to particle filter detection was 340 ms, which was less than half of the time from the incision to sensor detection, implicating that most of the delay is caused by the pneumatics of the prototype system rather than the surgical vacuum, which is, in practice, unoptimizable. In contrast to the first detection time, the molecules' residual time until the VOC concentration has decayed to 10% of its maximum was found to be long, with the median being 8.2 s.

Finally, we tested the impulse response of the system. The closest matching distribution function was Lévy distribution, which is characterized by a heavy tail. However, Lévy distribution still lacked heaviness in the tail when compared to the measured results.

5.3.1 Tube material characteristics

Desorption time distributions are presented in Figure 14. However, the small sample size and other limitations (described in detail in PII) limits the reliability of the figure. An additional study with temperature programmed desorption (TPD) would enhance the reliability of the results.

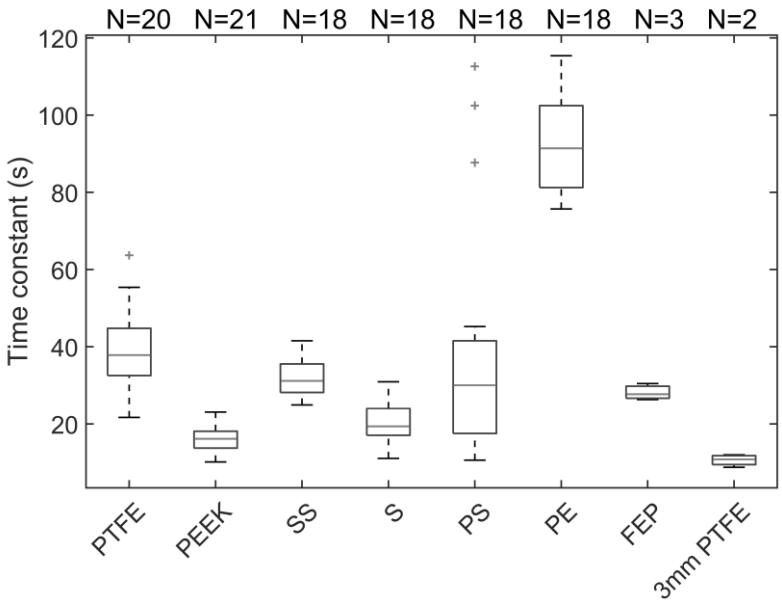

Figure 14. Recovery time constant distributions for different tube materials at room temperature. Tested tube materials were polyetheretherketone (PEEK), polytetrafluoroethylene (PTFE), fluorinated ethylene propylene (FEP), polyethylene (PE), steel 316 L (S), parylene C coated steel (PS), Silconert® coated steel (SS).

Shortest recovery times was obtained from small tube diameter PTFE tube. PEEK tube was next with 3.2 mm inner diameter. Uncoated steel tube was fastest from six mm inner diameter tubes. The parylene coating was partially detached during assemblies, which may explain outliers in Figure 14. PTFE-tube had longest recovery time from potential tube materials and PE had longest recovery time in overall. Removing the particles from the smoke reduced the signal levels by 13-47% and recovery times by 63-81%.

Tube material has a two-fold effect on the recovery from smoke exposure. First, compounds adsorb into the tube walls. The free surface energy of the tube material is a central parameter affecting the adhesion strength. A higher free surface energy causes higher adhesion strength. Free surface energy correlates with the inner bond strength of the substrate. Therefore, stronger materials, such as metals, generally have higher surface energies. However, another phenomenon affecting the recovery speed is tube permeation. Molecules diffuse into the tube substrate. Later, a portion of these molecules diffuses back into the sample stream. This is relevant with plastic tubes, but not with metal tubes. These two phenomena, permeation and surface bonding, could be mitigated with a non-permeable metal tube coated with a thin and soft material, such as parylene, that has low free surface energy. Another test was performed for PTFE tube material in different temperatures. An increase in temperature has a significant decreasing effect on the recovery time, as is seen in Figure 15.

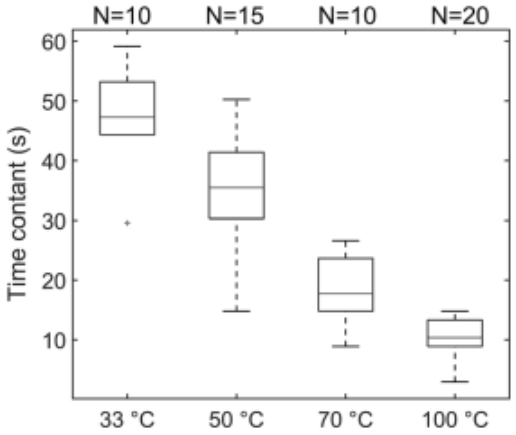

Figure 15. Recovery time constant of PTFE tubes in four temperatures. 30 cm long tubes were contaminated with surgical smoke. Reprinted from PIII.

A fast-response system should have minimum tube length and diameter to achieve maximal flow speed. The tubes should have minimal adsorption (in practice, minimal free surface energy) and minimal absorption. Notably, an increase in temperature increases permeation and, hence, absorption. At the same time, however, an increase in temperature also decreases adsorption. Therefore, we can assume that there is an optimal temperature for plastic tube materials, which absorb and adsorb

considerably. In contrast, metal tubes should benefit from a temperature increase with no permeation drawbacks at temperatures otherwise applicable for the instrumentation. A high temperature can, however, fragment sample molecules.

In addition, the exposure time is relevant with plastic tubes, since adsorption to a surface is faster than absorption into a bulk material. Similarly, desorption is faster from a surface than from within the bulk material. With plastics, long exposure times would increase recovery time more than with metal tubes.

Based on the present results, we suggest the following: 1) Tubes with a minimal length and diameter should be used. 2) Polyether ether ketone (PEEK) and fluoropolymers are suitable materials in low temperatures. High performance can be obtained with a high temperature and using metal tubes. In principle, an optimal tube would be a metal tube with a soft coating, but, in practice, an increase in temperature and the use of uncoated metal tubes can improve performance with lower costs.

5.3.2 Classification accuracy over recovery time and decaying signal

The results obtained in PIV regarding the relationship between recovery time and classification accuracy were surprising. The measurements consisted of binary randomized tissue incisions with the interval between the incisions being 2, 3, 5 or 11 seconds. The accuracies were 0.74, 0.8, 0,82 and 0.71 respectively. We concluded that the incision intervals did not reveal notable changes in classification accuracy. This is surprising, since the time for sensor recovery to less than 10% of the maximum signal was, on average, 8.6 seconds.

The data analysis capability to withstand carry-over is significant, as we considered a 2–3 s latency between incision and indication to be realistic for pneumatic systems, such as DMS or MS, since surgeons typically cut tissue at a speed of 5 –15 mm/s (Liboon, Funkhouser, and Terris 1997). Therefore, this latency is acceptable for the intended purpose of the analysis system.

In another test, we examined how the CA correlated with the impulse response of the system, as shown in Figure 16. Clearly, the best accuracy is obtained at the highest signal intensity. However, the CA decreased clearly more slowly than the signal strength. This indicates that there is a threshold level for correct classification rather than a straight correlation between signal intensity and classification accuracy.

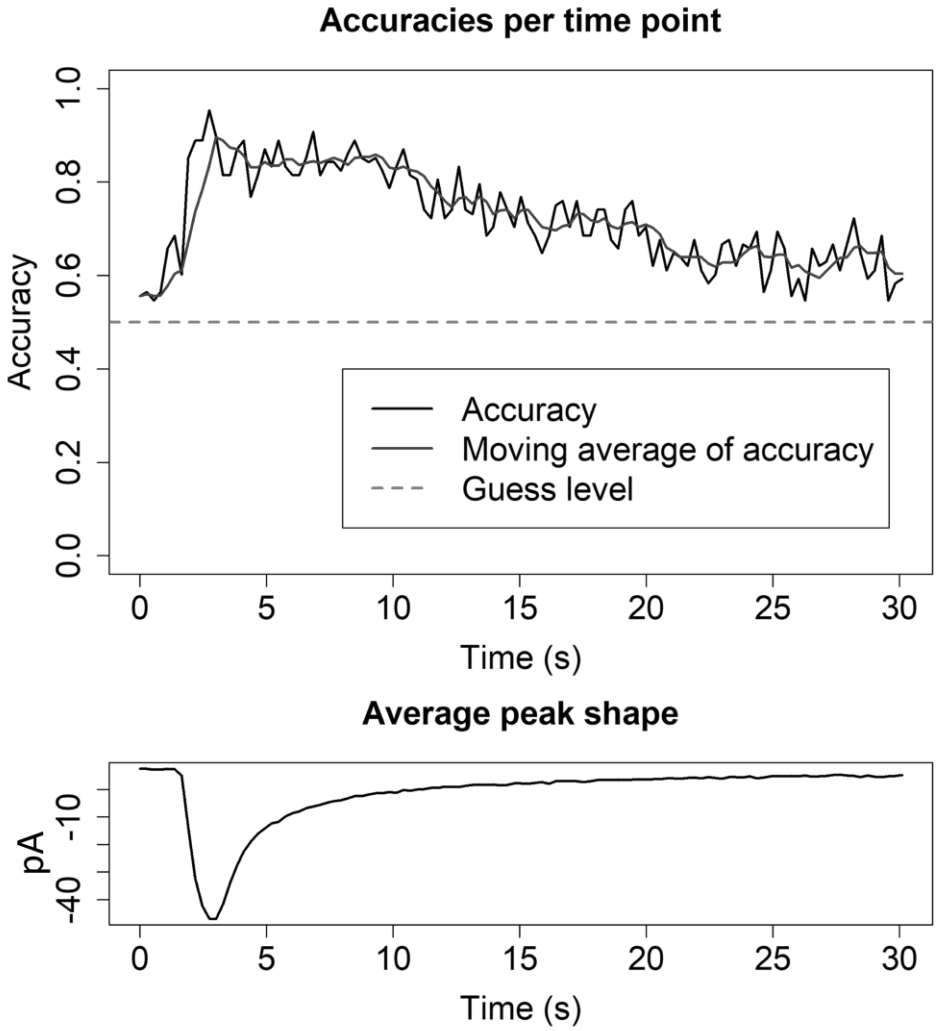

Figure 16. The classification accuracy of the impulse response as a function of the time from incision to performing the analysis. The decaying signal decreases the classification accuracy. An average peak shape with a 200 V separation voltage and 0.5 V compensation voltage is presented at the bottom. Reprinted from PIV.

6 CONCLUSIONS

A synthesis of the original research questions, literature survey and experimental studies is concluded in the following manner.

The first research question was formulated as: **What is the composition of surgical smoke?**

Surgical smoke consists of substances evaporated or burned off from cut tissue. The molecules are either in the gaseous phase or accumulated into particulates. The particulates are in a dynamic phase in which they constantly receive or evaporate molecules, depending on the surrounding environment, essentially on the partial pressure of the substances, which is highly dependent on the temperature.

This smoke is harmful to operating theatre personnel and should therefore be removed. The amount of smoke or the particles in it is strongly dependent on the type of the operated tissue. For instance, in our measurement, liver produced a 40 times higher particulate mass than did fat (PI).

The second research question was formulated as: **How should surgical smoke be analysed in order to obtain accurate tissue recognition?**

The gas-phase molecules and particles carry information on the cut tissue. These particles and molecules are in constant chemical reaction to their surroundings, mostly reacting to the molecules in the room air and with tube walls in case surgical smoke removal is used. The methods used for analysing this chemical information are sensitive to the same environmental factors as the chemical information itself. For instance, the DMS method is sensitive to humidity, temperature, pressure and other contaminants. In order to obtain undistorted information from the original surgical event, these factors must be under control. In addition, the smoke sampling causes a temporal delay. Especially, particulates stick onto tube walls and evaporate chemical signals from previous events, causing interference to the signal. The

dynamics of the particulate and gas molecule decay were found to be best described with Lévy distribution.

The third research question was formulated as: **How should surgical smoke be transported and modulated in order to obtain optimal tissue analysis?**

The tubing that transfers chemical information should be minimized and the flow speed maximized. The inner diameter of the tubing should be as small as possible. There are two good options for the tube materials. Polymers have a lower free surface energy, causing weaker interactions with molecules. However, polymers are porous and absorb molecules into the gaps in the polymer. Later, these molecules will be desorbed into the sample stream. Metal tubes do not absorb but have a higher free surface energy, which causes stronger bonding of the molecules to the surface than do polymers. This can be avoided by heating. However, heating increases absorption into the bulk material, which limits the benefits of heating polymer tubes.

Final conclusions

We were able to classify various brain cancer samples with clinically meaningful accuracy using DMS technology, thus demonstrating the possibilities of the method in medical use. However, real-life clinical applications would require more studies in varying environmental conditions, taking into account the device variances and the possibly higher heterogeneity of the patient material to secure robust performance in all situations.

With a robust predictive system design, some of the variance-induced challenges could be avoided. Similarly, by choosing the best available methods for each system function, patient safety should be maximized.

7 REFERENCES

Anttalainen, Anna, Meri Mäkelä, Pekka Kumpulainen, Antti Vehkaoja, Osmo Anttalainen, Niku Oksala, and Antti Roine. 2021. 'Predicting Lecithin Concentration from Differential Mobility Spectrometry Measurements with Linear Regression Models and Neural Networks'. *Talanta* 225: 121926.

Anttalainen, Osmo, Elie Lattouf, Tapio Kotiaho, and Gary Eiceman. 2021. 'Ion Density of Positive and Negative Ions at Ambient Pressure in Air at 12--136 Mm from 4.9 KV Soft x-Ray Source'. *Review of Scientific Instruments* 92 (5): 54104.

Anttalainen, Osmo, Jarosław Puton, Kaleva Peräkorpi, Edyta Budzyńska, Gary Eiceman, and Mika Sillanpää. 2018. 'Differential Mobility Spectrometers with Tuneable Separation Voltage--Theoretical Models and Experimental Findings'. *TrAC Trends in Analytical Chemistry* 105: 413–23.

Arevalo-Martinez, Damian L, Maya Beyer, Marita Krumbholz, Inga Piller, Annette Kock, Tobias Steinhoff, Arne Körtzinger, and Hermann W Bange. 2013. 'A New Method for Continuous Measurements of Oceanic and Atmospheric N 2 O, CO and CO 2: Performance of off-Axis Integrated Cavity Output Spectroscopy (OA-ICOS) Coupled to Non-Dispersive Infrared Detection (NDIR)'. *Ocean Science* 9 (6): 1071–87.

Asbach, C, T A J Kuhlbusch, and H Fissan. 2004. 'Development of an Electrostatic Partitioner for Highly Efficient Partitioning of Gas and Particles with Minimal Effect on the Gas Phase'. *Aerosol Science and Technology* 38 (4): 322–29.

Azordegan, Nazila, Virginia Fraser, Khuong Le, Lyn M Hillyer, David W L Ma, Gabor Fischer, and Mohammed H Moghadasian. 2013. 'Carcinogenesis Alters Fatty Acid Profile in Breast Tissue'. *Molecular and Cellular Biochemistry* 374 (1): 223–32.

Badger, Richard M. 1934. 'A Relation between Internuclear Distances and Bond Force Constants'. *The Journal of Chemical Physics* 2 (3): 128–31.

Balog, Júlia, László Sasi-Szabó, James Kinross, Matthew R Lewis, Laura J Muirhead, Kirill Veselkov, Reza Mirnezami, et al. 2013. 'Intraoperative Tissue Identification Using Rapid Evaporative Ionization Mass Spectrometry' 5 (194): 194ra93. https://doi.org/10.1126/SCITRANSLMED.3005623.

Barbosa, Arménio J M, Ana Rita Oliveira, and Ana C A Roque. 2018. 'Protein-and Peptide-Based Biosensors in Artificial Olfaction'. *Trends in Biotechnology* 36 (12): 1244–58.

Belan, Sergei, Itzhak Fouxon, and Gregory Falkovich. 2014. 'Localization-Delocalization Transitions in Turbophoresis of Inertial Particles'. *Physical Review Letters* 112 (23): 234502.

Blakeman, Kenion H, Craig A Cavanaugh, William M Gilliland Jr, and J Michael Ramsey. 2017. 'High Pressure Mass Spectrometry of Volatile Organic Compounds with Ambient Air Buffer Gas'. *Rapid Communications in Mass Spectrometry* 31 (1): 27–32.

Blakeman, Kenion H, Derek W Wolfe, Craig A Cavanaugh, and J Michael Ramsey. 2016. 'High Pressure Mass Spectrometry: The Generation of Mass Spectra at Operating Pressures Exceeding 1 Torr in a Microscale Cylindrical Ion Trap'. *Analytical Chemistry* 88 (10): 5378–84.

Bratu, AM, M Petrus, M Patachia, C Matei, C Popa, S Banita, and DC Dumitras. 2015. 'Quantitative Analysis of Laser Surgical Smoke: Targeted Study on Six Toxic Compounds'. *Romanian Journal of Physics* 60 (1): 215–27.

Brook, Robert D, Sanjay Rajagopalan, C Arden Pope 3rd, Jeffrey R Brook, Aruni Bhatnagar, Ana V Diez-Roux, Fernando Holguin, et al. 2010. 'American Heart Association Council on Epidemiology and Prevention, Council on the Kidney in Cardiovascular Disease, and Council on Nutrition, Physical Activity and Metabolism.' *Circulation* 121 (21): 2331–78.

Brown, Hannah Marie, Clint M Alfaro, Valentina Pirro, Mahua Dey, Eyas M Hattab, Aaron A Cohen-Gadol, and R Graham Cooks. 2021. 'Intraoperative Mass Spectrometry Platform for IDH Mutation Status Prediction, Glioma Diagnosis, and Estimation of Tumor Cell Infiltration'. *The Journal of Applied Laboratory Medicine* 6 (4): 902–16.

Broza, Yoav Y, Xi Zhou, Miaomiao Yuan, Danyao Qu, Youbing Zheng, Rotem Vishinkin, Muhammad Khatib, Weiwei Wu, and Hossam Haick. 2019. 'Disease Detection with Molecular Biomarkers: From Chemistry of Body

Fluids to Nature-Inspired Chemical Sensors'. *Chemical Reviews* 119 (22): 11761–817.

Calero, L, and T Brusis. 2003. 'Laryngeal Papillomatosis-First Recognition in Germany as an Occupational Disease in an Operating Room Nurse'. *Laryngo-Rhino-Otologie* 82 (11): 790–93.

Cardoso, Victor Gustavo Kelis, Guilherme Post Sabin, and Leandro Wang Hantao. 2022. 'Rapid Evaporative Ionization Mass Spectrometry (REIMS) Combined with Chemometrics for Real-Time Beer Analysis'. *Analytical Methods* 14 (15): 1540–46.

Chattopadhyay, Arnab, Andres Huertas, Andrew Rebeiro-Hargrave, Pak Lun Fung, Samu Varjonen, Tuomas Hieta, Sasu Tarkoma, and Tuukka Petäjä. 2022. 'Low-Cost Formaldehyde Sensor Evaluation and Calibration in a Controlled Environment'. *IEEE Sensors Journal* 22 (12): 11791–802.

DeBerardinis, Ralph J, and Navdeep S Chandel. 2016. 'Fundamentals of Cancer Metabolism'. *Science Advances* 2 (5): e1600200.

Do, Duong D. 1998. *Adsorption Analysis: Equilibria and Kinetics (with Cd Containing Computer MATLAB Programs)*. Vol. 2. World Scientific.

Dodds, James N, and Erin S Baker. 2019. 'Ion Mobility Spectrometry: Fundamental Concepts, Instrumentation, Applications, and the Road Ahead'. *Journal of the American Society for Mass Spectrometry* 30 (11): 2185–95.

Dutta, Dilip Kumar, and Indranil Dutta. 2016. 'The Harmonic Scalpel'. *The Journal of Obstetrics and Gynecology of India* 66 (3): 209–10.

Eiceman, Gary Alan, Zeev Karpas, and Herbert H Hill Jr. 2013. *Ion Mobility Spectrometry*. CRC press.

Elsayed, Elsayed A. 2012. 'Overview of Reliability Testing'. *IEEE Transactions on Reliability* 61 (2): 282–91.

Farsad, Nariman, Weisi Guo, and Andrew W Eckford. 2013. 'Tabletop Molecular Communication: Text Messages through Chemical Signals'. *PloS One* 8 (12): e82935.

Feider, Clara L, Rachel J DeHoog, Marta Sans, Jialing Zhang, Anna Krieger, and Livia S Eberlin. 2018. 'DESI Spray Stability in the Negative Ion Mode Is

Dependent on Relative Humidity'. *Journal of The American Society for Mass Spectrometry* 30 (2): 376–80.

Fennelly, Kevin P. 2020. 'Particle Sizes of Infectious Aerosols: Implications for Infection Control'. *The Lancet Respiratory Medicine* 8 (9): 914–24.

Fowler, Peter E, Jacob Zachary Pilgrim, Gyoung-il Lee, and Gary A Eiceman. 2020. 'Field Induced Fragmentation Spectra from Reactive Stage-Tandem Differential Mobility Spectrometry'. *Analyst*.

Friedmann-Morvinski, Dinorah. 2014. 'Glioblastoma Heterogeneity and Cancer Cell Plasticity'. *Critical Reviews™ in Oncogenesis* 19 (5).

Gamage, Radhya W, and Daniel E Austin. 2020. 'The Effects of Electrode Misalignments on the Performance of a Miniaturized Linear Wire Ion Trap Mass Spectrometer'. *International Journal of Mass Spectrometry* 453: 116344.

Gianella, Michele, and Markus W Sigrist. 2012. 'Chemical Analysis of Surgical Smoke by Infrared Laser Spectroscopy'. *Applied Physics B* 109: 485–96.

Giles, K, and D Gordon. 2010. 'A New Conjoined RF Ion Guide for Enhanced Ion Transmission'. In *Proc. 58th ASMS Conf. Mass Spectrometry and Allied Topics*.

Giles, Kevin, Steven D Pringle, Kenneth R Worthington, David Little, Jason L Wildgoose, and Robert H Bateman. 2004. 'Applications of a Travelling Wave-Based Radio-Frequency-Only Stacked Ring Ion Guide'. *Rapid Communications in Mass Spectrometry* 18 (20): 2401–14.

Greaves, John, and John Roboz. 2014. *Mass Spectrometry for the Novice*. CRC Press Boca Raton, FL.

Grinham, Rebecca, and Andrew Chew. 2017. 'A Review of Outgassing and Methods for Its Reduction'. *Applied Science and Convergence Technology* 26 (5): 95–109.

Guo, Qi, Lijuan Gao, Yanbing Zhai, and Wei Xu. 2018. 'Recent Developments of Miniature Ion Trap Mass Spectrometers'. *Chinese Chemical Letters* 29 (11): 1578–84.

Gurdak, Elzbieta, Felicia M Green, Paulina D Rakowska, Martin P Seah, Tara L Salter, and Ian S Gilmore. 2014. 'VAMAS Interlaboratory Study for Desorption Electrospray Ionization Mass Spectrometry (DESI MS) Intensity Repeatability and Constancy'. *Analytical Chemistry* 86 (19): 9603–11.

Haack, Alexander, Jeff Crouse, Femke-Jutta Schlüter, Thorsten Benter, and W Scott Hopkins. 2019. 'A First Principle Model of Differential Ion Mobility: The Effect of Ion-Solvent Clustering'. *Journal of The American Society for Mass Spectrometry* 30 (12): 2711–25.

Haapala, Ilkka, Anton Kondratev, Antti Roine, Meri Mäkelä, Anton Kontunen, Markus Karjalainen, Aki Laakso, et al. 2022. 'Method for the Intraoperative Detection of IDH Mutation in Gliomas with Differential Mobility Spectrometry'. *Current Oncology* 29 (5): 3252–58.

Hall, Adam B, Stephen L Coy, Amol Kafle, James Glick, Erkinjon Nazarov, and Paul Vouros. 2013. 'Extending the Dynamic Range of the Ion Trap by Differential Mobility Filtration'. *Journal of the American Society for Mass Spectrometry* 24 (9): 1428–36.

Henderson, Ben, Amir Khodabakhsh, Markus Metsälä, Irène Ventrillard, Florian M Schmidt, Daniele Romanini, Grant A D Ritchie, et al. 2018. 'Laser Spectroscopy for Breath Analysis: Towards Clinical Implementation'. *Applied Physics B* 124: 1–21.

Hierlemann, Andreas, and Ricardo Gutierrez-Osuna. 2008. 'Higher-Order Chemical Sensing'. *Chemical Reviews* 108 (2): 563–613.

Hinds, William C. 2012. *Aerosol Technology: Properties, Behavior, and Measurement of Airborne Particles*. John Wiley & Sons.

Ho, Emily, Keith Edmond, and David Peacock. 2002. 'Effect of Temperature and Pressure on Permeation, Ageing and Emissions of Elastomers'. *Sealing Technology* 2002 (10): 5–10.

Hodgkinson, Jane, and Ralph P Tatam. 2012. 'Optical Gas Sensing: A Review'. *Measurement Science and Technology* 24 (1): 12004.

Huang, Qingyu, Dayu Hu, Xiaofei Wang, Yahong Chen, Yan Wu, Lu Pan, Hongyu Li, et al. 2018. 'The Modification of Indoor PM2. 5 Exposure to Chronic Obstructive Pulmonary Disease in Chinese Elderly People: A Meet-in-Metabolite Analysis'. *Environment International* 121: 1243–52.

Huber, Ferdinand, Julian Berwanger, Svitlana Polesya, Sergiy Mankovsky, Hubert Ebert, and Franz J Giessibl. 2019. 'Chemical Bond Formation Showing a Transition from Physisorption to Chemisorption'. *Science* 366 (6462): 235–38.

Ieritano, Christian, Joshua Featherstone, Alexander Haack, Mircea Guna, J Larry Campbell, and W Scott Hopkins. 2020. 'How Hot Are Your Ions in Differential Mobility Spectrometry?' *Journal of the American Society for Mass Spectrometry* 31 (3): 582–93.

Intra, Panich, and Nakorn Tippayawong. 2008. 'An Overview of Differential Mobility Analyzers for Size Classification of Nanometer-Sized Aerosol Particles.' *Songklanakarin Journal of Science and Technology* 30 (2).

Jiao, Bin, Huimin Ye, Xinwei Liu, Jiexun Bu, Junhan Wu, Wenpeng Zhang, Yunfeng Zhang, and Zheng Ouyang. 2021. 'Handheld Mass Spectrometer with Intelligent Adaptability for On-Site and Point-of-Care Analysis'. *Analytical Chemistry* 93 (47): 15607–16.

Jones, Emrys A, Daniel Simon, Tamas Karancsi, Julia Balog, Steven D Pringle, and Zoltan Takats. 2019. 'Matrix Assisted Rapid Evaporative Ionization Mass Spectrometry'. *Analytical Chemistry* 91 (15): 9784–91.

Kim, Chuntae, Iruthayapandi Selestin Raja, Jong-Min Lee, Jong Ho Lee, Moon Sung Kang, Seok Hyun Lee, Jin-Woo Oh, and Dong-Wook Han. 2021. 'Recent Trends in Exhaled Breath Diagnosis Using an Artificial Olfactory System'. *Biosensors* 11 (9): 337.

Kontunen, Anton, Ulla Karhunen-Enckell, Markus Karjalainen, Anna Anttalainen, Pekka Kumpulainen, Leena Pitkänen, Osmo Anttalainen, Antti Vehkaoja, Niku Oksala, and Antti Roine. 2021. 'Tissue Identification from Surgical Smoke by Differential Mobility Spectrometry: An in Vivo Study'. *IEEE Access*, 1. https://doi.org/10.1109/ACCESS.2021.3136719.

Kumbhani, Sambhav R, Lisa M Wingen, Véronique Perraud, and Barbara J Finlayson-Pitts. 2017. 'A Cautionary Note on the Effects of Laboratory Air Contaminants on Ambient Ionization Mass Spectrometry Measurements'. *Rapid Communications in Mass Spectrometry* 31 (19): 1659–68.

Langmuir, Irving. 1916. 'The Constitution and Fundamental Properties of Solids and Liquids. Part I. Solids.' *Journal of the American Chemical Society* 38 (11): 2221–95.

Liboon, John, William Funkhouser, and David J Terris. 1997. 'A Comparison of Mucosal Incisions Made by Scalpel, CO2 Laser, Electrocautery, and Constant-Voltage Electrocautery'. *Otolaryngology--Head and Neck Surgery* 116 (3): 379–85.

Limchantra, Ice V, Yuman Fong, and Kurt A Melstrom. 2019. 'Surgical Smoke Exposure in Operating Room Personnel: A Review'. *JAMA Surgery* 154 (10): 960–67.

Ma, Jianfeng, Ting Li, Huiyao Chen, Chengde Wang, Haixing Wang, and Qun Li. 2021. 'Lipidomic Analysis and Diagnosis of Glioblastoma Multiforme with Rapid Evaporative Ionization Mass Spectrometry'. *Electrophoresis*.

Marjamäki, Marko, Jorma Keskinen, Da-Ren Chen, and David Y H Pui. 2000. 'Performance Evaluation of the Electrical Low-Pressure Impactor (ELPI)'. *Journal of Aerosol Science* 31 (2): 249–61.

Mason, Sam, Eftychios Manoli, Liam Poynter, James Alexander, Petra Paizs, Afeez Adebesin, Robert Goldin, Ara Darzi, Zoltan Takats, and James Kinross. 2020. 'Mass Spectrometry Transanal Minimally Invasive Surgery (MS-TAMIS) to Promote Organ Preservation in Rectal Cancer'. *Surgical Endoscopy* 34 (8): 3618–25.

Massarweh, Nader N., Ned Cosgriff, and Douglas P. Slakey. 2006. 'Electrosurgery: History, Principles, and Current and Future Uses'. *Journal of the American College of Surgeons*. https://doi.org/10.1016/j.jamcollsurg.2005.11.017.

McGuinn, Laura A, Alexandra Schneider, Robert W McGarrah, Cavin Ward-Caviness, Lucas M Neas, Qian Di, Joel Schwartz, et al. 2019. 'Association of Long-Term PM2. 5 Exposure with Traditional and Novel Lipid Measures Related to Cardiovascular Disease Risk'. *Environment International* 122: 193–200.

Menlyadiev, Marlen R, and Gary A Eiceman. 2014. 'Tandem Differential Mobility Spectrometry in Purified Air for High-Speed Selective Vapor Detection'. *Analytical Chemistry* 86 (5): 2395–2402.

Mitchell, Gerald D. 2000. 'A Review of Permeation Tubes and Permeators'. *Separation and Purification Methods* 29 (1): 119–28.

Moser, Emily, and Michael McCulloch. 2010. 'Canine Scent Detection of Human Cancers: A Review of Methods and Accuracy'. *Journal of Veterinary Behavior* 5 (3): 145–52.

Munro, Malcolm G. 2012. 'Fundamentals of Electrosurgery Part I: Principles of Radiofrequency Energy for Surgery'. In *The SAGES Manual on the*

Fundamental Use of Surgical Energy (FUSE), 15–59. https://doi.org/10.1007/978-1-4614-2074-3_2.

Nakhleh, Morad K., Haitham Amal, Raneen Jeries, Yoav Y. Broza, Manal Aboud, Alaa Gharra, Hodaya Ivgi, et al. 2017. 'Diagnosis and Classification of 17 Diseases from 1404 Subjects *via* Pattern Analysis of Exhaled Molecules'. *ACS Nano* 11 (1): 112–25. https://doi.org/10.1021/acsnano.6b04930.

Newsome, G Asher, Luke K Ackerman, and Kevin J Johnson. 2014. 'Humidity Affects Relative Ion Abundance in Direct Analysis in Real Time Mass Spectrometry of Hexamethylene Triperoxide Diamine'. *Analytical Chemistry* 86 (24): 11977–80.

Newsome, G Asher, Luke K Ackerman, and Kevin J Johnson. 2015. 'Humidity Effects on Fragmentation in Plasma-Based Ambient Ionization Sources'. *Journal of The American Society for Mass Spectrometry* 27 (1): 135–43.

O'Daly, Brendan J, Edmund Morris, Graham P Gavin, John M O'Byrne, and Garrett B McGuinness. 2008. 'High-Power Low-Frequency Ultrasound: A Review of Tissue Dissection and Ablation in Medicine and Surgery'. *Journal of Materials Processing Technology* 200 (1–3): 38–58.

O'Dowd, Adrian. 2010. 'Long Term Cancer Survival Rates Double in England and Wales in Past 40 Years'. *BMJ: British Medical Journal (Online)* 341.

Ogrinc, Nina, Philippe Saudemont, Zoltan Takats, Michel Salzet, and Isabelle Fournier. 2021. 'Cancer Surgery 2.0: Guidance by Real-Time Molecular Technologies'. *Trends in Molecular Medicine*.

Oliveira, Rafael Furlan de, Verónica Montes-García, Artur Ciesielski, and Paolo Samorí. 2021. 'Harnessing Selectivity in Chemical Sensing via Supramolecular Interactions: From Functionalization of Nanomaterials to Device Applications'. *Materials Horizons* 8 (10): 2685–2708.

Ouyang, Zheng, Guangxiang Wu, Yishu Song, Hongyan Li, Wolfgang R Plass, and R Graham Cooks. 2004. 'Rectilinear Ion Trap: Concepts, Calculations, and Analytical Performance of a New Mass Analyzer'. *Analytical Chemistry* 76 (16): 4595–4605.

Palanker, Daniel, Alexander Vankov, and Pradeep Jayaraman. 2008. 'On Mechanisms of Interaction in Electrosurgery'. *New Journal of Physics* 10 (12): 123022.

Pane, Josep, Reynold D C Francisca, Katia M C Verhamme, Marcia Orozco, Hilde Viroux, Irene Rebollo, and Miriam C J M Sturkenboom. 2019. 'EU Postmarket Surveillance Plans for Medical Devices'. *Pharmacoepidemiology and Drug Safety* 28 (9): 1155–65.

Pillinger, S. H., L. Delbridge, and D. R. Lewis. 2003. 'Randomized Clinical Trial of Suctionversus Standard Clearance of the Diathermy Plume'. *British Journal of Surgery* 90 (9): 1068–71. https://doi.org/10.1002/bjs.4214.

Pirro, Valentina, Clint M Alfaro, Alan K Jarmusch, Eyas M Hattab, Aaron A Cohen-Gadol, and R Graham Cooks. 2017. 'Intraoperative Assessment of Tumor Margins during Glioma Resection by Desorption Electrospray Ionization-Mass Spectrometry'. *Proceedings of the National Academy of Sciences* 114 (26): 6700–6705.

Pirrone, Federica, and Mariangela Albertini. 2017. 'Olfactory Detection of Cancer by Trained Sniffer Dogs: A Systematic Review of the Literature'. *Journal of Veterinary Behavior* 19: 105–17.

Pu, Fan, Clint M Alfaro, Valentina Pirro, Zhuoer Xie, Zheng Ouyang, and R Graham Cooks. 2019. 'Rapid Determination of Isocitrate Dehydrogenase Mutation Status of Human Gliomas by Extraction Nanoelectrospray Using a Miniature Mass Spectrometer'. *Analytical and Bioanalytical Chemistry* 411 (8): 1503–8.

Puzio-Kuter, Anna M. 2011. 'The Role of P53 in Metabolic Regulation'. *Genes & Cancer* 2 (4): 385–91.

Reznik, Ed, Augustin Luna, Bülent Arman Aksoy, Eric Minwei Liu, Konnor La, Irina Ostrovnaya, Chad J Creighton, A Ari Hakimi, and Chris Sander. 2018. 'A Landscape of Metabolic Variation across Tumor Types'. *Cell Systems* 6 (3): 301–13.

Roberts, Keith, Bruce Alberts, Alexander Johnson, Peter Walter, and Tim Hunt. 2002. 'Molecular Biology of the Cell'. *New York: Garland Science.*

Roine, Antti, Markus Karjalainen, Niku Oksala, Anton Kontunen, and Sampo Saari. 2021. 'Method and Apparatus for Analyzing Biological Samples'. Google Patents.

Ruskin, Keith J, and Dirk Hueske-Kraus. 2015. 'Alarm Fatigue: Impacts on Patient Safety'. *Current Opinion in Anesthesiology* 28 (6): 685–90.

Safaei, Zahra, Timothy J Willy, Gary A Eiceman, John A Stone, and Mika Sillanpää. 2019. 'Quantitative Response in Ion Mobility Spectrometry with Atmospheric Pressure Chemical Ionization in Positive Polarity as a Function of Moisture and Temperature'. *Analytica Chimica Acta* 1092: 144–50.

Sanai, Nader, and Mitchel S Berger. 2008. 'Glioma Extent of Resection and Its Impact on Patient Outcome'. *Neurosurgery* 62 (4): 753–66.

Sankaranarayanan, Ganesh, Rajeswara R Resapu, Daniel B Jones, Steven Schwaitzberg, and Suvranu De. 2013. 'Common Uses and Cited Complications of Energy in Surgery'. *Surgical Endoscopy* 27 (9): 3056–72.

Schäfer, Karl-Christian, Júlia Dénes, Katalin Albrecht, Tamás Szaniszló, Júlia Balog, Réka Skoumal, Mária Katona, Miklós Tóth, Lajos Balogh, and Zoltán Takáts. 2009. 'In Vivo, in Situ Tissue Analysis Using Rapid Evaporative Ionization Mass Spectrometry'. *Angewandte Chemie International Edition* 48 (44): 8240–42.

Schneider, Bradley B, Thomas R Covey, Stephen L Coy, Evgeny V Krylov, and Erkinjon G Nazarov. 2010. 'Control of Chemical Effects in the Separation Process of a Differential Mobility Mass Spectrometer System'. *European Journal of Mass Spectrometry* 16 (1): 57–71.

Schwartz, Laurent, Claudiu T Supuran, and Khalid O Alfarouk. 2017. 'The Warburg Effect and the Hallmarks of Cancer'. *Anti-Cancer Agents in Medicinal Chemistry (Formerly Current Medicinal Chemistry-Anti-Cancer Agents)* 17 (2): 164–70.

Song, Yee Jiun, Wendy Tobagus, Jeff Raymakers, and Armando Fox. 2004. 'Is MTTR More Important Than MTTF For Improving User-Perceived Availability?' *Computer Science Department, Stanford University*.

St John, Edward R, Julia Balog, James S McKenzie, Merja Rossi, April Covington, Laura Muirhead, Zsolt Bodai, et al. 2017. 'Rapid Evaporative Ionisation Mass Spectrometry of Electrosurgical Vapours for the Identification of Breast Pathology: Towards an Intelligent Knife for Breast Cancer Surgery'. *Breast Cancer Research* 19 (1): 1–14.

Taghipour, Sharareh, Dragan Banjevic, and Andrew K S Jardine. 2011. 'Reliability Analysis of Maintenance Data for Complex Medical Devices'. *Quality and Reliability Engineering International* 27 (1): 71–84.

Takats, Zoltan, Justin M Wiseman, Bogdan Gologan, and R Graham Cooks. 2004. 'Mass Spectrometry Sampling under Ambient Conditions with Desorption Electrospray Ionization'. *Science* 306 (5695): 471–73.

Tian, Yuan, Jessica Higgs, Ailin Li, Brandon Barney, and Daniel E Austin. 2014. 'How Far Can Ion Trap Miniaturization Go? Parameter Scaling and Space-Charge Limits for Very Small Cylindrical Ion Traps'. *Journal of Mass Spectrometry* 49 (3): 233–40.

Tzafetas, Menelaos, Anita Mitra, Maria Paraskevaidi, Zsolt Bodai, Ilkka Kalliala, Sarah Bowden, Konstantinos Lathouras, et al. 2020. 'The Intelligent Knife (IKnife) and Its Intraoperative Diagnostic Advantage for the Treatment of Cervical Disease'. *Proceedings of the National Academy of Sciences* 117 (13): 7338–46.

Uhlén, Mathias, Linn Fagerberg, Björn M Hallström, Cecilia Lindskog, Per Oksvold, Adil Mardinoglu, Åsa Sivertsson, et al. 2015. 'Tissue-Based Map of the Human Proteome'. *Science* 347 (6220).

Utriainen, Mikko, Esko Kärpänoja, and Heikki Paakkanen. 2003. 'Combining Miniaturized Ion Mobility Spectrometer and Metal Oxide Gas Sensor for the Fast Detection of Toxic Chemical Vapors'. *Sensors and Actuators B: Chemical* 93 (1–3): 17–24.

Virtanen, Annele, Marko Marjamäki, Jyrki Ristimäki, and Jorma Keskinen. 2001. 'Fine Particle Losses in Electrical Low-Pressure Impactor'. *Journal of Aerosol Science* 32 (3): 389–401.

Wang, Hong-Kai, Fei Mo, Chun-Guang Ma, Bo Dai, Guo-Hai Shi, Yao Zhu, Hai-Liang Zhang, and Ding-Wei Ye. 2015. 'Evaluation of Fine Particles in Surgical Smoke from an Urologist's Operating Room by Time and by Distance'. *International Urology and Nephrology* 47 (10): 1671–78. https://doi.org/10.1007/s11255-015-1080-3.

Waraksa, Emilia, Urszula Perycz, Jacek Namieśnik, Mika Sillanpää, Tomasz Dymerski, Marzena Wójtowicz, and Jarosław Puton. 2016. 'Dopants and Gas Modifiers in Ion Mobility Spectrometry'. *TrAC Trends in Analytical Chemistry* 82: 237–49.

Warburg, Otto. 1956. 'On the Origin of Cancer Cells'. *Science* 123 (3191): 309–14.

Wilmoth, Richard Gordon. 1973. 'Measurement of Surface Stay Times for Physical Adsorption of Gases.'

Woodard, H Q, and D R White. 1986. 'The Composition of Body Tissues'. *The British Journal of Radiology* 59 (708): 1209–18.

Zhang, Feng, and Guangwei Du. 2012. 'Dysregulated Lipid Metabolism in Cancer'. *World Journal of Biological Chemistry* 3 (8): 167.

PUBLICATION I

The characterization of surgical smoke from various tissues and its implications for occupational safety

Markus Karjalainen, Anton Kontunen, Sampo Saari, Topi Rönkkö, Jukka Lekkala, Antti Roine, Niku Oksala

PLoS One. 2018 Apr 12;13(4):e0195274.

doi: 10.1371/journal.pone.0195274. eCollection 2018.

RESEARCH ARTICLE

The characterization of surgical smoke from various tissues and its implications for occupational safety

Markus Karjalainen[1]*, Anton Kontunen[1], Sampo Saari[2], Topi Rönkkö[2], Jukka Lekkala[1], Antti Roine[3☯], Niku Oksala[4☯]

1 BioMediTech Institute and Faculty of Biomedical Sciences and Engineering, Tampere University of Technology, Tampere, Finland, **2** Aerosol Physics, Faculty of Natural Sciences, Tampere University of Technology, Tampere, Finland, **3** Department of Surgery, Hatanpää Hospital, Tampere, Tampere, Finland, **4** Division of Vascular Surgery, Tampere University Hospital and Faculty of Medicine and Life Sciences, University of Tampere, Tampere, Finland

☯ These authors contributed equally to this work.
* markus.karjalainen@tut.fi

Citation: Karjalainen M, Kontunen A, Saari S, Rönkkö T, Lekkala J, Roine A, et al. (2018) The characterization of surgical smoke from various tissues and its implications for occupational safety. PLoS ONE 13(4): e0195274. https://doi.org/10.1371/journal.pone.0195274

Editor: Sachiko Matsuzaki, CHU Clermont-Ferrand, FRANCE

Received: September 11, 2017

Accepted: March 19, 2018

Published: April 12, 2018

Data Availability Statement: All relevant data are within the paper and its Supporting Information files.

Funding: This study was supported by grants from following foundations: Finnish Foundation for Technology Promotion (TES) to M.K., Tampereen Tuberkuloosisäätiö (Tampere Tuberculosis Foundation), Emil Aaltonen foundation, and Pirkanmaan sairaanhoitopiiri (PSHP) grants 9s045, 151B03, 9T044, 9U042, 150618, and 9V044 to N. O., which were used partially for salaries for

Abstract

Electrosurgery produces surgical smoke. Different tissues produce different quantities and types of smoke, so we studied the particle characteristics of this surgical smoke in order to analyze the implications for the occupational health of the operation room personnel. We estimated the deposition of particulate matter (PM) from surgical smoke on the respiratory tract of operation room personnel using clinically relevant tissues from Finnish landrace porcine tissues including skeletal muscle, liver, subcutaneous fat, renal pelvis, renal cortex, lung, bronchus, cerebral gray and white matter, and skin. In order to standardize the electrosurgical cuts and smoke concentrations, we built a customized computer-controlled platform. The smoke particles were analyzed with an electrical low pressure impactor (ELPI), which measures the concentration and aerodynamic size distribution of particles with a diameter between 7 nm and 10 μm. There were significant differences in the mass concentration and size distribution of the surgical smoke particles depending on the electrocauterized tissue. Of the various tissues tested, liver yielded the highest number of particles. In order to better estimate the health hazard, we propose that the tissues can be divided into three distinct classes according to their surgical smoke production: 1) high-PM tissue for liver; 2) medium-PM tissues for renal cortex, renal pelvis, and skeletal muscle; and 3) low-PM tissues for skin, gray matter, white matter, bronchus, and subcutaneous fat.

Introduction

Electrosurgery is an essential tool in a surgeon's repertoire and is now used in almost every surgical procedure. It is used both to cut tissue, and to control bleeding by coagulating the blood vessels. The procedure involves administering a high-frequency electric current through the target tissue, causing its temperature to increase [1]. The heating effect of the surgical

authors M.K. and A.K. The funders had no role in study design, data collection and analysis, decision to publish, or preparation of the manuscript. The specific roles of these authors are articulated in the 'author contributions' section. Olfactomics Ltd did not provide any funding for the study and did not play any role in the study design.

Competing interests: Authors Markus Karjalainen, Jukka Lekkala, Antti Roine and Niku Oksala are shareholders of Olfactomics Ltd, a company developing applications for eNose technology. This does not alter our adherence to PLOS ONE policies on sharing data and materials.

instrument used for the procedure is controlled by the waveform of the current. A low-voltage, high-frequency current causes a rapid increase in temperature, causing the tissue to evaporate rapidly; essentially cutting the tissue. A high-voltage, low-frequency current results in a more gradual heating effect that denatures the proteins in the tissue, resulting in the coagulation and occlusion of the affected blood vessels [2]. In modern electrosurgical procedures, high-frequency "cut" and low-frequency "coag" modes are interweaved to achieve a clinically optimal combination of cutting and coagulation. It is the evaporation of the tissue that produces the plume of smoke, herein referred to as "surgical smoke" (SS).

SS causes technical, physical, and occupational health problems. One obvious challenge is the visual obfuscation that occurs, particularly in laparoscopic surgery. SS has also been shown to contain living bacteria [3] and viruses [4], thus exposing surgical staff to the risk of infection. In addition, exposure to aerosol particles is associated with an increased risk of respiratory diseases and strokes [5–10]. Some of the harmful effects are mediated by carcinogenic volatile molecules such as acrylonitrile (a precursor of cyanide) and carbon monoxide [11]. Other health hazards are caused by airborne particles, especially those with a diameter at or below 2.5 μm ($PM_{2.5}$), as these are known to have long-term negative health effects. Such particles are able to penetrate the defense mechanisms of the upper respiratory tract and enter the alveoli, as well as systemic circulation. The deposition of inhaled particles has been documented in the brain, liver, heart and kidneys [12–14]. The standard surgical mask alone does not protect the wearer from SS due to leakages around the mask and the filtration efficiency of small particles [15,16]. Even though the risks of SS are acknowledged, smoke evacuation units are not yet routinely used in many healthcare centers [17,18].

There has been little research in the literature on the effects exposure to SS has on operation room personnel during various clinical procedures. Although one study [18] has provided evidence of particle production during a specific surgical procedure, the procedures followed for electrosurgery vary from surgeon to surgeon. To our knowledge, there is no data available on the composition and levels of the particles in SS from different tissues with standardized electrosurgery. Therefore, our goal was to analyze the particle composition of SS from various types of landrace porcine tissues during standard electrosurgical procedures in order to estimate the potential lung depositions of these particles, and their implications for the health of the surgical personnel in the operating room.

Materials and methods

Particle analyzer

We used an electrical low pressure impactor (ELPI, Dekati Inc., Finland) [19] with a filter stage [20] and an additional impactor stage [21] for real-time particle number, mass, and size distribution measurements. The ELPI measures the concentration of all the aerodynamic particles with a diameter between 7 nm and 10 μm. We calculated the particle mass distribution from the ELPI number distribution using standard water density for the particles (1 g/cm^3). This approximation in particle mass calculations from ELPI data typically gives correct results [22]. Because of the high particle concentration, we first diluted the smoke sample using an ejector type diluter (Dekati Diluter DI-1000, Dekati Inc.) with a 1:8 dilution ratio, and a second dilution step was performed by mixing 8.5 l/min pure air with 2 l/min sample flow from the Dekati Diluter. Therefore, the total dilution ratio was 1:45.

Testing platform

In order to control the smoke production, we standardized the electrosurgical cuts (i.e. length, depth and duration of the cut) with a custom-made computer-controlled platform, a

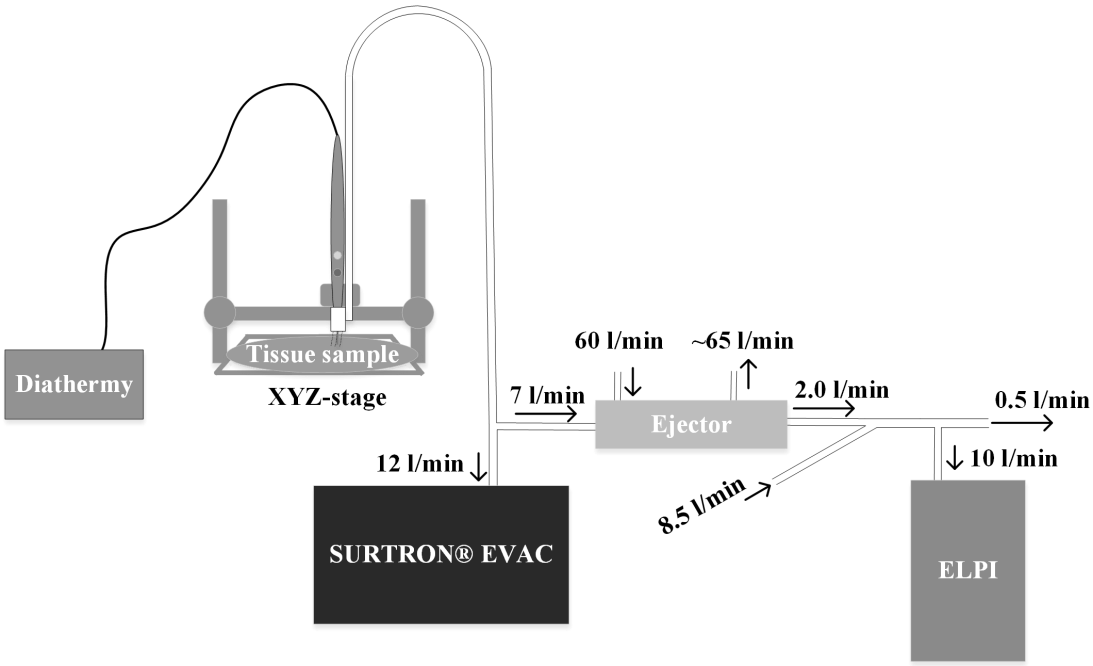

Fig 1. The measurement system.

https://doi.org/10.1371/journal.pone.0195274.g001

schematic diagram of which is presented in Fig 1. In the system, a diathermy knife was moved with an automated xyz-stage and the measured tissue sample was placed on a custom-built ground electrode. We used conductive tubes (Tygon, Saint-Gobain, France) for aerosol sampling to minimize the electrical losses of the particles. The tubes were connected to a commercially available smoke evacuator (Surtron Evac, Quirumed, Spain). The evacuator power was set at five (out of nine), which equals a suction of 12 l/min. We measured the flow settings with a commercial flow calibrator (Gilian Gilibrator 2, Sensidyne, Germany). We collected the smoke at 2 cm from the diathermy tip, so that a high proportion of the smoke was captured. We conducted the measurements in a laboratory located in the faculty of Biomedical Sciences and Engineering at Tampere University of Technology. During the study, the testing platform was located inside a fume hood in order to prevent the measurement laboratory being contaminated by the smoke.

Testing platform evaluation with a weight scale

We tested tissue weight loss during diathermal cutting with a regular weighing scales (XR 205SM-DR, Precisa, Switzerland). We used a cutting time of 7 seconds, and the mean weight loss of liver during the nine tests was 41 (±12) mg, which suggests an evaporation speed of 5.9 (±1.2) mm^3/s, assuming a unit mass of 1 g/cm^3. In a surgical evacuator stream of 12 l/min, this would indicate that there could be a maximum mass concentration of 29 g/m^3 of aerosol particles, discounting any losses. According to the ELPI measurements, the calculated total mass concentration of aerosol particles from the liver was 9.1 (±4.2) g/m^3, which would indicate a

loss of 20 (±9.2) g/m^3. This indicates significant losses from the evaporated tissue mass into the measured aerosol mass. The diathermy knife and the head of the suction tube collected a noticeable amount of evaporated tissue matter, indicating that some of the evaporated mass is deposited near the surgical event. Additional losses in concentration, which are not detectable in the ELPI measurements, could be due to the particulate mass vaporizing into gaseous molecules. The diathermy smoke may contain up to 95% water [23], although in our experiment the amount of particulate-gas in the evaporated water was undefined.

Diathermy device

We used a commercially available electrosurgery unit (Itkacut 350MB, Innokas Medical, Finland) set at a nominal 120 W power. Such a high power level was used to avoid the sample sticking to the diathermy tip. We used direct cut settings at a cutting frequency of 450 kHz. We made a flat, steel custom-ground electrode (19 x 19 cm) for the robot stage, and measured the cutting voltage at slightly under 800 V peak-to-peak.

Samples

The test materials were fresh, (unfrozen) Finnish landrace porcine tissues, purchased from a local slaughterhouse (Paijan Tilateurastamo, Urjala, Finland). The smoke from ten different tissue types was measured: skeletal muscle, liver, subcutaneous fat, renal pelvis, renal cortex, lung, bronchus, cerebral gray and white matter, and skin, all taken from the same animal. We performed the sampling with the automated xyz-stage to ensure that the cuts were all the same size. A typical cutting pattern is presented in Fig 2. The numbers and dark lines in the Fig 2 show the 10 mm spacing in the ground electrode. Each electrosurgical cut was 5 mm in length, and we took ten test samples from every tissue type. The 2.4 mm-wide blade (HF 9805–24 Hebu medical, Germany) had a sharp tip, and we aimed for 4 mm deep-cuts, although these varied slightly due to variations in the height of the tissue.

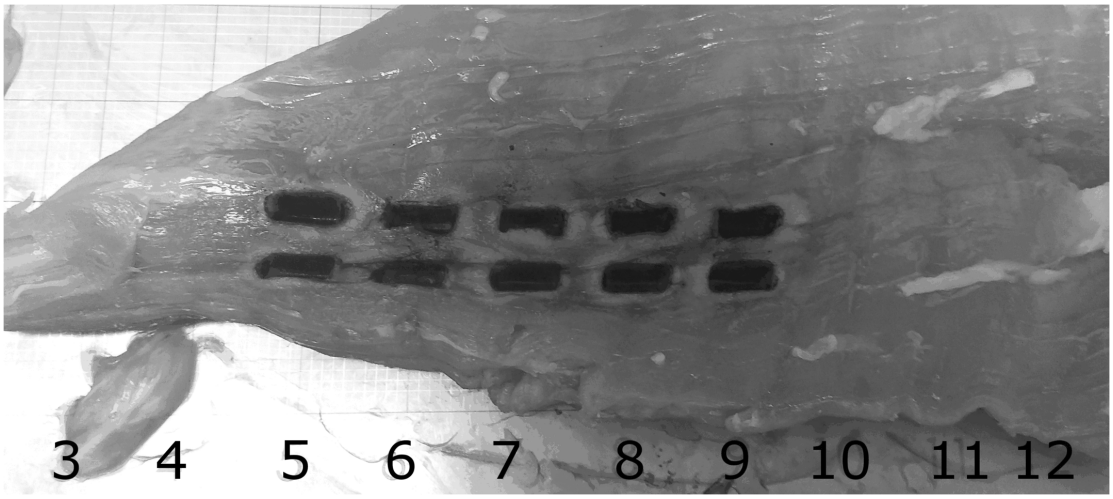

Fig 2. Representative image of a pig skeletal muscle sample after being exposed to the ten sample burns.

https://doi.org/10.1371/journal.pone.0195274.g002

Particle deposition model

Only a certain proportion of the emitted particles will be deposited in the respiratory tract, and so we calculated the level of deposition with models used by the International Commission on Radiological Protection (ICRP, 1994) [15]. We estimated the airway deposition fractions for the upper airways (UA), the bronchial tube (BT) and the alveoli (AL) from the measured aerosol particle mass distributions. We calculated the particulate matter (PM) depositions from these distributions using a unit density of 1 g/cm^3. The toxicity of atmospheric aerosols is commonly calculated from the PM values, which are typically PM_{10}, $PM_{2.5}$, and PM_1 for particulate total mass for particles with diameters smaller than 10 μm, 2.5 μm, and 1 μm, respectively.

The sample size was relatively small for statistical evaluation of the data, having only ten particle measurements per tissue. This small sample size was necessary in order to maintain the heterogeneity of the tissues, which limited their physical size. For example, although we had plenty of excess liver tissue, which would have been enough for several additional measurements, there was only enough macroscopically homogenous tissue area from certain tissues, such as the gray and white matter, for ten electrosurgical cuts if all the samples were to be taken from a single animal.

We performed a two-sample analysis with a confidence interval (CI) of 99% between the mass distributions of every different tissue. We subjected the sample groups to the Shapiro-Wilk normality test individually. The test indicated non-normality within the sample groups and thus a non-parametric method was chosen to validate the statistical difference between the levels of various tissue SS. Since all the tissues came from the same animal, the Mann-Whitney U test was used for the analysis.

An inverse spherical model

We evaluated the SS hazard for OR personnel with an inverse spherical model [24], in which the smoke intensity decreases inversely to the square of the distance from the source. Since we used an unusually high power for the surgical diathermy (120 W), we made a linear assumption for the smoke that would be produced with 40 W, which is the most common power limit in surgical operations. This linear assumption is in line with previous results in the literature [25]. In our model, we also used smoke evacuation efficiencies reported in the literature for integrated and general-purpose evacuation. In an integrated smoke evacuator, the smoke suction is integrated with the electric scalpel, which produces a high suction efficiency of 88% [26]. A general purpose surgical suction is commonly a hand-help pump unit, used for collecting blood and other liquids, which is not optimized to remove SS. The smoke suction efficiency of the general purpose evacuation is approximately 50% [24].

Results

The particulate number distributions of each tissue type are presented in Fig 3A, while Fig 3B shows the mass distributions. The curves in the Fig 3 are the medians from ten tests. The results of each individual test can be found in S1 Dataset and S1 File. Based on the corresponding particle number and mass distributions (Fig 3), three tissue type groups can be distinguished: high-PM tissues, medium-PM tissues, and low-PM tissues. The mass distributions varied significantly between the tissue types and the particle sizes, so logarithmic distribution axes were used. Furthermore, due to the diffusional losses of the smallest particles in the ELPI stages, the accuracy of the presented PM values increases as a function of decreasing particle size.

The majority of mass in the smoke is explained by the large particles, as can be seen from the curve trends in Fig 3B. In contrast, the particle number concentration is highest in the

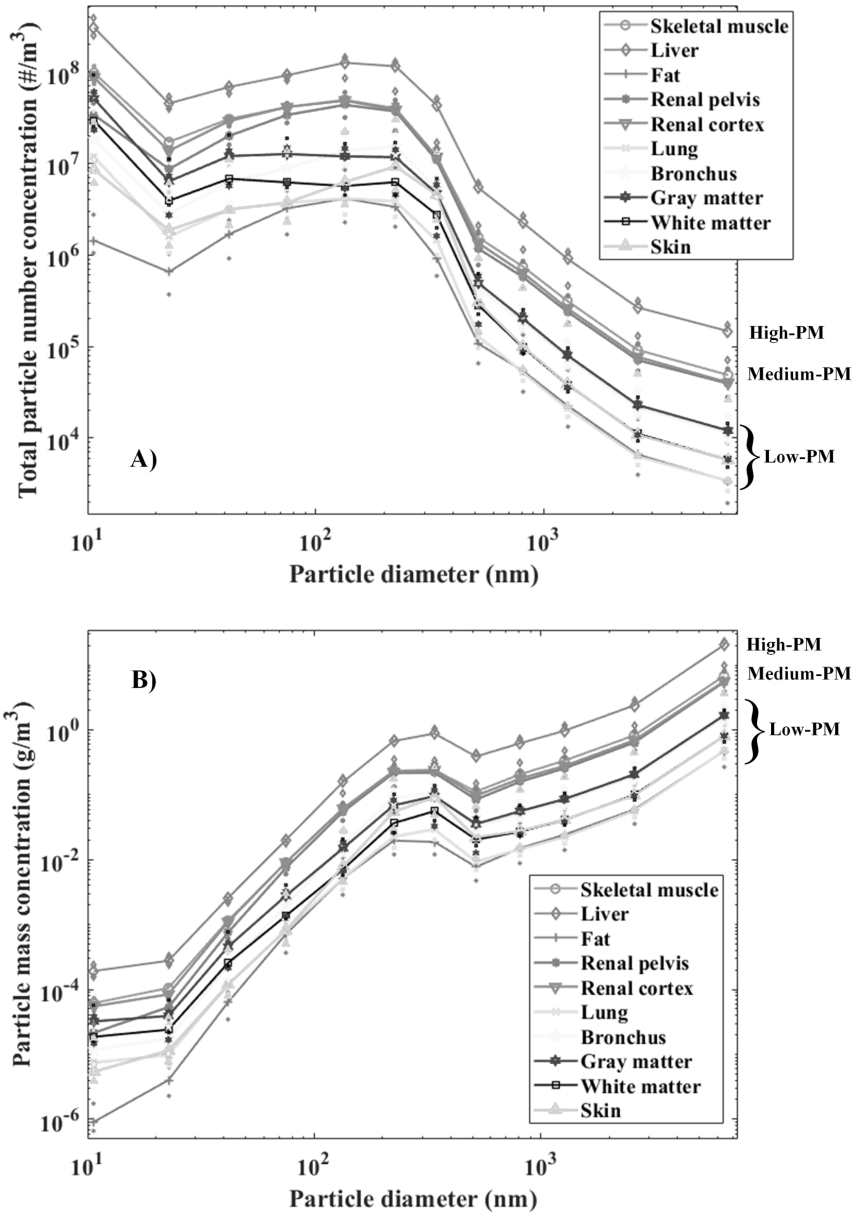

Fig 3. Median particle number (A) and mass (B) concentrations of different tissue types, produced with the diathermy knife. The particulate concentrations form three groups: high-PM, medium-PM, and low-PM.

https://doi.org/10.1371/journal.pone.0195274.g003

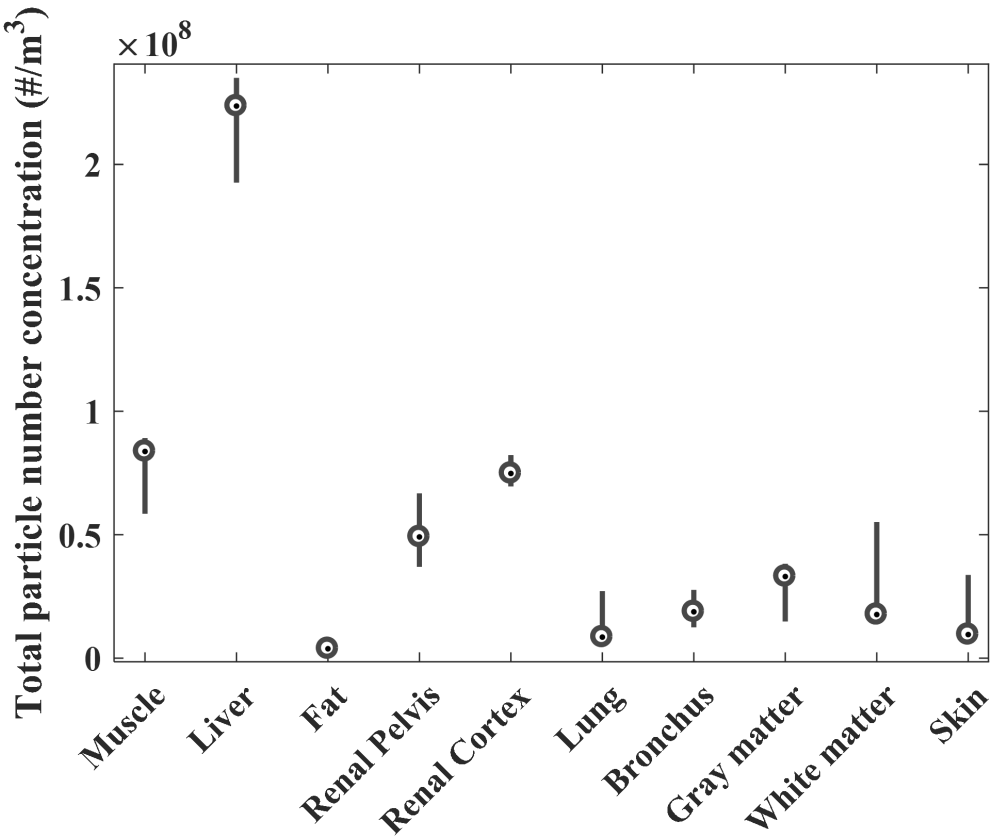

Fig 4. Boxplot presentation of the distributions of the measured total particle number for each tissue. Medians are presented as dots between the quartile lines.

https://doi.org/10.1371/journal.pone.0195274.g004

smallest particle size range (Fig 3A). The particle size distribution curves presented in Fig 3 indicate that there are at least two particle modes: the first around 10 nm and the second around 100 nm. The variations in the concentration of the total number of particles between the individual tests are presented in Fig 4. The variations within each tissue, and the deviation of the liver from the other tissues, are clearly visible. Some of the tissues, such as those of the renal cortex and bronchus, only exhibited moderate variation ($<1.3x10^7$ #/m3 difference in the particle number concentration between the first and third quartiles), but the variation between the quartiles in the liver tissue was substantial ($>4.2x10^7$ #/m3) (Fig 4).

The deposition fractions of the different mass fractions, PM_{10}, $PM_{2.5}$ and PM_1, are presented in Table 1, which shows that $PM_{2.5}$ and PM_1 particles constitute only slightly more than one tenth of the total particulate mass.

A statistical analysis of the total particle masses revealed that only the liver was significantly different from the rest of the tissues. The results for all the tissues can be seen in Table 2, as the p-values of the two-sample Mann Whitney U test (99% CI). Any p-values under 0.01 are in bold type.

Table 1. Measured aerosol median masses inside the surgical smoke evacuation stream from different tissue types, and the calculated mass depositions to the upper airways (UA), the bronchus (B), and the alveoli (AL) for particles under 10 μm (PM_{10}), under 2.5 μm ($PM_{2.5}$) and under 1 μm (PM_1).

PM_{10} (mg/m^3)	Muscle	Liver	Fat	Renal pelvis	Renal cortex	Lung	Bronchus	Gray matter	White matter	Skin
Measured total mass	3000	9100	210	2400	2500	210	720	760	370	370
Mass deposited to UA	1900	5700	130	1500	1600	130	440	470	230	220
Mass deposited to B	110	320	7.4	85	88	7.4	25	26	13	13
Mass deposited to AL	160	460	11	120	130	11	37	39	19	20
$PM_{2.5}$ (mg/m^3)	Muscle	Liver	Fat	Renal pelvis	Renal cortex	Lung	Bronchus	Gray matter	White matter	Skin
Measured total mass	370	1100	28	300	330	29	100	100	52	61
Mass deposited to UA	110	320	7.9	85	92	7.7	26	28	14	14
Mass deposited to B	23	66	1.6	18	19	1.6	5.4	5.8	2.8	2.8
Mass deposited to AL	53	160	3.9	42	46	3.9	14	14	7.0	7.4
PM_1 (mg/m^3)	Muscle	Liver	Fat	Renal pelvis	Renal cortex	Lung	Bronchus	Gray matter	White matter	Skin
Measured total mass	150	470	12	130	140	14	52	47	25	34
Mass deposited to UA	9.9	31.0	0.74	8.0	8.9	0.83	3.0	3.0	1.6	1.9
Mass deposited to B	1.6	4.9	0.12	1.4	1.5	0.14	0.49	0.48	0.25	0.29
Mass deposited to AL	12	38	0.94	10	11	1.1	3.9	3.7	2.0	2.5

https://doi.org/10.1371/journal.pone.0195274.t001

We concluded from both Tables 1 and 2 that even though some of the tissues are similar in terms of the mass of the produced particles, three separate groups can be distinguished, based on their corresponding particle mass size distributions, as seen in Fig 3, where three PM-classes are presented.

Table 3 shows estimates of the particle concentrations from various distances. Three user cases are included: surgery without any smoke removal, surgery with a general-purpose suction device and surgery with an integrated smoke evacuator. These concentrations are compared to the air quality index (AQI) [27]. In general, low-PM tissues do not pose a significant risk of particulate exposure for the surgical team, but high-PM tissues pose a significant risk of exposure to operating room personnel even if they are away from the immediate vicinity of the source. Based on our estimates in Table 3, we can see that in high-PM procedures, even with integrated smoke evacuation, the AQI classification at 30 cm distance from the cutting point remains Very High. Very Low classifications are only achieved at distances of 1 m (or more) when using integrated evacuation, and at 2 m when using general-purpose surgical suction.

Table 2. The result matrix for the p-values of the statistical analysis* based on the total mass of the particles created in tissue electrosurgery.

	Muscle	Liver	Fat	Renal pelvis	Renal cortex	Lung	Bronchus	Gray matter	White matter	Skin
Muscle		**0.0028**	**0.0006**	0.5205	0.1041	**0.0002**	**0.0002**	**0.0002**	**0.0002**	**0.0003**
Liver	-		**0.0003**	**0.0028**	**0.0028**	**0.0002**	**0.0002**	**0.0002**	**0.0002**	**0.0004**
Fat	-	-		**0.0022**	**0.0017**	0.9698	0.0452	0.1859	0.1212	0.3847
Renal pelvis	-	-	-		1.0000	**0.0002**	**0.0006**	**0.0002**	**0.0006**	**0.0028**
Renal cortex	-	-	-	-		**0.0002**	**0.0002**	**0.0002**	**0.0002**	**0.0002**
Lung	-	-	-	-	-		0.0257	0.1859	0.0757	0.3447
Bronchus	-	-	-	-	-	-		0.4727	0.2123	0.3847
Gray matter	-	-	-	-	-	-	-		0.9698	0.6776
White matter	-	-	-	-	-	-	-	-		0.7913
Skin	-	-	-	-	-	-	-	-	-	

*Mann-Whitney U test (99% CI).

https://doi.org/10.1371/journal.pone.0195274.t002

Table 3. Spherical model approximation for particle concentrations from various distances, for the tested tissues.

Extrapolated particulate exposures	Distance (cm)	High-PM µg/m3, AQI		Medium-PM µg/m3 AQI		Low-PM µg/m3 AQI	
40 W, without any smoke removal	30	1700	VH	500	VH	86	H
	50	360	VH	110	VH	19	L
	100	46	M	14	VL	2.3	VL
	200	5.6	VL	1.7	VL	0.29	VL
40 W, with general purpose surgical suction (-50%)	30	870	VH	260	VH	44	M
	50	190	VH	56	VH	9.7	VL
	100	24	L	7.1	VL	1.2	VL
	200	2.9	VL	0.88	VL	0.15	VL
40 W, with integrated smoke evacuator (-88%)	30	200	VH	60	H	10	VL
	50	44	M	13	VL	2.3	VL
	100	5.6	VL	1.7	VL	0.28	VL
	200	0.68	VL	0.21	VL	0.036	VL

A high-PM (liver), medium-PM (kidney, skeletal muscle) and low-PM (skin, subcutaneous fat, lung and brain). $PM_{2.5}$ Air quality index (AQI) for one hour exposure. Very low (VL), Low (L), Medium (M), High (H), Very High (VH).

https://doi.org/10.1371/journal.pone.0195274.t003

Discussion

Our results show significant differences in the mass concentration and size distribution of the particles in SS from different porcine tissues. The tissues can be divided into three groups according to their particle production. Liver produces by far the highest number of particles. Renal tissues and skeletal muscle produce a medium mass of particulate matter, while subcutaneous fat, lung tissue, bronchus, cerebral gray and white matter, and skin produce significantly less particulate mass. Some of the tested tissues have large variations in the number of particles that they produce (Fig 4). These variations can be explained by the heterogeneity of the histologic structures within the tissue specimens, such as connective tissue, blood vessels and hematomas, which can result in significant differences in the composition of the smoke produced by the same specimen.

Our results differ from those of Hinz et al. [28]. While they observed similar particle distributions from the liver and the kidney, we noted a pronounced difference between these tissues. However, other research groups, such as Bruske-Hohlfeld et al. [29] and Pillinger et al. [26], have presented results that support our findings. Bruske-Hohlfeld et al. reported the largest particle concentrations from the surgery of hemangioma of liver, which is in line with our results, even though a liver hemangioma and a porcine liver differ from each other histologically.

According to Pillinger et al., the mean mass concentration of particle exposure for a surgeon was 137 $\mu g/m^3$ when a smoke evacuation unit was not used [26]. This result is well in line with our estimate for the surgeon's particle exposure using the spherical model. At operating distances, without a dedicated smoke evacuation system, high-PM and medium-PM tissues produce $PM_{2.5}$ concentrations over 150 $\mu g/m^3$. According to European Union air quality indices [28] this is unhealthy. Wang et al. [24] observed that a wall-installed smoke evacuation unit reduced the $PM_{2.5}$ concentration by approximately half. Additionally, Pillinger et al. observed a particle mass reduction of 88% [26], when a suction device was integrated into the surgical blade. According to our results, is seems that with a smoke evacuation system, the surgeon is only exposed to unhealthy concentrations of particulate matter when operating on high-PM tissues, whereas general wall suction is adequate only for low-PM tissues.

In addition to smoke evacuators, the concentration of inhaled particles can be reduced with surgical masks. Nevertheless, there are vast differences in the filtering efficiencies of such masks, which can range from 13% to 99% [16]. In fact, it appears that only N95-respiratory protectors can be regarded as being more efficient than smoke evacuators in reducing surgical operating personnel's exposure to particulates in SS [30]. According to the AQI classification [27], surgical theatre personnel can be exposed from very low to very high doses of PM during electrosurgery, so we suggest using a combination of masks and smoke evacuators for electrosurgery on high-PM tissues, depending on the filtering options and the tissue being operated on. Even though there have been no epidemiological studies that show an elevated lung cancer risk in OR personnel [31], PM exposure is associated with an increased risk of lung cancer, higher mortality [32] and a higher risk of persistent airway problems [33]. Even though electrosurgery is used only for a fraction of the time during a whole surgical procedure, some OR personnel, especially plastic surgeons, and urologic and general surgical practitioners do make extensive use of electrosurgery. Without adequate protection, this population may be at risk of long-term health problems related to PM exposure. Our results and the proposed PM class division could be used as a reference for any surgeon when selecting protective measures for an operation. For example, if the surgery only involves low-PM tissue surgery, the workplace safety requirements for surgical masks would be lower than for medium-PM and high-PM tissue operations. However, in order to validate these PM classes as a standard practice, more particle measurements with a larger sample sizes are needed, including further testing of the filtering efficiency of different types of surgical masks.

It must be acknowledged that there may be some limitations and contradictions in our study. Krones et al. studied the production of volatile compounds (VOC) in electrosurgery with porcine tissue samples and found that the VOC ratio between liver and fat was significantly less than our aerosol ratio between the liver and subcutaneous fat [34]. However, VOC and aerosol ratios may not be uniform. Another possible source of inaccuracy could be that our diathermy unit does not compensate for variations in the tissue impedance, but instead operates with a constant voltage. Tissue impedance compensation is used in some diathermy devices to produce more balanced cutting efficiency for different tissue types [35]. As the tested tissue types had different impedances, the results may have been different if the experiment had been done with an instrument with impedance compensation. On the other hand, our results do accurately reflect the relation between natural tissue impedance and smoke production, without any bias from such compensation features. We standardized the cuts, so we could directly measure the variations in smoke production from the heterogeneous samples without any significant variance in the cuts themselves.

Natural aerosol particle size distributions typically have multiple modes, e.g. the aerosol emission from a vehicle exhaust typically contains a nucleation particle mode (median particle diameter around 10 nm) and a soot particle mode (median particle diameter around 50 nm). Unfortunately, the ELPI size range is limited and particles smaller than 10 nm are only partly detected. The particle size distribution curves presented in Fig 3 indicate that there are two particle modes: the first around 10 nm and the second around 100 nm, but the curves are similar to those of ELPI measurements in vehicle exhaust emissions [36] [37].

Conclusions

Our results indicate significant differences in particle production from different types of tissue during electrosurgery. The results suggest that the tissues can be divided into three groups according to their particle emissions: high-PM tissues (liver), medium-PM tissues (renal cortex, renal pelvis, muscle), and low-PM tissues (skin, cerebral gray matter, cerebral white

matter, bronchus, subcutaneous fat). These classes can be related to surgery-specific PM doses. These results are of clinical importance for the protective measures used by surgeons and OR staff who employ electrosurgery extensively. We recommend smoke evacuation and particulate filtration masks, especially for high-PM and medium-PM tissue surgery. More studies on smoke production and mask efficiency are still needed in order to produce yet more accurate health hazard limits and practical recommendations for electrosurgical procedures.

Supporting information

S1 Dataset. Raw data from the ELPI. Consists the ELPI measurement data from the performed experiments.
(MAT)

S1 File. Calculations and visualization for the particle size and number distributions. Including the results of each individual burning test. To execute this file, Matlab® R2016a or later is required.
(M)

S1 Table. Tissue specific timing in the experiments. This file is required to execute the S1 File.
(MAT)

Acknowledgments

This study was supported by grants from the following foundations: Finnish Foundation for Technology Promotion (TES), Tampereen Tuberkuloosisäätiö (Tampere Tuberculosis Foundation), Emil Aaltonen foundation and Pirkanmaan sairaanhoitopiiri (PSHP) grants 9s045, 151B03, 9T044, 9U042, 150618 and 9V044.

The authors would like to thank Jari Viik for his comments and contributions for the statistical analysis.

Author Contributions

Conceptualization: Markus Karjalainen, Sampo Saari, Topi Rönkkö, Antti Roine, Niku Oksala.

Data curation: Markus Karjalainen, Anton Kontunen, Sampo Saari, Antti Roine.

Formal analysis: Anton Kontunen, Sampo Saari.

Funding acquisition: Jukka Lekkala, Antti Roine, Niku Oksala.

Investigation: Markus Karjalainen, Anton Kontunen, Sampo Saari, Antti Roine.

Methodology: Markus Karjalainen, Anton Kontunen, Sampo Saari, Antti Roine.

Project administration: Jukka Lekkala, Antti Roine, Niku Oksala.

Resources: Topi Rönkkö, Jukka Lekkala, Antti Roine, Niku Oksala.

Supervision: Sampo Saari, Topi Rönkkö, Jukka Lekkala, Antti Roine, Niku Oksala.

Validation: Anton Kontunen, Antti Roine, Niku Oksala.

Visualization: Markus Karjalainen, Anton Kontunen, Sampo Saari, Antti Roine.

Writing – original draft: Markus Karjalainen, Anton Kontunen, Sampo Saari, Antti Roine, Niku Oksala.

Writing – review & editing: Markus Karjalainen, Anton Kontunen, Sampo Saari, Topi Rönkkö, Jukka Lekkala, Antti Roine, Niku Oksala.

References

1. Munro MG. Fundamentals of Electrosurgery Part I: Principles of Radiofrequency Energy for Surgery. The SAGES Manual on the Fundamental Use of Surgical Energy (FUSE). 2012. pp. 15–59. https://doi.org/10.1007/978-1-4614-2074-3_2
2. Massarweh NN, Cosgriff N, Slakey DP. Electrosurgery: History, principles, and current and future uses. Journal of the American College of Surgeons. 2006. pp. 520–530. https://doi.org/10.1016/j.jamcollsurg.2005.11.017 PMID: 16500257
3. Capizzi PJ, Clay RP, Battey MJ. Microbiologic activity in laser resurfacing plume and debris. Lasers Surg Med. 1998; 23: 172–4. Available: http://www.ncbi.nlm.nih.gov/pubmed/9779652 PMID: 9779652
4. Garden JM, O'Banion MK, Bakus AD, Olson C. Viral disease transmitted by laser-generated plume (aerosol). Arch Dermatol. 2002; 138: 1303–7. Available: http://www.ncbi.nlm.nih.gov/pubmed/12374535 PMID: 12374535
5. Maheswaran R, Pearson T, Smeeton NC, Beevers SD, Campbell MJ, Wolfe CD. Outdoor Air Pollution and Incidence of Ischemic and Hemorrhagic Stroke. Stroke. 2011; 43. Available: http://stroke.ahajournals.org/content/43/1/22
6. Lin H, Guo Y, Di Q, Zheng Y, Kowal P, Xiao J, et al. Ambient PM2.5 and Stroke. Stroke. 2017; 48. Available: http://stroke.ahajournals.org/content/48/5/1191
7. Matsuo R, Michikawa T, Ueda K, Ago T, Nitta H, Kitazono T, et al. Short-Term Exposure to Fine Particulate Matter and Risk of Ischemic Stroke. Stroke. 2016; 47. Available: http://stroke.ahajournals.org/content/47/12/3032
8. Maheswaran R, Haining RP, Brindley P, Law J, Pearson T, Fryers PR, et al. Outdoor Air Pollution and Stroke in Sheffield, United Kingdom. Stroke. 2005; 36. Available: http://stroke.ahajournals.org/content/36/2/239
9. Ljungman PL, Mittleman MA. Ambient Air Pollution and Stroke. Stroke. 2014; 45. Available: http://stroke.ahajournals.org/content/45/12/3734
10. Desikan A, Crichton S, Hoang U, Barratt B, Beevers SD, Kelly FJ, et al. Effect of Exhaust- and Nonexhaust-Related Components of Particulate Matter on Long-Term Survival After Stroke. Stroke. 2016; 47. Available: http://stroke.ahajournals.org/content/47/12/2916
11. Choi SH, Kwon TG, Chung SK, Kim T-H. Surgical smoke may be a biohazard to surgeons performing laparoscopic surgery. Surg Endosc. 2014; 28: 2374–2380. https://doi.org/10.1007/s00464-014-3472-3 PMID: 24570016
12. Semmler M, Seitz J, Erbe F, Mayer P, Heyder J, Oberdörster G, et al. Long-Term Clearance Kinetics of Inhaled Ultrafine Insoluble Iridium Particles from the Rat Lung, Including Transient Translocation into Secondary Organs. Inhal Toxicol. 2004; 16: 453–459. https://doi.org/10.1080/08958370490439650 PMID: 15204761
13. Bellmann B, Creutzenberg O, Ale H, Mermelstein R. Models for deposition, retention and clearance of particles after dust overloading of lungs in rats. Ann Occup Hyg. The British Occupational Hygiene Society; 1994; 38: 303–311.
14. Lehnert BE, Valdez YE, Tietjen GL. Alveolar macrophage-particle relationships during lung clearance. Am J Respir Cell Mol Biol. Am Thoracic Soc; 1989; 1: 145–154.
15. Hinds WC. Aerosol technology: properties, behavior, and measurement of airborne particles. John Wiley & Sons; 2012.
16. Redmayne a. C, Wake D, Brown RC, Crook B. Measurement of the Degree of Protection Afforded by Respiratory Protective Equipment Against Microbiological Aerosols. Ann Occup Hyg. 1997; 41: 636–640. https://doi.org/10.1093/annhyg/41.inhaled_particles_VIII.636
17. Spearman J, Tsavellas G, Nichols P. Current attitudes and practices towards diathermy smoke. Ann R Coll Surg Engl. Royal College of Surgeons of England; 2007; 89: 162–5. https://doi.org/10.1308/003588407X155752 PMID: 17346413
18. Hill DS, O'Neill JK, Powell RJ, Oliver DW. Surgical smoke—A health hazard in the operating theatre: A study to quantify exposure and a survey of the use of smoke extractor systems in UK plastic surgery units. J Plast Reconstr Aesthetic Surg. 2012; 65: 911–916. https://doi.org/10.1016/j.bjps.2012.02.012 PMID: 22445358
19. Keskinen J, Pietarinen K, Lehtimäki M. Electrical low pressure impactor. J Aerosol Sci. 1992; 23: 353–360. https://doi.org/10.1016/0021-8502(92)90004-F

20. Marjamäki M, Lemmetty M, Keskinen J. ELPI Response and Data Reduction I: Response Functions. Aerosol Sci Technol. 2005; 39: 575–582. https://doi.org/10.1080/027868291009189

21. Yli-Ojanperä J. Improving the Nanoparticle Resolution of the ELPI. Aerosol Air Qual Res. 2010; https://doi.org/10.4209/aaqr.2009.10.0060

22. Charvet A, Bau S, Bémer D, Thomas D. On the Importance of Density in ELPI Data Post-Treatment. Aerosol Sci Technol. Taylor & Francis; 2015; 49: 1263–1270. https://doi.org/10.1080/02786826.2015.1117568

23. González-Bayón L, González-Moreno S, Ortega-Pérez G. Safety considerations for operating room personnel during hyperthermic intraoperative intraperitoneal chemotherapy perfusion. Eur J Surg Oncol. Elsevier; 2006; 32: 619–624.

24. Wang H-K, Mo F, Ma C-G, Dai B, Shi G-H, Zhu Y, et al. Evaluation of fine particles in surgical smoke from an urologist's operating room by time and by distance. Int Urol Nephrol. 2015; 47: 1671–1678. https://doi.org/10.1007/s11255-015-1080-3 PMID: 26271645

25. Wardoyo AYP. The relation of ultrafine particle emission production to temperature from wood burning. Int J Eng Sci Innov Technol. 2012; 1: 161–169.

26. Pillinger SH, Delbridge L, Lewis DR. Randomized clinical trial of suctionversus standard clearance of the diathermy plume. Br J Surg. 2003; 90: 1068–1071. https://doi.org/10.1002/bjs.4214 PMID: 12945072

27. van den Elshout S, Léger K, Heich H. CAQI Common Air Quality Index—Update with PM2.5 and sensitivity analysis. Sci Total Environ. 2014; 488: 461–468. https://doi.org/10.1016/j.scitotenv.2013.10.060 PMID: 24238948

28. Hinz K-P, Gelhausen E, Schäfer K-C, Takats Z, Spengler B. Characterization of surgical aerosols by the compact single-particle mass spectrometer LAMPAS 3. Anal Bioanal Chem. 2011; 401: 3165–3172. https://doi.org/10.1007/s00216-011-5465-6 PMID: 22002560

29. Brüske-Hohlfeld I, Preissler G, Jauch K-W, Pitz M, Nowak D, Peters A, et al. Surgical smoke and ultrafine particles. J Occup Med Toxicol. 2008; 3: 31. https://doi.org/10.1186/1745-6673-3-31 PMID: 19055750

30. Oberg T, Brosseau LM. Surgical mask filter and fit performance. Am J Infect Control. Elsevier; 2008; 36: 276–282.

31. Gates MA, Feskanich D, Speizer FE, Hankinson SE. Operating room nursing and lung cancer risk in a cohort of female registered nurses. Scand J Work Environ Health. 2007; 33: 140–7. Available: http://www.ncbi.nlm.nih.gov/pubmed/17460802 PMID: 17460802

32. Beelen R, Hoek G, Raaschou-Nielsen O, Stafoggia M, Andersen ZJ, Weinmayr G, et al. Natural Cause Mortality and Long-Term Exposure to Particle Components: An Analysis of 19 European Cohorts within the Multi-Center ESCAPE Project. Environ Health Perspect. 2015; 123: 525–33. https://doi.org/10.1289/ehp.1408095 PMID: 25712504

33. Le Moual N, Varraso R, Zock JP, Henneberger P, Speizer FE, Kauffmann F, et al. Are operating room nurses at higher risk of severe persistent asthma? The Nurses' Health Study. J Occup Environ Med. NIH Public Access; 2013; 55: 973–7. https://doi.org/10.1097/JOM.0b013e318297325b PMID: 23887704

34. Krones CJ, Conze J, Hoelzl F, Stumpf M, Klinge U, Möller M, et al. Chemical composition of surgical smoke produced by electrocautery, harmonic scalpel and argon beaming—a short study. Eur Surg. Springer-Verlag; 2007; 39: 118–121. https://doi.org/10.1007/s10353-006-0305-1

35. Tokar JL, Barth BA, Banerjee S, Chauhan SS, Gottlieb KT, Konda V, et al. Electrosurgical generators. Gastrointest Endosc. Saunders/Elsevier, St. Louis (Mo); 2013; 78: 197–208. https://doi.org/10.1016/j.gie.2013.04.164 PMID: 23867369

36. Saari S, Karjalainen P, Ntziachristos L, Pirjola L, Matilainen P, Keskinen J, et al. Exhaust particle and NOx emission performance of an SCR heavy duty truck operating in real-world conditions. Atmos Environ. 2016; 126: 136–144. https://doi.org/10.1016/j.atmosenv.2015.11.047

37. Pirjola L, Lähde T, Niemi J V, Kousa A, Rönkkö T, Karjalainen P, et al. Spatial and temporal characterization of traffic emissions in urban microenvironments with a mobile laboratory. Atmos Environ. Elsevier; 2012; 63: 156–167.

PUBLICATION II

Identifying brain tumors by differential mobility spectrometry analysis of diathermy smoke

Ilkka Haapala, Markus Karjalainen, Anton Kontunen, Antti Vehkaoja, Kristiina Nordfors, Hannu Haapasalo, Joonas Haapasalo, Niku Oksala, Antti Roine

Journal of Neurosurgery. 2019 Jun 14;133(1):100-6.

doi:10.3171/2019.3.JNS19274.

JNS

LABORATORY INVESTIGATION

Identifying brain tumors by differential mobility spectrometry analysis of diathermy smoke

Ilkka Haapala, MD,[1] Markus Karjalainen, MSc,[2] Anton Kontunen, MSc,[2] Antti Vehkaoja, MSc, PhD, DSc(Tech),[2] Kristiina Nordfors, MD, PhD,[3] Hannu Haapasalo, MD, PhD,[4] Joonas Haapasalo, MD, PhD,[1,2] Niku Oksala, MD, PhD, DSc(Med),[2,5] and Antti Roine, MD, PhD[2,6]

[1]Unit of Neurosurgery, Tampere University Hospital; [2]Faculty of Medicine and Health Technology, Tampere University; [3]Department of Pediatrics, Tampere University Hospital; [4]Fimlab Laboratories Ltd., Tampere University Hospital; [5]Centre for Vascular Surgery and Interventional Radiology, Tampere University Hospital; and [6]Department of Surgery, Tampere University Hospital, Hatanpää Hospital, Tampere, Finland

OBJECTIVE There is a need for real-time, intraoperative tissue identification technology in neurosurgery. Several solutions are under development for that purpose, but their adaptability for standard clinical use has been hindered by high cost and impracticality issues. The authors tested and preliminarily validated a method for brain tumor identification that is based on the analysis of diathermy smoke using differential mobility spectrometry (DMS).

METHODS A DMS connected to a special smoke sampling system was used to discriminate brain tumors and control samples ex vivo in samples from 28 patients who had undergone neurosurgical operations. They included meningiomas (WHO grade I), pilocytic astrocytomas (grade I), other low-grade gliomas (grade II), glioblastomas (grade IV), CNS metastases, and hemorrhagic or traumatically damaged brain tissue as control samples. Original samples were cut into 694 smaller specimens in total.

RESULTS An overall classification accuracy (CA) of 50% (vs 14% by chance) was achieved in 7-class classification. The CA improved significantly (up to 83%) when the samples originally preserved in Tissue-Tek conservation medium were excluded from the analysis. The CA further improved when fewer classes were used. The highest binary classification accuracy, 94%, was obtained in low-grade glioma (grade II) versus control.

CONCLUSIONS The authors' results show that surgical smoke from various brain tumors has distinct DMS profiles and the DMS analyzer connected to a special sampling system can differentiate between tumorous and nontumorous tissue and also between different tumor types ex vivo.

https://thejns.org/doi/abs/10.3171/2019.3.JNS19274

KEYWORDS differential mobility spectrometry; brain tumor identification; oncology

In present clinical practice, frozen section analysis is the gold standard for intraoperative tumor identification, yet the histopathological examination is often limited to a very small number of separate samples and the diagnosis is achieved with a delay.[15] Especially in cases of low-grade tumors, frozen section analysis is difficult, and often the pathologist can only provide a morphological description of the tumor, with a lot of interobserver variability. Also, the assessment of more accurate molecular characteristics of the tumor is achieved only after several days and extensive tissue preparation.[11] Furthermore, a precise intraoperative tissue identification would, in many cases, have a direct effect on the surgeon's resection strategy. For example, in the case of a low-grade glioma (LGG), a surgeon would attempt an aggressive gross-total resection for maximal survival gain, whereas in glioblastoma (GBM) resections it is especially important to preserve remaining functions and be careful with eloquent cerebral areas.[4,14] Therefore, there is a need for real-time, intraoperative tissue identification technology.

Several technologies are under development for intraoperative brain tumor identification. Optical coherence

ABBREVIATIONS CA = classification accuracy; DMS = differential mobility spectrometry; GBM = glioblastoma; LDA = linear discriminant analysis; LGG = low-grade glioma; LOOCV = leave-one-out cross-validation; OCT = optical coherence tomography; REIMS = rapid evaporate ionization mass spectrometry; 10-f-CV = 10-fold cross-validation.

SUBMITTED January 30, 2019. **ACCEPTED** March 24, 2019.
INCLUDE WHEN CITING Published online June 14, 2019; DOI: 10.3171/2019.3.JNS19274.

tomography (OCT) provides a high-resolution microscopic view of the tissue by illuminating the tissue with near-infrared light and measuring the reflected light with a spectrometer. OCT has been used to provide structural information about the dissected tissue.[3]

Raman spectroscopy is a modality that gives spectral tissue characteristics based on molecular signatures resulting from inelastic scattering of incident light. The resulting spectrum provides a fingerprint by which different molecular species can be identified. Raman spectroscopy reached sensitivity of 93% and specificity of 91% in binary classification when used for WHO grades II–IV brain tumor detection.[8]

The rapid evaporative ionization mass spectrometry (REIMS) setup, developed by the Imperial College, London, United Kingdom, has already been incorporated into a commercialized device by Waters Corp. as the "intelligent knife" or iKnife. It has reached an impressive identification capability with 100% of the given diagnoses matching the postoperative histopathology.[1] A mass spectrometry–based sampling system has also been coupled with the Cavitron Ultrasonic Surgical Aspirator (CUSA) with a formidable ex vivo identification performance of 100% in GBMs and healthy brain samples, which the authors speculated to be a slight overestimation due to the limited number of samples.[16] There is also a laser-based adoption of iKnife REIMS technology. Laser-based sampling systems such as PIRL and SpirerMass have also been developed.[5,20] Both have been validated in analysis of animal tissues, but data from human tissues are not yet available. MasSpec Pen is yet another mass spectrometry–based sampling approach that uses water flushing of the analyzed tissue as the sampling modality.[21] The system has achieved high performance in ex vivo analysis on cancerous tissues and has been demonstrated in vivo in a murine model, although sensitivity and specificity were not reported. On their website, the team states that research on MasSpec Pen in CNS malignancies is underway.

Electrosurgical resection is currently a widely used technique in neurosurgery. It produces surgical smoke, which is evacuated from the resection cavity to improve visibility and to avoid inhalation of toxic smoke. Surgical smoke carries information about the excised tissue in the form of biomarkers or tissue-specific metabolites.[17] Electric discharge of the diathermy blade disperses particulates and causes evaporation of molecules from the tissue. The gold standard for the analysis of such molecules is mass spectrometry, which identifies molecules based on their mass-to-charge ratio. In various REIMS studies, the phospholipid content of the tissue has been identified as a key distinguishing factor.[1] Mass spectrometry operates in a high vacuum, which poses considerable costs and mechanical challenges. In particular, ion mobility spectrometry (IMS) characterizes substances in atmospheric pressure based on cross-sectional area and electrical charge of the molecules.[18] Differential mobility spectrometry (DMS) is an advanced adaptation of IMS. It uses a high-frequency electric field to break molecule clusters, thus creating additional information about the cluster strength that can be used in the analysis. Compared with mass spectrometry, the DMS is technically less complex and does not require a vacuum. Therefore, DMS is potentially a more affordable solution with less required maintenance and a smaller size.

Previously, the DMS has been studied as a diagnostic tool in various cancers with promising results.[7] We have previously shown that DMS is capable of discriminating animal tissues and benign and malignant human breast tissue with high accuracy from surgical smoke.[10,19] To our knowledge, this is the first time when DMS is used for brain tumor identification and classification.

Methods

Tissue Samples

We retrospectively obtained samples from 28 patients who had undergone neurosurgical operations in Tampere University Hospital between 2005 and 2017. The original samples included 6 meningiomas (WHO grade I), 3 pilocytic astrocytomas (grade I), 3 other grade II LGGs, 9 GBMs (grade IV), 5 CNS metastases, and 3 control samples. Primary tumors for the metastases were lung, endocervix, breast, endometrium, and prostate carcinomas. A total of 9 GBM samples were collected from 8 patients; otherwise, we had one sample per patient. The control samples were hemorrhagic or traumatically damaged brain tissue. Seventeen samples were originally preserved in Tissue-Tek (Sakura Finetek), a gel-like medium consisting of polyethylene glycol and polyvinyl alcohol.[2] It penetrates the tissue and preserves the sample's suitability for morphological examination with a microscope. Diagnoses of the tumor types were obtained from an experienced neuropathologist. The study was approved by the ethics review board of Pirkanmaa Hospital District, Finland.

All samples were stored in a freezer at –70°C. The samples were thawed and cut into smaller specimens that were placed in a custom-made aluminum well plate. The wells were 3.9 mm deep and 3 mm in diameter. The size of the smaller specimens was determined by the size of the wells. Each well contained a fitting of 3–5 wt/wt agar and 0.9 wt/wt NaCl to simulate body conductivity and to avoid arcing from the blade to the well plate that acted as a grounding electrode for the electrosurgical blade. Samples were analyzed with the DMS system in 9 sessions with a total numer of 694 tissue specimens prepared; 331 specimens were derived from patient samples preserved in Tissue-Tek. The specimens included in total 121 meningiomas, 154 CNS metastases, 35 pilocytic astrocytomas, 257 GBMs, 32 LGGs, and 20 control samples.

Tissue Analysis System

The measurement system consisted of 4 distinct parts: a tissue sampling unit (I), sample conditioning unit (II), DMS sensor (III), and computational data analysis (IV) as illustrated in Fig. 1 (a photograph of the system appears in Supplemental Fig. 2). The sampling system is described in detail in an earlier study.[10]

An automated tissue sampling unit (I) was developed to produce standardized incisions from tissue samples. This eliminated the sampling variations arising from free-hand use of the surgical blade. The sampling unit consisted of a commercial diathermy blade (Itkacut 350 MB, Innokas Medical) used with a nominal 100-W cut mode. The high

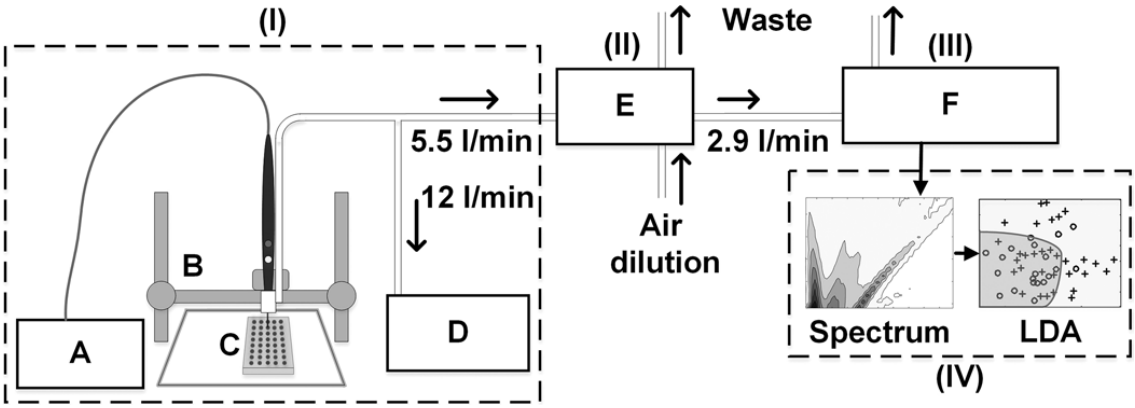

FIG. 1. Illustration of the measurement system consisting of a tissue sampling unit (I), sample conditioning unit (II), DMS sensor (III), and computational data analysis (IV). The tissue sampling unit further includes a diathermy power unit (A), robot stage (B), sample well plate (C), surgical smoke evacuator (D), filter and dilution system (E), and ENVI-AMC differential mobility spectrometer (F). The numbered values depict the input flow rate to each device. The LDA is a sketch of the operating principle, where 2 classes, + and o, are projected onto a 2D plane.

power was used to avoid adhesion of the samples to the blade. The blade was attached to a modified 3D printer (RepRap Mendel Prusa i3, Kit Printer 3D) and a smoke evacuator (Surtron Evac, LED SpA), which directed the surgical smoke to the sample conditioning unit. The diathermy blade incised each specimen once. The duration of time from the capture of smoke to the readout was 1 minute. The blade used in this study was 2.5 mm in width; thus, the spatial resolution is in the same order.

The sample conditioning unit (II) separated contaminating particulate matter from the smoke and kept the sample concentration constant. In addition to biomarkers, electrosurgery produces a significant amount of particulate matter,[9] which has 2 unwanted consequences. First, the particulate matter contaminates the sensor and second, it causes increased carryover. Thus, an electric particle filter was used as the first active component in the sample conditioning unit for removing the particulate matter from the sampling stream. After filtering, we diluted the sample with cleaned air, using variable dilution ratio from 1:85 to 1:440 due to the high concentration of the sample. Compressed diluting air was cleaned with active carbon and 5-Å molecular sieves. Moreover, the sample flow path of the sample conditioning unit was heated to 40°C–50°C to minimize carryover from previous sampling events.

The sample was passed from the conditioning unit to a DMS analyzer (III) (ENVI-AMC, Environics Oy). The DMS consists of a radioactive ^{241}Am source to ionize the molecules and a sensor unit, which separates ions with low and high electric fields. A 2D spectrum is obtained by altering the radiofrequency electric field strength and direct current field. With these fields, ions partially separate and partially stay clustered. This ion separation can be used as a characteristic dispersion spectrum, or "smell fingerprints," of the sample, as seen in Fig. 2.

Analysis of the measurement data (IV) was performed

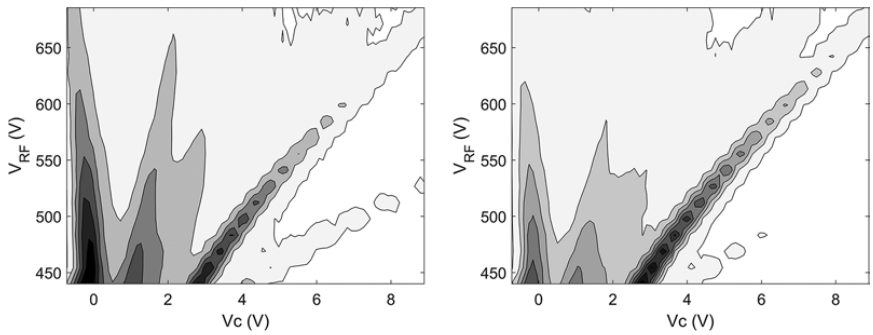

FIG. 2. Example spectral images from a single control tissue sample (**left**) and a GBM (**right**). The areas of the dispersion plot that are in the 1- to 2-V compensation voltage range are the most prone to exhibit the differences in the DMS spectra between the tissues. In this instance, the differential mobility peaks near the 2-V compensation voltage differ in shape and size. V_C = compensation voltage; V_{RF} = peak-to-peak amplitude of the radiofrequency waveform voltage.

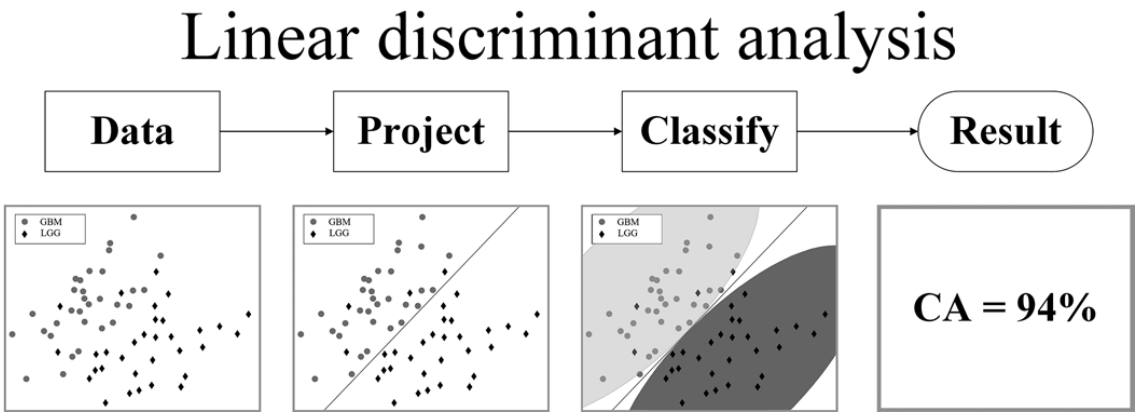

FIG. 3. The principle of LDA classification. The LDA classification model aims to find a linear combination that best separates two or more classes based on given features. In this study, the features were the pixels in the DMS spectra, but for visualization purposes, the data for GBM and LGG are presented in 2 dimensions as Sammon projections of the DMS spectrum data.

using MATLAB (MathWorks Ltd.)–based processing and classification algorithms. The samples were classified into 7, 5, or 2 categories with linear discriminant analysis (LDA). LDA is a simple and commonly used supervised classification method that is based on feature projection to reduce the dimensionality of the initial measurement data. The principle of LDA classification is presented in Fig. 3. The LDA classification was performed using the full raw data matrices (1620 pixels) of the DMS output spectra as features. To avoid overfitting, leave-one-out cross-validation (LOOCV) or 10-fold cross-validation (10-f-CV) was performed, depending on the sample size. LOOCV is a valid method for small sample size classifications, but when the size increases to hundreds, a more unbiased estimation is achieved with 10-f-CV. Furthermore, in cases in which the sample sizes of the binary classification were significantly skewed, the classes were balanced by only including a portion of the samples from the larger class in the classification. Exclusion of the samples from the larger class was randomized. In addition to the cross-validated and balanced LDA models, blind hierarchical clustering was also carried out to test unsupervised classification.

Results

When classifying the full measurement data set to the 7 tissue classes, a classification accuracy (CA) of 50% was achieved. The average CA by chance would be 14%. The confusion matrix is presented in Table 1. Blind hierarchical clustering did not show relevant grouping.

When only focusing on distinguishing CNS metastases from meningiomas, the cross-validated classifier produced a CA of 74% (sensitivity 71%, specificity 77%). For separating the control samples from tumors (the class consisted of 4 samples of each tumor type), the CA was 83% (sensitivity 78%, specificity 89%). In differentiation of LGGs (grade II) from GBMs, the CA was 94% (sensitivity 88%, specificity 100%). For the differentiation of pilocytic

TABLE 1. Results of 7-class classification

		Assigned Class										
		Meningioma	No Sample	Met	PA	GBM	LGG	Control	Total	Sensitivity	Specificity	CA
True class	Meningioma	**63**	0	22	2	33	1	0	121	52%	91%	
	No sample	2	**72**	0	0	1	0	0	75	96%	99%	
	Met	18	2	**63**	6	63	1	1	154	40%	77%	
	PA	2	1	11	**2**	17	1	1	35	6%	98%	
	GBM	27	0	75	3	**144**	5	3	257	56%	68%	
	LGG	4	1	10	0	15	**2**	0	32	6%	99%	
	Control	0	0	5	3	11	0	**1**	20	5%	99%	
	Total											50%

Met = metastasis; PA = pilocytic astrocytoma.

Correctly classified samples appear in boldface type. Sensitivity is the percentage of correctly identified positive samples. Specificity is the percentage of correctly identified negative samples. In the sensitivity and specificity columns, the positive sample is determined as the sample on the given row, while all others are considered as negative samples. For example, in the first row for meningioma, there are 121 positive samples and 573 negative samples, which gives a sensitivity of 63/121 = 52% and specificity of 520/573 = 91%.

TABLE 2. Results of selected relevant binary classifications

Comparison	No. of Samples	CA	Sensitivity	Specificity	PPV	NPV
Tumor (+) vs control (–)*,†	40	83%	78%	89%	87%	80%
Meningioma (+) vs met (–)‡	275	74%	71%	77%	70%	77%
LGG (grade II) (+) vs GBM (–)†	64	94%	88%	100%	100%	89%
PA (+) vs diffusively infiltrating glioma (–; grades II & IV)†	70	70%	77%	63%	68%	73%
LGG (+; grade II) vs control (–)†	52	94%	97%	90%	94%	95%

NPV = negative predictive value; PPV = positive predictive value; + = positive; – = negative.
Positive predictive value is the ratio of true positives to all (predicted and true) positives. Negative predictive value is the ratio of true negatives to all (predicted and true) negatives.
* Five randomly selected tumor samples of every class.
† LOOCV.
‡ 10-f-CV.

astrocytomas from diffusely infiltrating gliomas (grades II and IV), the CA was 70% (sensitivity 77%, specificity 63%). The differentiation of LGGs (grade II) from control samples produced a CA of 94% (sensitivity 97%, specificity 90%). Table 2 shows the results for each binary classification case.

Classifications were also conducted separately in samples that were not preserved in Tissue-Tek, which improved the CA significantly. The results for the classification of the remaining 5 classes are presented in Table 3. In addition, the binary classification (LDA with 10-f-CV) of meningioma from metastases without the Tissue-Tek samples produced a CA of 95% with 87% sensitivity and 98% specificity.

Discussion

Our results show that surgical smoke produced by various brain tumors has distinct DMS profiles. The DMS accompanied with a specialized sampling system can distinguish different brain tumors from each other ex vivo. With 7-class classification by LDA, we reached the CA of 50%, which is considerably better than the discrimination of 14% achieved by chance. We also carried out binary classifications in order to better simulate the factual intraoperative use of the DMS. In clinical reality, the physician often has some thought as to the tumor diagnosis even before surgery, based on imaging study findings, patient age, tumor location, and other factors. Therefore, the diagnostic alternatives for DMS can often be narrowed down beforehand. Binary classifications yielded significantly higher CAs. Particularly promising is the 94% CA in LGG (grade II) versus control setting. Low-grade glioma patients compose a subgroup that may have the greatest survival benefit from more accurate resection,[14] and their identification by frozen section analysis is especially difficult. The CA also largely improved when the samples originally conserved in Tissue-Tek were excluded from the analysis, suggesting that Tissue-Tek was a major confounding factor. As an example, a Sammon projection image about the dispersion of GBMs and empty samples is shown in Supplemental Fig. 1.

From a clinician's standpoint, a DMS-based tumor identification system has several advantages. It can be connected to the instrumentation already present in neurosurgical operating rooms and does not require a separate probe. The DMS provides data that can be translated by relatively simple algorithms to tissue classifications that can be interpreted by the surgical staff without substantial training. Thus, the system is user friendly, provides near–real-time information, and preserves the surgical workflow. OCT requires a visual analysis of the image and thus is ultimately a subjective method for cancer margin evaluation. The image analysis is sensitive to surgical artifacts (blood and cauterized tissue), and surgical personnel would need additional training and qualification to manage the analysis. In OCT, the analysis does not happen in vivo but instead the surgically removed tissue piece is imaged on a separate platform.[3] Raman spectroscopy requires a specialized probe to be inserted into the resection

TABLE 3. Classification results for samples not preserved in Tissue-Tek

		Assigned Class								
		Meningioma	No Sample	Met	PA	GBM	Total	Sensitivity	Specificity	CA
True class	Meningioma	**32**	1	3	0	3	39	82%	99%	
	No sample	0	**74**	0	0	1	75	99%	99%	
	Met	0	1	**82**	2	17	102	80%	90%	
	PA	1	1	10	**11**	6	29	38%	99%	
	GBM	0	0	17	0	**101**	118	86%	89%	
	Total									83%

Correctly classified samples appear in boldface type.

cavity.[8] Therefore, all such systems are likely to interfere with the surgeon's workflow.

Compared with mass spectrometry, a clinical use of DMS is analogous. DMS is a technically less complex system than mass spectrometry and does not require a vacuum. The adaptability of the iKnife for standard clinical use has been hindered by its high cost, expertise required for its use, need for regular and intensive maintenance, and impractically large size for operating rooms. The same challenge applies to other described mass spectrometry–based methods. DMS is a potentially more affordable solution with less required maintenance and a smaller size.

A major limitation of our study is that we had only 29 patient samples from which we obtained 694 specimens for the analysis. However, in the studies of many competing solutions, the number of patient samples is similar or even smaller.[3,8,16] Even though a small number of patients may introduce selection bias and affect the generalizability of the results, it was considered to be enough for a proof-of-concept study.

We used hemorrhagic or traumatically damaged brain tissue as control samples. Even though these samples were nontumorous, pathological injuries could have had an impact on metabolic profiles of these cells. Therefore, these specimens cannot be directly contrasted with healthy brain tissue.

When the entire sample is taken into consideration, our CA does not seem to match the identification capabilities of the competing solutions. The performance, however, is significantly improved when the samples processed with Tissue-Tek were excluded, with a total CA of 84% (5 classes) and CAs of greater than 90% in several binary scenarios. This suggests that tissue preservation medium is a significant confounding factor. Tissue-Tek penetrates the tissue and preserves it for morphological examination with a microscope.[2] Yet because it penetrates the tissue, it is likely that the electrosurgical smoke will contain some of the medium, thereby disturbing the DMS classifier. Since 2016, Tissue-Tek has been a part of standard processing of brain tumor samples in the Department of Pathology, Tampere University Hospital, Finland. We collected our samples retrospectively, so all the samples newer than 2016 were conserved in Tissue-Tek.

Further shortcomings in classification accuracy may be explained by intratumoral heterogeneity. It is obvious that CNS metastases are histologically heterogeneous, since they arise from completely different primary tumors.[12] Thus, it is expected that they can be troublesome for the classifier. Also, intratumoral histological heterogeneity is a common phenomenon in gliomas, especially in GBMs. Different areas of a glioma (grades II–IV) has been shown to vary in terms of cellular density, nuclear pleomorphism, necrosis, histological architecture, vasculature, and mitoses, which causes the WHO grade to vary within a tumor.[13] Structural differences between separate tumor areas also cause variation in tissue impedance.[22] We dissected the original tissue samples into smaller pieces. Therefore, different tissue pieces with the same pathological diagnosis most likely varied in terms of histological structure and bioelectrical qualities, which may have affected the results. The classifier also performed better with meningiomas, which are considered to be rather homogeneous tumors.[6]

In addition to histological heterogeneity, different brain tumors also vary a lot in terms of macroscopic composition. Therefore, even with the custom-made well plate, standardized incisions, and our best preparation of the samples, the depth of the incisions and the amount of smoke provided was somewhat varied. This issue was only partly managed with the supervised learning method in the data analysis (LDA) with its ability to reduce the variance and noise of the original data set. Since significantly better results were achieved by excluding samples preserved in Tissue-Tek, we examined the possibility of bias in distribution of sample types analyzed in different sessions with no significant bias observed.

In the future, the DMS will be tested to detect elevated levels of D-2-hydroxyglutarate and thereby intraoperatively determine the IDH mutation status of a tumor. Further studies are also needed to validate the DMS analyzer for tissue identification in vivo, with more accurate histopathological validation. Instead of the current diathermy blade, we will need to develop a bipolar scissors–integrated sampling system that conforms the routine instruments used by neurosurgeons. The speed of the analysis will also be improved by optimizing the DMS analysis window and the sampling system. Along with further in vivo research and technical development, we can also assess the system's suitability for the evaluation of neurosurgical resection margins.

Conclusions

This proof-of-concept study demonstrates that surgical smoke from various brain tumors has distinct DMS profiles, and that the DMS connected to a special sampling system can differentiate between tumorous and nontumorous brain tissue and also between different tumor types ex vivo. A DMS analyzer could potentially become a simple, user-friendly, and affordable tool for intraoperative brain tumor tissue identification.

Acknowledgments

This study was supported by grants from the following foundations: Finnish Foundation for Technology Promotion (TES); Tampereen Tuberkuloosisäätiö (Tampere Tuberculosis Foundation); Emil Aaltonen Foundation; Finnish Cultural Foundation; Finnish Medical Foundation; Pediatric Research Foundation; Finnish Neurosurgical Society; Competitive State Research Financing of the Expert Responsibility area of the Tampere University Hospital and Pirkanmaa Hospital District grants 9s045, 151B03, 9T044, 9U042, 150618, 9U042, and 9V044; and Academy of Finland, grant 292477.

References

1. Balog J, Sasi-Szabó L, Kinross J, Lewis MR, Muirhead LJ, Veselkov K, et al: Intraoperative tissue identification using rapid evaporative ionization mass spectrometry. **Sci Transl Med 5:**194ra93, 2013
2. Barthel LK, Raymond PA: Improved method for obtaining 3-microns cryosections for immunocytochemistry. **J Histochem Cytochem 38:**1383–1388, 1990
3. Böhringer HJ, Lankenau E, Stellmacher F, Reusche E, Hütt

mann G, Giese A: Imaging of human brain tumor tissue by near-infrared laser coherence tomography. **Acta Neurochir (Wien) 151:**507–517, 2009
4. Brown TJ, Brennan MC, Li M, Church EW, Brandmeir NJ, Rakszawski KL, et al: Association of the extent of resection with survival in glioblastoma: a systematic review and meta-analysis. **JAMA Oncol 2:**1460–1469, 2016
5. Fatou B, Saudemont P, Leblanc E, Vinatier D, Mesdag V, Wisztorski M, et al: In vivo real-time mass spectrometry for guided surgery application. **Sci Rep 6:**25919, 2016
6. Filippi CG, Edgar MA, Uluğ AM, Prowda JC, Heier LA, Zimmerman RD: Appearance of meningiomas on diffusion-weighted images: correlating diffusion constants with histopathologic findings. **AJNR Am J Neuroradiol 22:**65–72, 2001
7. Fitzgerald JE, Bui ETH, Simon NM, Fenniri H: Artificial nose technology: status and prospects in diagnostics. **Trends Biotechnol 35:**33–42, 2017
8. Jermyn M, Mok K, Mercier J, Desroches J, Pichette J, Saint-Arnaud K, et al: Intraoperative detection of glioma invasion beyond MRI enhancement with Raman spectroscopy in humans. **Proc SPIE 9318:**93180D-1–93180D-6, 2015
9. Karjalainen M, Kontunen A, Saari S, Rönkkö T, Lekkala J, Roine A, et al: The characterization of surgical smoke from various tissues and its implications for occupational safety. **PLoS One 13:**e0195274, 2018
10. Kontunen A, Karjalainen M, Lekkala J, Roine A, Oksala N: Tissue identification in a porcine model by differential ion mobility spectrometry analysis of surgical smoke. **Ann Biomed Eng 46:**1091–1100, 2018
11. Longuespée R, Wefers AK, De Vita E, Miller AK, Reuss DE, Wick W, et al: Rapid detection of 2-hydroxyglutarate in frozen sections of IDH mutant tumors by MALDI-TOF mass spectrometry. **Acta Neuropathol Commun 6:**21, 2018
12. Nayak L, Lee EQ, Wen PY: Epidemiology of brain metastases. **Curr Oncol Rep 14:**48–54, 2012
13. Paulus W, Peiffer J: Intratumoral histologic heterogeneity of gliomas. A quantitative study. **Cancer 64:**442–447, 1989
14. Sanai N, Berger MS: Glioma extent of resection and its impact on patient outcome. **Neurosurgery 62:**753–766, 2008
15. Santagata S, Eberlin LS, Norton I, Calligaris D, Feldman DR, Ide JL, et al: Intraoperative mass spectrometry mapping of an onco-metabolite to guide brain tumor surgery. **Proc Natl Acad Sci U S A 111:**11121–11126, 2014
16. Schäfer KC, Balog J, Szaniszló T, Szalay D, Mezey G, Dénes J, et al: Real time analysis of brain tissue by direct combination of ultrasonic surgical aspiration and sonic spray mass spectrometry. **Anal Chem 83:**7729–7735, 2011
17. Schäfer KC, Dénes J, Albrecht K, Szaniszló T, Balog J, Skoumal R, et al: In vivo, in situ tissue analysis using rapid evaporative ionization mass spectrometry. **Angew Chem Int Ed Engl 48:**8240–8242, 2009
18. Schneider BB, Nazarov EG, Londry F, Vouros P, Covey TR: Differential mobility spectrometry/mass spectrometry history, theory, design optimization, simulations, and applications. **Mass Spectrom Rev 35:**687–737, 2016
19. Sutinen M, Kontunen A, Karjalainen M, Kiiski J, Hannus J, Tolonen T, et al: Identification of breast tumors from diathermy smoke by differential ion mobility spectrometry. **Eur J Surg Oncol 45:**141–146, 2019
20. Tata A, Gribble A, Ventura M, Ganguly M, Bluemke E, Ginsberg HJ, et al: Wide-field tissue polarimetry allows efficient localized mass spectrometry imaging of biological tissues. **Chem Sci (Camb) 7:**2162–2169, 2016
21. Zhang J, Rector J, Lin JQ, Young JH, Sans M, Katta N, et al: Nondestructive tissue analysis for ex vivo and in vivo cancer diagnosis using a handheld mass spectrometry system. **Sci Transl Med 9:**eaan3968, 2017
22. Zhang Y, Xu S, Min W, Shen L, Zhang Y, Yue Z: Surg-25. A novel bio-impedance spectroscopy system real-time intraoperatively discriminates glioblastoma from brain tissue in mice. **Neuro Oncol 19:**240, 2017

Disclosures

Mr. Karjalainen, Mr. Kontunen, Dr. Oksala, and Dr. Roine: direct stock ownership in Olfactomics Ltd. Dr. Roine: employee of Olfactomics Ltd.

Author Contributions

Conception and design: Karjalainen, H Haapasalo, J Haapasalo, Oksala, Roine. Acquisition of data: H Haapasalo, J Haapasalo. Analysis and interpretation of data: Haapala, Karjalainen, Kontunen, H Haapasalo, Roine. Drafting the article: Haapala, Karjalainen, Kontunen, Roine. Critically revising the article: all authors. Reviewed submitted version of manuscript: Haapala. Approved the final version of the manuscript on behalf of all authors: Haapala. Statistical analysis: Haapala, Karjalainen, Kontunen. Administrative/technical/material support: Karjalainen, Kontunen, Vehkaoja, Nordfors, H Haapasalo, J Haapasalo, Oksala, Roine. Study supervision: J Haapasalo, Oksala, Roine.

Supplemental Information

Online-Only Content

Supplemental material is available with the online version of the article.

Supplemental Figs. 1 and 2. https://thejns.org/doi/suppl/10.3171/2019.3.JNS19274.

Previous Presentations

Portions of this work were presented in poster form at the 3rd Annual Symposium on Brain Tumors, Finnish Brain Tumor Research Association, Turku, Finland, October 26–27, 2017.

Correspondence

Ilkka Haapala: Tampere University Hospital, Tampere, Finland. ilkka.haapala@fimnet.fi.

PUBLICATION III

Recovery characteristics of different tube materials in relation to combustion products

Markus Karjalainen, Anton Kontunen, Meri Mäkelä, Osmo Anttalainen Antti Vehkaoja, Niku Oksala, Antti Roine

International Journal for Ion Mobility Spectrometry (2020) 23:83–90

https://doi.org/10.1007/s12127-020-00266-z

International Journal for Ion Mobility Spectrometry (2020) 23:83–90
https://doi.org/10.1007/s12127-020-00266-z

ORIGINAL RESEARCH

Recovery characteristics of different tube materials in relation to combustion products

M. Karjalainen[1] · A. Kontunen[1] · M. Mäkelä[1] · O. Anttalainen[2] · A. Vehkaoja[1] · N. Oksala[1,3] · A. Roine[1]

Received: 29 May 2020 / Revised: 1 July 2020 / Accepted: 2 July 2020 / Published online: 22 July 2020

Abstract
Common challenge in gas analyzers such as Ion Mobility Spectrometers (IMS) integrated into a measurement system is the reduced analysis speed that is partially limited by the temporal carry-over of sample molecules. It is caused by adsorption and absorption of the molecules into the gas tubes of the analyzer. We studied the recovery times of common tube materials: polyether ether ketone (PEEK), polytetrafluoroethylene (PTFE), fluorinated ethylene propylene (FEP), polyethylene (PE), steel 316 L, parylene C coated steel and Silconert® coated steel from organic combustion products. The tests were performed in two temperatures, at 25 °C and at 70 °C. In addition, detailed analysis was performed for PTFE tube material at 33, 50, 70 and 100 °C to observe the temperature relation of desorption. Uncoated steel was found to have the best performance in increased temperature applications due lack of absorption. Major advantages from coatings compared to plane steel were not found. Plastics were found suitable materials in lower temperatures where adsorption exceeds absorption.

Keywords Carry over · Instrumenting · Recovery · Tubing · Sorption

Introduction

Gas analyzers based on ion mobility spectrometry (IMS) are used in various application areas such as medicine, process industry, security and research ([1, 2]. Due to its relative simplicity and ability to function at atmospheric pressure, IMS technology enables low-maintenance gas analysis even outside laboratory conditions. However, residual signal produced by the previously sampled gas results in so called carry-over effect that should be addressed in all applications. Recovery time, i.e. the time required for the system to clear out the carry-over is dependent on analyzer materials, temperature, volume and control of the contaminating molecules. Recovery time can be improved by increasing the temperature, reducing surface area, and by optimizing material selection and filtration methods utilized in the system ([3, 4]. These methods also have their downsides. Heating inherently increases the complexity and energy consumption of the system, reduces the number of applicable materials, and in some cases may also affect to the analyte composition by promoting chemical reactions. Minimizing the surface area by reducing of physical dimensions beyond a certain point further complicates the manufacturing of the system, and filtering potentially limits the range of detection.

With correct material selection, the recovery time of the system can be improved without energy draw and material limitations posed by heating to high temperatures. An ideal material would be flexible with minimal adsorption and absorption and with no degassing when heated up. Any material is a compromise between these factors. Typical materials in gas analysis are plastics such as fluoropolymers, metals or ceramics. Steel is typically used in high performance applications where minimal adsorption is critical because of its heat tolerance. In order to further improve the performance of steel, special coatings can also be deployed.

Our team focuses on the development of methods for the analysis of surgical smoke that is produced in electrosurgery operation to classify the tissue types being operated ([5, 6]. The 95% of the mass of surgical smoke is water and the remainder consists of volatile organic compounds (VOCs)

✉ M. Karjalainen
Markus.karjalainen@tuni.fi

[1] Faculty of Medicine and Health Technology, Tampere University, Tampere, Finland

[2] Olfactomics Oy, Tampere, Finland

[3] Centre for Vascular Surgery and Interventional Radiology, Tampere University Hospital, Tampere, Finland

and cellular debris [7]. Majority of VOCs and water is condensed into particulates ([8, 9]. This application area is particularly challenging as the combination of molecular and particulate matter easily condenses into the analytical system causing excessive carry-over effect. The particulates dominate the carry-over through dissolving back to the sample stream after the partial pressure in the stream is decreased below the vapor pressure of the molecules.

There is no literature on optimal material selection for sampling and analysis of surgical smoke. We chose seven common materials used in pneumatics and gas analyzers and evaluated their effect on the recovery times as a function of temperature by using differential mobility spectrometer (DMS).

From physicochemical perspective, we focused on different forms of sorption, namely adsorption, absorption, and desorption. We aimed to find out the sorption properties of the different materials by using the DMS for measuring carry-over after sample introduction.

Materials and methods

Tube materials and tubes

We chose the most common materials used in VOC analyzers for the test tubes: polyether ether ketone (PEEK), polytetrafluoroethylene (PTFE), fluorinated ethylene propylene (FEP), polyethylene (PE), steel 316 L, parylene C coated steel and Silconert® coated steel. The purpose of the Parylene and Silconert® coatings is to reduce the adsorption on the steel tube surface. The length of the test tubes from each material was 30 cm. The length of the test tubes was chosen to reflect the tubing of typical desktop-sized. Tubes had 4 mm Inner diameter (ID) except 3.2 mm PEEK-tube and additional 3 mm ID PTFE-tube.

Comparison of the materials was performed in the procedure and the setup described in Test setup 1. More detailed testing for the effect of temperature on the recovery time was performed for the PTFE tube with the procedure described in Test setup 2.

Test setup 1: Material comparison for recovery times.

The test procedure consisted of two phases: sorption phase by contaminating smoke, and a desorption measurement phase. The smoke production setup consisted of a commercial electrosurgical knife (Itkacut MB350, Innokas Medical, Finland) attached to a stepper motor controlled xyz-stage modified from a 3D printer (REPRAP Mendel Prusa i3, Kitprinter3d, Spain) and a smoke evacuator (Surtron Evac, Quirumed, Spain). The smoke production setup is illustrated in Fig. 1 a). A similar setup has been used in previous studies, where the aim was to identify tissue types by DMS measurements of surgical smoke ([5, 6, 10]. The setup in the desorption and the measurement phase consisted only the individual 30 cm long sample tubes and the DMS device (Envi-AMC, Environics Ltd., Mikkeli, Finland). An illustration of the desorption phase setup is presented in Fig. 1 b). Where six-channel tube holder was attached to setup in sorption phase and single tubes in the measurement phase.

For tube sorption phase, a fresh porcine kidney was cut with the electrosurgical knife. Kidney slices were around 1 cm thick in order to guarantee appropriate cutting depth for the knife. The sample tubes were cleaned with steam after each measurement for approximately two minutes and subsequent drying with pressurized air. This brought the sorption level (described in DMS Sensor section) back to the initial baseline value before the next sorption phase.

The movements of the diathermy knife used in the smoke production phase were controlled with the xyz-stage. The cuts made to the sample were 3 mm deep, 5 mm long. Blade width was 2.35 mm. The surgical smoke evacuator was used to lead the smoke into the tubes as presented in Fig. 1 a). The smoke evacuator was immediately switched off once the smoke production ended to avoid driving excess ambient air through the sample tubes. The six-channel platform holding the sample tubes was then detached from the smoke production setup. The placement of the tubes in the six-channel platform was shuffled between the sorption cycles. Secondly, the sample tube order was shuffled in the measurement phase to take into account that some of the VOCs might desorb from the tubes between sorption and measurement. For reference, we sorbted two samples per material without particulates. This was performed with HEPA-filter between xyz-stage and test tubes.

The actual desorption measurement phase for each tube consisted of three stages:

1. The sample tube was connected to the sample input of the DMS device.
2. For the first 15 s of the 5-min measurement, clean air was measured to provide a baseline reference value for the desorption.
3. The airflow was changed to go through the sample tube for the rest of the measurement. The measurements were conducted in room temperature. Second set of measurements was conducted in a heating cabinet (MICRO, Temperature Applied Sciences (TAS), UK) where the tubes were warmed up at 70 °C for 5 min before the measurement was started. Desorption was approximated to follow first order dynamics, where the time constant τ equals approximately 63% reduction in the intensity from the beginning of the measurement phase. Half-life in first order rate equation compares to time constant with Eq. 1.

$$t_{\S} = \tau * \ln(2) \quad (1)$$

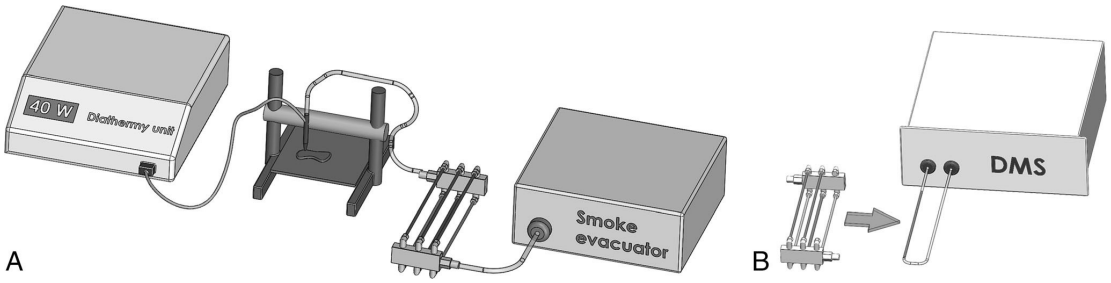

Fig. 1 Test setup 1: a) The sample tubes were connected into a flow divider that had six channels and the tubes were sorbted with surgical smoke from porcine renal tissue. b) Residual molecules were measured from each tube individually with the DMS

Test setup 2: The Effect of Temperature on PTFE recovery.

The second test setup consisted of a single PFTE-tube and a flow rate controller (AS2000, SMC Japan), which were heated to target temperature in a heat cabinet. The flow rate controller was included to simulate typical gas analyzer composition with tubes and other components. The surgical smoke sample was generated with electrosurgical knife and the xyz-stage as in Test setup 1. Since there was no need for changing tubes between sorption and desorption, the desorption phase was begun immediately after the sorption phase.

Figure 2 illustrates the test setup 2. Produced smoke was injected using flow injection principle. In the sorption phase, valve V1 was closed and valve V2 opened, resulting in a flow of 10 l/min from the diathermy system and additional 2 l/min flow from the clean air source. In the desorption phase valve V1 was open and valve V2 was closed causing 1.5 l/min flow through the sample tube from the clean air source. Excess 0.5 l/min clean air flow from 2 l/min was directed to the smoke evacuator.

DMS sensor

Sample tubes were measured with Envi-AMC® (Environics Oy, Finland), a Differential ion Mobility Spectrometer (DMS). It contains a radioactive Americium-241 source to ionize the volatile molecules in the sample gas and a sensor unit, which separates the ions with a high amplitude asymmetric radio frequency (RF) -electric field and a low amplitude DC compensation field. Two-dimensional spectrum is obtained by altering the strength RF of the electric fields and recording the amount of ionized molecules landing on the detector element at each pair of fields. The operation of the DMS is recently presented in detail elsewhere [11].

To assess the desorption, we performed a time series DMS sweep, where the aim was to particularly monitor the release and the amount of the sorbted heavy VOCs, instead of a normal sweep to measure a wide range of substances. For this purpose, the amplitude of the voltage generating the radio frequency field (Vrf) was kept nearly constant, at 450 V - 451 V. The reason for varying the amplitude by one volt was due to technical limitations of the DMS sensor. The compensation voltage (Vc) was scanned from −1 to 5 V in steps of 0.3 V, (Fig. 3). The time constant values were obtained at Vc = −0.3 V.

We analyzed obtained recovery times with Mann-Whitney U-test (MWU) with 95% confidence interval. This means that the statistical difference between the results was analyzed with the Mann Whitney U test, and the presented result of significant statistical difference has a 95% confidence interval. The confidence interval of 95% means that the null hypothesis (the distributions are the same i.e. no statistical difference) is rejected, if the p value from the Mann Whitney U

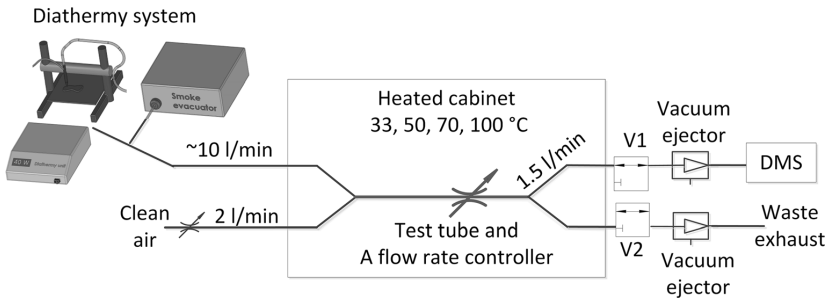

Fig. 2 The test setup for rapid adsorption-desorption cycle in elevated temperatures

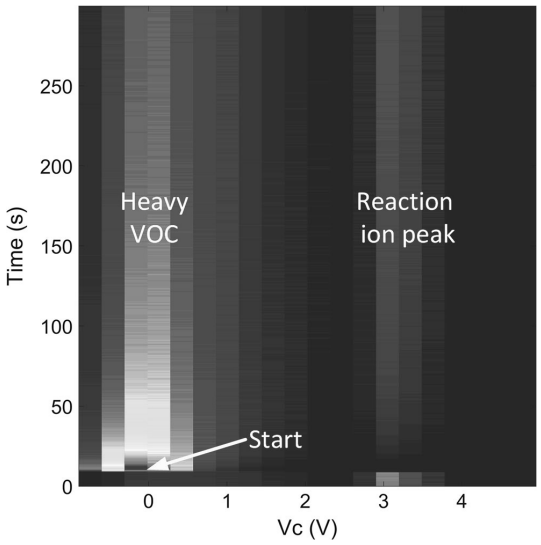

Fig. 3 Typical measurement spectrum from an individual desorption measurement. Scan consist two clusters, excessive undispersed heavy VOC cluster and reaction ion peak (RIP) consisting mainly of ionized water. The discontinuity at the beginning (start) is the moment when toggled to direct sample to DMS

test is under 0.05. In practice this conveys the probability that the portrayed result of statistically significant difference is correct.

Results

Test setup 1: Material comparison for recovery times.

The results of the recovery time measurements for different materials are illustrated in Table 1. Shortest desorption time at room temperature was obtained with a smaller diameter (3 mm) PTFE tube. PEEK tube was next, but it also had a smaller inner diameter than other tubes (3.2 mm compared to the 4 mm in other materials). Uncoated steel tube had the third shortest recovery time. Silconert®-coated and parylene-coated steel were nearly equal in terms of recovery time. Furthermore, the parylene-coating was partially detached during assemblies, which may explain the outliers between the test repetitions (Fig.4). The longest recovery time was obtained with PE-material. From the potential tube materials, diameter (4 mm) PTFE-tube had the worst recovery time. The sample number for FEP material is significantly lower than the rest of the materials, since the material arrived at the final stages of the measurement period. Box plots showing the distribution of the recovery time constants in room temperature are presented in Fig. 4.

We excluded PE-tubes from heated tests after two measurements, since heated PE itself was found to emit plasticizer molecules to the measurement gas. Heated 4 mm PTFE and FEP-tubes performed clearly worse than in unheated case. In opposite parylene-coated steel tube benefited from the heating the most and Silconert®-coated and plain steel tube slightly. Box plots showing the distribution of the recovery time constants in the heated condition are presented in Fig. 5. The measurements in elevated temperature were conducted after the room temperature measurements, and due to limited equipment availability, the sample numbers had to be left lower. Filtering particulates before the sample tubes reduced both recovery times and signal levels. Precisely 63–81% reduction in recovery times and 13–47% reduction in signal peak. The only exception was parylene-coated steel, but this might be due to the coating that had damaged during repetitive testing.

(PEEK) polyether ether ketone, (PTFE) polytetrafluoroethylene, (FEP) fluorinated ethylene propylene, (PE) polyethylene, (S) steel 316 L, (PS) parylene C coated steel, (SS) Silconert® coated steel.

Data in boxplots preferably have N greater than 5. Therefore, we excluded measurement with FEP: 30.5, 26.3, 27.7 s recovery times and 3 mm PTFE: 10.2, 8.8, 12.0, 11.5 s from Fig. 4. In addition, from Fig. 5 FEP: 34.6, 35.5, 26.3, PVDF (3 mm) 6.9, 6.5 s.

Test setup 2: The Effect of Temperature on PTFE recovery.

In test setup 2, the recovery time of a PTFE tube was measured in 33, 50, 70, 100 °C ambient temperature. Recovery time constants for the heated PTFE tubes are presented in Fig. 6.

Statistical analysis

Mann-Whitney U-test was performed for the time constant values to assess the statistical validity of the results gained in this study. A 95% confidence level (i.e. $p < 0.05$) was considered as the threshold for statistical significance. The results are presented in Table 2 and Table 3 for room temperature and 70 °C conditions, respectively. As seen in Table 2, statistically significant difference in the time constants was found between most material pairs. However, PE and PEEK were the only materials that have a statistically significant difference in the clearance time constants in room temperature compared to any other material. In the elevated temperature of 70 °C, statistically relevant differences were only observed between some material pairs, but no material could be completely differentiated, as shown in Table 3.

Table 1 Measured tube recovery times. τ is the recovery time constant in sec. MAX is maximum current signal in the beginning of the measurement. END is the remnant signal after 5 min of the measurement. N is the number of samples measured

	Room temperature				70 °C				HEPA-filtered			
Material	**τ (s)**	**MAX (pA)**	**END (pA)**	**N**	**τ (s)**	**MAX (pA)**	**END (pA)**	**N**	**τ (s)**	**MAX (pA)**	**END (pA)**	**N**
PTFE, 3 mm	10.9	163	23.5	4	6.69	208	51.2	2	–	–	–	–
PEEK, 3.2 mm	16.2	314	62.8	21	15.2	305	98.7	6	6.00	202	82.4	2
S, 4 mm	19.4	290	63.6	18	17.8	280	90.9	6	6.00	153	92.4	2
FEP, 4 mm	27.7	239	33.4	3	34.6	298	76.2	3	7.38	179	70.3	2
PS, 4 mm	30.0	222	63.6	18	14.1	274	86.3	6	35.1	189	89.0	2
SS, 4 mm	31.2	381	66.9	18	30.0	352	90.7	6	10.4	332	83.1	2
PTFE, 4 mm	37.9	319	71.5	20	49.9	294	89.9	8	7.15	210	75.9	2
PE, 4 mm	91.4	221	125	18	NaN	459	425	2	–	–	–	–

Discussion

Recovery time constants

Shortest recovery time for unheated materials was achieved with tubes with smaller diameter, PEEK and PTFE. For the tubes with a larger inner diameter, 4 mm, pure steel tube had the shortest recovery time. In the heated experiment, parylene coated steel performed best. Silconert coating performed worse than pure steel, but may perform better in higher temperatures, since the recommended temperature range of the manufacturer goes up to 450 °C. This could explain the reason why Silconert-coated steel was inferior in terms of recovery times when compared to uncoated steel. The difference between the two materials decreases along with rising temperature and it is possible that Siclonert-coating performs superiorly when temperature is elevated significantly above those used in our study. As demonstrated by these results the inner diameter is a noteworthy factor in terms of recovery time. These results are in line with the results of Dowker and Hardwick [12], where the recovery time was found being dependent on the cross-sectional area of the tubes. In addition, Moschou et al. have showed that the recovery time correlates with the sample flow speed and water evaporation speed correlating sample flow speed [13].

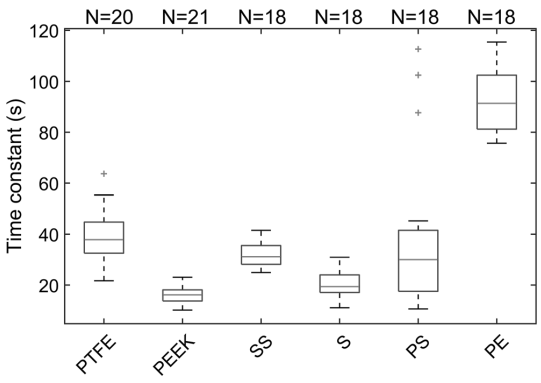

Fig. 4 Distributions of the recovery time constants at room temperature. N is the number of test repetitions

Summary about sorption related factors

Our results showed unexpected effect in the recovery times for PTFE between the heated and the unheated conditions (Fig. 4 and Fig. 5). The recovery times were somewhat slower in the heated test compared to the unheated. In the first experiment, we heated the tubes after the sorption phase for five minutes. This heating time could provide moment for adsorption. The heating increased permeability of PTFE and thus absorption into the tube material due to elevated temperature and relatively long five-minute diffusion time. This could be significant compared to decreased adhesion to the heated plastic surface.

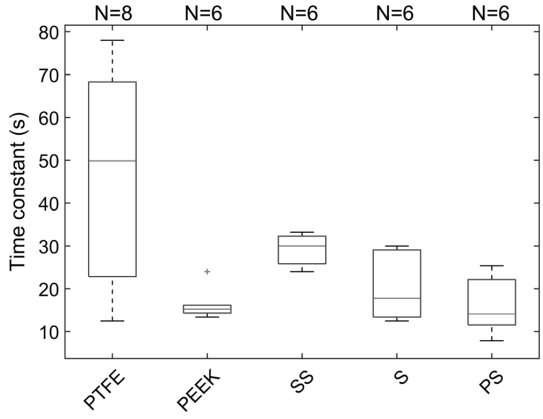

Fig. 5 *Distributions of the recovery time constants at 70 °C temperature.* N is the number of measurements included in the analysis

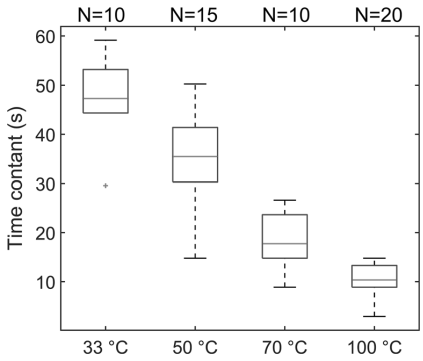

Fig. 6 Recovery time constant of a PTFE tube in various temperatures. Differences were statistically significant between all temperatures, according to Mann-Whitney U test with 95% confidence interval

The effect of increased absorption is also supported by the results obtained in additional PTFE heating test. As shown in Fig. 6, increase in temperature decreased the recovery time, as opposed to Fig. 5, where the tubes had the five-minute heating and an even longer assembly-disassembly period. In the second test (Fig. 6), tubes had only few second transition times and no assembly time. As metals have lower permeability than plastics, this could also explain why metal tubes recovered faster than plastic tube when heated.

In general, the recovery time of a tube depends on the desorption speed and the amount of the contaminating sorption, consisting absorption and adsorption. Adsorption consists of physisorption and chemisorption. We interpreted these results only through physisorption, since we assumed chemisorption to be irrelevant, having too strong bond energies to match these desorption kinetics (Grinham and Chew 2017). Energy in hydrogen bonds in water falls between physisorption and chemisorption. Therefore, steam is convenient for removal of physisorpted molecules. Similarly, we excluded competitive adsorption models, which could be fitted to data in respect of competition between different bond strengths in molecule alignment on surface (Singh et al. 2019). The exclusion was made based on the limited theoretical background and references.

Table 3 The result matrix of the statistical analysis based on the recovery times of the tubes at 70 °C. Table presents P-values, where bolded values indicate a statistically significant difference (MWU 95%-CI)

	SS	S	PS	FEP	PTFE	PEEK
SS		0.0649	**0.0043**	0.2619	0.4136	**0.0043**
S	–		0.3095	0.0952	0.0626	0.4848
PS	–	–		**0.0238**	**0.0293**	0.5887
FEP	–	–	–		0.6303	**0.0238**
PTFE	–	–	–	–		**0.0293**
PEEK	–	–	–	–	–	

The quantity of sorption is the sum of adsorption and absorption. Adsorption is dependent on the surface area, surface free energy of the surface and inversely on the vapor pressure of the adsorpted molecule. [14] In contrast, absorption depends on solubility, permeability and diffusion, ([15, 16], and the quantity of diffused molecules depends on exposure time (Fig.7). Solubility and diffusion are exponentially dependent on temperature [16] [15]. A rule of thumb is that every 10 °C increase in temperature doubles the permeability and therefore absorption as well. The surface free energy, unlike vapor pressure, does not increase dramatically in relation to temperature [17]. Thus, adsorption decreases on elevating temperatures.

The surface free energies of the materials used in this study have substantial differences that can partly explain the changes in recovery times. According to acid-base theorem, surface free energy can be approximated by the single component model where it is divided into dispersive (van der Waals type) and acid and base components [18] [19]. Eq. 2 shows the model for total surface free energy

$$\gamma^{Tot.} = \gamma^{LW} + 2\sqrt{\gamma^{+}\gamma^{-}} \tag{2}$$

, where γ^{LW} is the van der Waals component, γ- is the electron donor component, and $\gamma+$ is the electron acceptor component.

Table 2 The result matrix of a statistical analysis based on the recovery times of the tubes at room temperature. Table presents *P*-values, where bolded values indicate a statistically significant difference with Mann-Whitney U test with 95% confidence interval

	SS	S	PS	PE	FEP	PTFE	PTFE 3 mm	PEEK
SS		**$<10^{-5}$**	0.7042	**$<10^{-5}$**	0.1912	**0.0186**	**0.0025**	**$<10^{-5}$**
S	–		0.0597	**$<10^{-5}$**	**0.0269**	**$<10^{-5}$**	**0.0043**	**0.0071**
PS	–	–		**0.0001**	0.9599	0.1321	**0.0043**	**0.0008**
PE	–	–	–		**0.0077**	**$<10^{-5}$**	**0.0025**	**$<10^{-5}$**
FEP	–	–	–	–		0,0912	0,0571	**0,0068**
PTFE	–	–	–	–	–		**0,0022**	**0,0000**
3 mm	–	–	–	–	–	–		**0.0034**
PEEK	–	–	–	–	–	–	–	

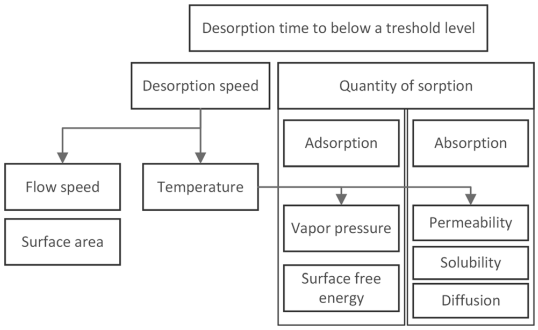

Fig. 7 Estimation schematic for major affecting parameters for tube recovery time

Surface free energy components for steel are γ^{LW} = 38.7 mJ/m^2, γ- = 39.1 mJ/m^2, and y + = 1.4 mJ/m^2 resulting in total surface free energy y^{tot} of 54 mJ/m^2. For PTFE γ^{LW} = 18.1 mJ/m^2, γ- = 2.2 mJ/m^2, and γ + = 0.1 mJ/m^2, thus yielding y^{tot} = 19 mJ/m^2 [20]. According to a single component model parylene has total surface free energy of 27.64 mJ/m^2 [21], FEP 16.9–22.7 mJ/m^2 [22], PEEK 42.4–49.8 mJ/m^2 [23], and PE 31 mJ/m^2 [24].

Since increase in surface free energy increases adsorption, we can conclude that softer materials (less surface energy) adsorb less, but due to the material porosity, they absorb more, especially in higher temperatures. For example, H_2O permeability for PTFE is at 20 °C 0.0045 gmm/m^{2}day, at 40 °C 0.0174 gmm/m^{2}day, and at 80 °C 0.241 gmm/m^{2}day [25, 26]. For metals, the absorption is insignificant.

In addition to surface free energy, the flow speed of the sample and carrier gas is a factor that contributes to the recovery time. More specifically, the flow speed affects to the desorption rate. Lyulin and Kabov described an evaporation correlation as Eq. 3 [27],

$$Q = 1.5{*}10^{-4} T^{1.82} U_g^{0.147} \quad (3)$$

Where Q is the mass flow, T is the temperature in Celsius and U_g is the mass flow in a test chamber. This would imply that the difference between tubes having 4 and 2 mm inner diameter (id) is only 23%, but temperature elevation from 20 to 40 °C produce a 3.5 times faster response. On the contrary [13], studied evaporation where the results indicated that 2 mm (id) tube recovers 4 times faster than a 4 mm tube. This is also closer to the results reported in a study by [12]. We observed a 3.5-fold increase in recovery time, in unheated situation and 7.4-fold increase in heated situation between 4 and 3 mm PTFE tubes being clearly larger than expected.

Figure 7 presents major affecting parameters for tube recovery time. The recovery time depends on desorption speed and the amount of sorption. The sorption can be divided to adsorption and absorption, where vapor pressure and surface free energy affects to adsorption. Permeability, solubility and diffusion affects to absorption. Desorption speed is affected by airflow speed, tube diameter and surface area. In addition, temperature affects to desorption, adsorption and absorption.

Limitations

The key limitation of this study is the relatively small sample size of the different materials in the test setups. The sample size restricted the ability to draw statistically valid conclusions regarding the recovery times between some of the materials. With substantially more measurements, statistically significant differences between more tubing materials could most likely be seen. In addition, some of the parylene coatings partially detached during assembly and might cause some additional adhesion due to the increased surface area. These tests revealed direct desorption time constants for a specific application. However, temperature programmed desorption (TPD) is another possible approach. Using TDB all sorpted substances are desorpted and measured, which should decrease measurement uncertainties.

Conclusions

Optimal tubes should have maximal flow speed, minimal surface area, and minimal adsorption and absorption. Because increase in temperature decreases adsorption but increases absorption and since plastics absorb considerably, there should, in principle be an optimal temperature for the plastics. The exposure time may play a major role in this feature because the adsorption is faster than absorption. Therefore, short exposure times would elevate the optimal temperature for plastics. For metal tubes, the absorption is minimal and therefore there may not be such an optimal temperature. In this case, increase in temperature explicitly improves the performance by decreasing the amount of contamination.

Based on our results, we suggest that people working with gas analyzers would:

1. Use tubes with minimal inner diameter
2. Avoid using PE
3. Use PEEK or fluoropolymers in moderate temperature and demanding applications
4. Use metal tubing's in high performance and high temperature applications

Authors' contributions Markus Karjalainen, experiment design, data collection, data processing, manuscript writing,

Anton Kontunen, experiment design, data collection, data processing, manuscript writing, manuscript revision.

Meri Mäkelä, data collection, manuscript writing.

Osmo Anttalainen, design of experiments, manuscript writing, revision.

Antti Vehkaoja, manuscript writing, manuscript revision.
Niku Oksala, manuscript writing, manuscript revision, support.
Antti Roine, experiment design, manuscript writing, manuscript revision, support.

Funding information This study was financially supported (or partly supported) by The Finnish Cultural Foundation, Pirkanmaa Regional Fund; by The Finnish Foundation for Technology Promotion; by the Competitive State Research Financing of the Expert Responsibility area of Tampere University Hospital (9s045, 151B03, 9T044, 9U042, 150618, 9V044 and 9X040, 9AA057); by Competitive funding to strengthen university research profiles funded by Academy of Finland, decision number 292477; and by Tampereen Tuberkuloosisäätiö (Tampere Tuberculosis Foundation).

Compliance with ethical standards

Conflict of interest Markus Karjalainen, Anton Kontunen, Meri Mäkelä, Osmo Anttalainen, Niku Oksala and Antti Roine are employed by Olfactomics Ltd. Markus Karjalainen, Anton Kontunen, Osmo Anttalainen, Niku Oksala and Antti Roine are shareholders of Olfactomics Oy.

Declarations The funder provided support in the form of salaries for authors M.K., A.K., but did not have any additional role in the study design, data collection and analysis, decision to publish, or preparation of the manuscript. The specific roles of these authors are articulated in the 'author contributions' section. Olfactomics Ltd. did not provide any funding for the study and did not play any role in the study design.

References

1. Armenta S, Alcala M, Blanco M (2011) A review of recent, unconventional applications of ion mobility spectrometry (IMS). Anal Chim Acta 703(2):114–123
2. Röck F, Barsan N, Weimar U (2008) Electronic nose: current status and future trends. Chem Rev 108(2):705–725
3. Giles K, Gordon D (2010) A new conjoined RF ion guide for enhanced ion transmission. In: Proc. 58th ASMS Conf. Mass spectrometry and allied topics
4. Guttman M, Wales TE, Whittington D, Engen JR, Brown JM, Lee KK (2016) Tuning a high transmission ion guide to prevent gas-phase proton exchange during H/D exchange MS analysis. J Am Soc Mass Spectrom 27(4):662–668
5. Haapala I, Karjalainen M, Kontunen A et al (2019) Identifying brain tumors by differential mobility spectrometry analysis of diathermy smoke. J Neurosurg 1:1–7
6. Sutinen M, Kontunen A, Karjalainen M, Kiiski J, Hannus J, Tolonen T, Roine A, Oksala N (2019) Identification of breast tumors from diathermy smoke by differential ion mobility spectrometry. Eur J Surg Oncol 45(2):141–146
7. Ulmer BC (2008) The hazards of surgical smoke. AORN J 87(4): 721–738
8. Brüske-Hohlfeld I, Preissler G, Jauch K-W, Pitz M, Nowak D, Peters A, Wichmann HE (2008) Surgical smoke and ultrafine particles. J Occup Med Toxicol 3(1):31. https://doi.org/10.1186/1745-6673-3-31
9. Karjalainen M, Kontunen A, Saari S, Rönkkö T, Lekkala J, Roine A, Oksala N (2018) The characterization of surgical smoke from various tissues and its implications for occupational safety. PLoS One 13(4): e0195274. https://doi.org/10.1371/journal.pone.0195274
10. Kontunen A, Karjalainen M, Lekkala J, Roine A, Oksala N (2018) Tissue identification in a porcine model by differential ion mobility spectrometry analysis of surgical smoke. Ann Biomed Eng 46(8): 1091–1100
11. Anttalainen O, Puton J, Kontunen A et al (2019) Possible strategy to use differential mobility spectrometry in real time applications. Int J Ion Mobil Spectrom:1–8
12. Dowker K, Hardwick K (2008) RR-635 effect of tubing type on gas detector sampling systems, research reports of health and safety. Executive, UK https://www.hse.gov.uk/research/rrhtm/rr635.htm,
13. Moschou P, de Croon M, Van Der Schaaf J, Schouten JC (2013) Liquid flow rate effects during partial evaporation in a falling film micro contactor. Chem Eng Process Process Intensif 69:95–103
14. Do DD, others (1998) Adsorption analysis: equilibria and kinetics. Imperial college press London
15. Mitchell GD (2000) A review of permeation tubes and permeators. Sep Purif Methods 29(1):119–128
16. Wang X, Wolfbeis OS (2014) Optical methods for sensing and imaging oxygen: materials, spectroscopies and applications. Chem Soc Rev 43(10):3666–3761
17. Rulison C (2006) Effect of temperature on the surface energy of solids. COATING-ST Gall 39:52
18. Van Oss CJ, Good RJ, Chaudhury MK (1986) The role of van der Waals forces and hydrogen bonds in hydrophobic interactions between biopolymers and low energy surfaces. J Colloid Interface Sci 111:378–390
19. Rulison C (1999) So you want to measure surface energy. Charlotte NC (cf p 99)
20. Rosmaninho R, Rizzo G, Müller-Steinhagen H, Melo LF (2003) Study of the influence of bulk properties and surface tension on the deposition process of calcium phosphate on modified stainless steel
21. Chindam C, Lakhtakia A, Awadelkarim OO (2015) Surface energy of Parylene C. Mater Lett 153:18–19
22. Ebnesajjad S, Ebnesajjad C (2013) Surface treatment of materials for adhesive bonding. William Andrew
23. Heimer S, Schmidlin PR, Stawarczyk B (2016) Effect of different cleaning methods of polyetheretherketone on surface roughness and surface free energy properties. J Appl Biomater Funct Mater 14(3):e248–e255
24. Fox HW, Zisman WA (1952) The spreading of liquids on low-energy surfaces. III Hydrocarbon surfaces J Colloid Sci 7:428–442
25. Massarweh NN, Cosgriff N, Slakey DP (2006) Electrosurgery: history, principles, and current and future uses. J Am Coll Surg 202(3): 520–530
26. Massey LK (2003) Permeability properties of plastics and elastomers: a guide to packaging and barrier materials. William Andrew
27. Lyulin YV, Kabov OA (2013) Measurement of the evaporation mass flow rate in a horizontal liquid layer partly opened into flowing gas. Tech Phys Lett 39(9):795–797

PUBLICATION IV

Characterization of signal kinetics in real time surgical tissue classification system

Markus Karjalainen, Anton Kontunen, Anna Anttalainen, Meri Mäkelä, Soma Varga, Maiju Lepomäki, Osmo Anttalainen, Pekka Kumpulainen, Niku Oksala, Antti Roine, Antti Vehkaoja

Sensors and Actuators B: Chemical. 2022 Aug 15;365:131902.

https://doi.org/10.1016/j.snb.2022.131902

Sensors & Actuators: B. Chemical 365 (2022) 131902

Contents lists available at ScienceDirect

Sensors and Actuators: B. Chemical

journal homepage: www.elsevier.com/locate/snb

Characterization of signal kinetics in real time surgical tissue classification system

Markus Karjalainen [a,b,*], Anton Kontunen [a,b], Anna Anttalainen [b], Meri Mäkelä [b], Soma Varga [c], Maiju Lepomäki [d,e], Osmo Anttalainen [b], Pekka Kumpulainen [b], Niku Oksala [b,d,f], Antti Roine [b], Antti Vehkaoja [a]

[a] Sensor Technology and Biomeasurements, Faculty of Medicine and Health Technology, Tampere University, Hervanta Campus, Korkeakoulunkatu 3, FI-33720 Tampere, Finland
[b] Olfactomics Ltd, Kampusareena, Korkeakoulunkatu 7, FI-33720 Tampere, Finland
[c] Pázmány Péter Catholic University, Faculty of Information Technology and Bionics, Budapest Práter u. 50/A 1083, Hungary
[d] Surgery, Faculty of Medicine and Health Technology, Tampere University, Kauppi Campus, Arvo Building, Arvo Ylpön katu 34, FI-33520 Tampere, Finland
[e] Department of Pathology, Fimlab Laboratories, Arvo Ylpön katu 4, FI-33520 Tampere, Finland
[f] Vascular Centre, Tampere University Hospital, Central Hospital, P.O. Box 2000, FI-33521 Tampere, Finland

ARTICLE INFO

Keywords:
Differential ion mobility spectrometry
Surgical margin analysis
Tissue classification
Signal carry-over

ABSTRACT

Effective surgical margin assessment is paramount for good oncological outcomes and new methods are in active development. One emerging approach is the analysis of the chemical composition of surgical smoke from tissues. Surgical smoke is typically removed with a smoke evacuator to protect the operating room staff from its harmful effects to the respiratory system. Thus, analysis of the evacuated smoke without disturbing the operation is a feasible approach. Smoke transportation is subject to lags that affect system usability. We analyzed the smoke transportation delay and evaluated its effects to tissue classification with differential mobility spectrometry in a simulated setting using porcine tissues. With a typical smoke evacuator setting, the front of the surgical plume reaches the analysis system in 380 ms and the sensor within one second. For a typical surgical incision (duration 1.5 s), the measured signal reaches its maximum in 2.3 s and declines to under 10% of the maximum in 8.6 s from the start of the incision. Two-class tissue classification was tested with 2, 3, 5, and 11 s repetition rates resulting in no significant differences in classification accuracy, implicating that signal retention from previous samples is mitigated by the classification algorithm.

1. Introduction

Cancer is a major cause of death and disability. The majority of cancer patients are treated with surgery involving the excision of the tumor with clear margins to ensure that all of the tumor tissue is removed [1]. Margin assessment largely relies on palpation and visual examination by the surgeon in support with imaging (e.g., specimen radiography), frozen section analysis, and imprint cytology. These methods extend the operation time, only partially consider the resection margin, and may even lead to reoperation if the analysis is performed postoperatively. Less applied margin assessment methods include ultrasound imaging, optical methods, and radiofrequency spectroscopy. However, these disturb the normal surgical workflow and hence potentially delay the operation [2]. An ideal method should be accurate and integrate into the existing devices and the surgical workflow.

Schäfer et al. proposed a method based on mass spectrometry (MS), in which the resected tissue is recognized from surgical smoke [3]. Analysis of surgical smoke is compelling since electrocautery is widely used in soft tissue surgery and an analyzer directly coupled with the surgical device could enable thorough margin assessment without disrupting the workflow. Another advantageous aspect is that the means to capture the smoke are already available, as smoke evacuation systems are widely used in operation rooms, and an analyzer could be coupled with these devices enabling contact-free margin assessment.

However, MS is a complex and resource-intensive technology. Our team has developed a differential mobility spectrometry (DMS) based system as a potential and more cost-effective alternative [4–6]. In order to enable the accurate localization and re-incision of the positive

* Correspondence to: Tampere University, Korkeakoulunkatu 6, FI-33101 Tampere, Finland.
E-mail address: markus.karjalainen@tuni.fi (M. Karjalainen).

https://doi.org/10.1016/j.snb.2022.131902
Received 27 December 2021; Received in revised form 7 April 2022; Accepted 12 April 2022
Available online 22 April 2022

margin, the surgeon requires rapid feedback. While the effect of delay has not been studied in this application, even relatively small latencies of 150–700 ms have been shown to affect the surgical performance in telesurgery [7–9]. Both MS and DMS-based systems are subject to delays caused by the limited sample gas flow rate, signal spreading due to flow profile, adhesion of molecules to the tubing as well as computing. Alongside latency, signal carry-over (i.e., the overlap between consecutive samples) is a significant challenge and likely the limiting factor for very fast systems.

The purpose of this study is to experimentally analyze the kinetics of an analytical system consisting of a standard smoke evacuator, sample pre-processing system, and DMS. The findings of this study provide a framework to all gas analysis systems that operate in time-sensitive applications.

2. Materials and methods

2.1. Experimental setup

Our experimental setup consists of commercial diathermy surgery equipment combined with a system intended for diathermy smoke analysis. The setup was constructed with the following devices: Itkacut 350MB diathermy device (Innokas Medical, Finland); *SafeAir® Smoke Evacuator compact* surgical smoke evacuator (Stryker Corp, USA) with a 3-meter surgical evacuation tube and 50 l/min flow rate; Ionvision DMS spectrometer (Olfactomics Oy, Finland); and a custom-made filtration unit. We used commercial porcine muscle and renal tissues purchased from a local grocery store as the test sample.

We applied a nominal cutting power of 40 W and a frequency of 450 kHz to produce electrosurgical incisions to the porcine tissue samples. The surgical smoke produced by the incisions was analyzed by DMS. A DMS sensor device is essentially an electric field-tunable ion filter [9]. The filter has two separation electrode channels sized to $6\times20\times0.25$ mm. Channel doubling enhances sensitivity by doubling the ion flow compared to a single channel. Electrodes are driven with two adjustable electrical field parameters, a high-frequency asymmetric alternating field, and a sequentially tuned constant compensation field. IonVision DMS can be flexibly set-up to sample the datapoints anywhere in its measurement range (any pair of high-frequency and compensation fields). Waveform generation is implemented as direct pulsing without resonators allowing for a rectangular pulse shape. The frequency of the separation field is adjustable from 250 kHz to 1 MHz. In this study, we used 1 MHz frequency. Separation field voltage is software-limited to 1 kV. Analog to digital converter (ADC) sampling rate is 333 kHz and features user-adjustable averaging between 1 and 2^{15} samples. Used averages are presented in Table S1.

We used eleven pre-selected pairs of compensation and separation fields ranging from 0 to 22 V/mm and from 800 to 3668 V/mm, respectively. The field strengths and the number of averaged data points used in this study are provided in Table S1. Each DMS timepoint consisted of eleven datapoints from the positive and eleven datapoints from the negative ions. A small number of measurement points was used to enable high temporal sampling rate. We used forward feature selection from a detailed scan to select the used voltage pairs [10].

The filtration unit was an in-house developed prototype, of which the main purpose was to remove smoke particulates and deliver molecules to the spectrometer. The measurement setup is shown in Fig. 1. Transfer delays are estimated between the surgical scalpel, the filter and the spectrometer unit.

2.2. Description of variables

Time-dependent signals from the experiment setup were:

1. The diathermy current, which indicated the current flown through the porcine tissue
2. The corona discharge current in the filtration unit, in which the current was relative to the amount of smoke particulates and molecules
3. The DMS response to molecules. From these we derived six numerical indicators expressing the delay.

These times are illustrated in Fig. 1 and presented in Table 1.

2.3. Experiments

Two separate experiments were conducted to study the transfer line characteristics (the delays) and to assess the effect of delay on the performance of tissue classification. The experiments were executed with a fixed time delay to study transfer line kinetics and with a varying delay to assess its effect on classification. Data was captured with 3.7 Hz frequency in all experiments. The performance of tissue classification was evaluated using a shrinkage linear discriminant analysis (sLDA) model.

2.3.1. Time series with fixed delays – kinetics testing dataset

The first dataset comprised tissue vapor impulses from 1.5 s electrocautery incisions to porcine renal cortex and skeletal muscle in a randomized order. Examples of data generated in this test are illustrated in Fig. 1. We repeated the incisions 50 times in 20 s intervals. Intervals were kept even so that all the remnants from the previous cut dissipated.

2.3.2. Time series with varying delays – impulse interference effect for classifier

To study the effect of sampling (incision) intervals on the classification, we created a dataset in which the delays between the 1 s incisions varied between 2 s and 11 s (2, 3, 5, and 11 s). The one second incision duration was chosen to simulate a surgical procedure. Porcine renal cortex and skeletal muscle were incised in a randomized order. The dataset included ten subsets. Each of the first five subsets included twenty incisions, between which the order of the delays was the same for each repeat. The order of the tissues was the same for the first three and the next two sets.

For the latter five subsets, the order of the delays and tissues was randomized separately for each set. Also, the number of incisions was increased to 21 to fit 20 spaces in each set as illustrated in Fig. 2.

2.4. Data analysis

2.4.1. Impulse response shape analysis

We studied the structure of signal tailing with curve fitting to understand the overall system behavior. An accurate tailing function would benefit the system simulations in later studies. Four different distribution functions were fitted to the averaged intensity responses obtained with the DMS data from 50 incisions. The distributions were inverse gaussian, Lévy distribution, lognormal distribution, and geometric Brownian motion distribution. Signals were synchronized by the time of a threshold crossing at the rising edge of a signal. For diathermy, we used a multiplier of 1.1 from the baseline level as the threshold level and for DMS, a multiplier of 1.6. The duration of the cuts varied around the targeted 1.5 s, which led to accumulation in the averaged peak shapes.

2.4.2. Temporal classification

In the analysis of time dependency on tissue classification, we used leave-one-set-out as the cross-validation method. On each round, four sets were used as the training set and the fifth dataset was in turn assigned as the testing set. The datasets consisted of 50 randomized samples of porcine renal tissue and 50 randomized samples of porcine muscle. The intensity peaks were isolated to use individual time points for tissue classification. To remove linear drifting during the data collection, the data was detrended pixelwise based on the baseline values before each incision. For each time point in the extracted and

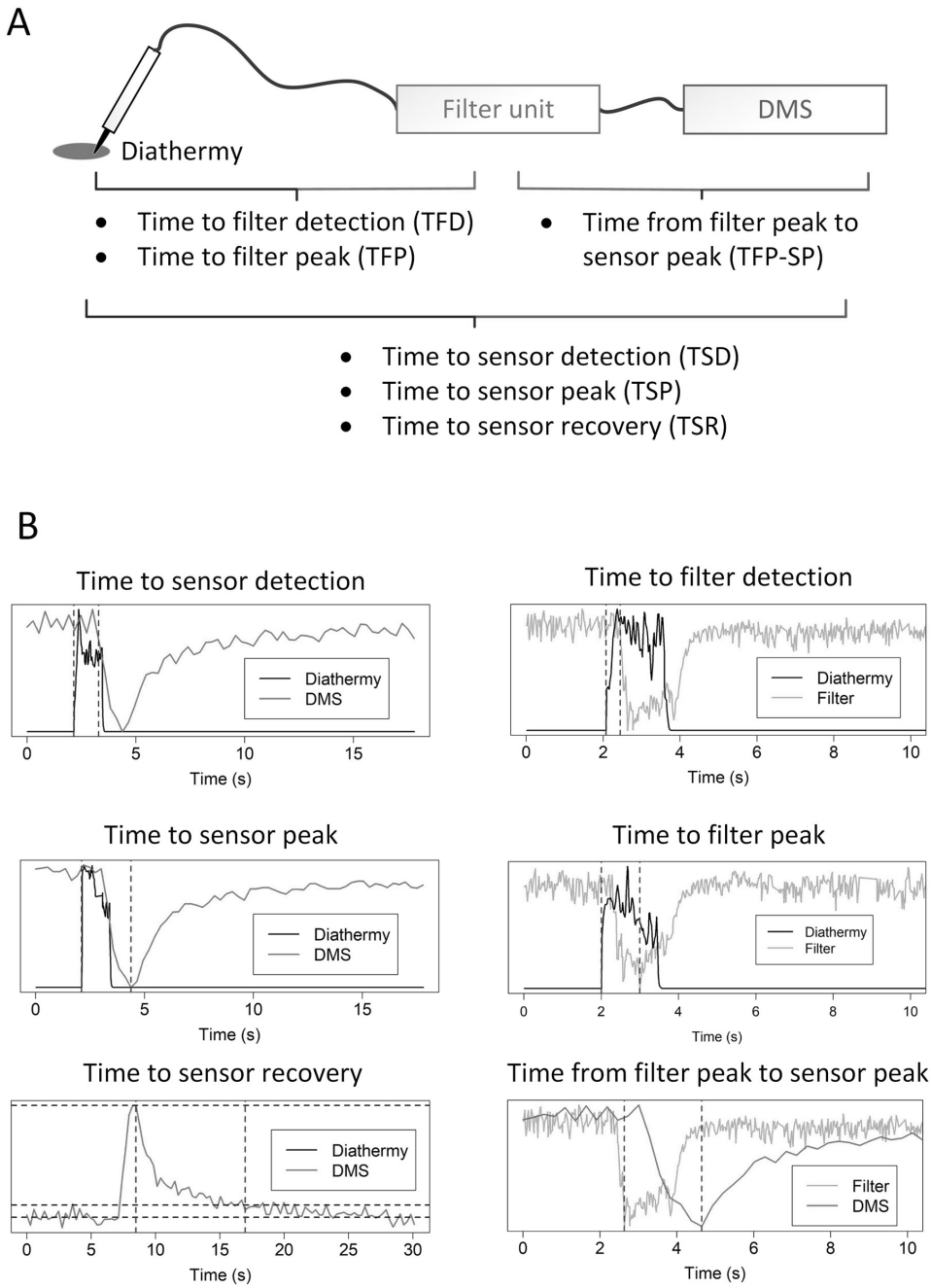

Fig. 1. Figurative explanations for the six delay indicators characteristic to each transfer line (A) and example signals visualizing the delays (B). Time to sensor detection describes the delay from the surgical incision to the first response in the DMS. Time to filter detection describes the time from the surgical incision to the filter unit. This is roughly the delay in the surgical tube. Time to sensor peak describes the delay from the incision to the peak response in DMS. Time to filter peak describes the delay from the incision to the strongest response in the filter unit. Time to sensor recovery describes the delay from the maximum signal to the 10% level of the baseline. Time from filter peak to sensor peak describes the delay in the device without the surgical tube.

Table 1
Delay indicators used to characterize and quantify transport kinetics.

Indicator	Description
Time to sensor detection (TSD)	Delay from the beginning of the dissection to the beginning of the DMS response
Time to sensor peak (TSP)	Delay from the beginning of the dissection to the DMS signal maximum
Time to sensor recovery (TSR)	Decay time from the DMS signal maximum to the 10% level from the baseline
Time to filter detection (TFD)	Delay from the dissection beginning to the first response in the filter
Time to filter peak (TFP)	Delay from the dissection beginning to the maximum corona filter current
Time from filter peak to sensor peak (TFP-SP)	Delay between the corona filter maximum current and the DMS maximum signal

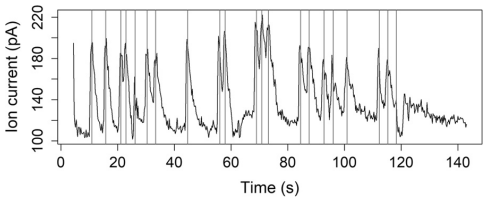

Fig. 2. One fifth of the randomized delay dataset from a single voltage pair channel. Red vertical lines indicate peaked signals, where classification is analyzed.

synchronized signals, separate, cross-validated (sLDA) classification models were created, and the classification accuracy was reported as a function of time from the peak signal strength. Impulse tailing interferes with later impulses. Therefore, we also studied how these earlier impulses affect the classification results. We studied how the classifier performs as a function of the time from the previous signal peak at the highest intensity value. In this analysis, the classifier was also trained with the leave-one-set-out method.

2.4.3. Similarity metrics between tissue types

To evaluate the generalizability of animal tissue signal kinetics to actual surgery, we compared our data to measurements from a separate study with malignant and benign breast tissues [11]. These tissue samples were vaporized by a CO_2-laser and analyzed with DMS. The samples included 192 measurements from two breast cancer specimens. We estimated the similarity between malignant and benign breast tissue, and between muscle and renal tissue by using the Euclidian distance of the classes from the respective archetypes (mean spectrums) of benign breast tissue and renal tissue. The Euclidean distance depicts the shortest distance between the two data vectors and can thus be used to estimate the relative differences of sample distributions [12]. If the relative differences between the tissue types are similar, we can expect similar temporal classification behavior.

3. Results

3.1. Delay induced during sample transfer

After sample incision, the first response is measured from the diathermy current probe. Second, as the smoke reaches the filter unit, the current in the corona discharge changes. Last, the molecules reach the DMS sensor unit. The delayed signal is illustrated in Fig. 3.

The smoke evacuator tube used in the study was three meters long with a 10 mm inner diameter. Thus, the volumetric flow rate would approximate to 50 l/min and the travel time of an ideal plug flow to 300 ms. However, we recorded a mean delay of 340 (SD 170) ms. Similarly, an ideal plug flow from the corona discharge of the filter to

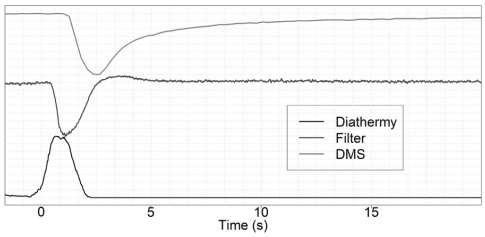

Fig. 3. Averaged and synchronized molecular transfer delays in the surgical sampling system.

DMS detection would be 350 ms. However, the recorded delay (TSD-TFD) was more than 700 ms.

The first detectable signal in the DMS was measured 1.1 (SD 0.3) seconds after the beginning of cutting. Then, the intensity increased for approximately 1.2 s and diminished to under 10% from the maximum within 8.2 (SD 2.3) seconds. All measured delays had outliers due to irregularities in the manual sampling. The delay distributions are presented as boxplots (Fig. 4).

We modeled the averaged impulse response with four heavy tailed distributions. The best fit was obtained with the Lévy distribution, a special case of inverse gaussian distribution, followed from a Lévy random walk [13] The result is illustrated in Fig. 5. Other functions included the Log-normal, which is a maximum entropy probability distribution, and Geometric Brownian motion distribution, which follows the random walk with a gaussian distribution. The residual standard errors for the fittings were as follows: Lévy distribution 0.030, Inverse gaussian 0.037, Log-normal 0.047, and geometric Brownian motion 0.052, respectively. None of the fitting functions managed to describe the extra heavy tail after the peak well. The properties of the handmade input impulse affected the signal. The duration and the incision depth varied considerably and thus affected the sample concentration.

Based on the impulse response test, the classification accuracy of renal cortex and skeletal muscle correlated with the average signal intensity of the test set with some delay (Fig. 6). However, decaying of the signal weakened the classification. Many of the 11 voltage pair channels on higher separation field values posed lower signal-to-noise ratios than the channel illustrated in Fig. 6. Although an increase in the DMS separation field enhances ion cluster separation, it simultaneously decreases ion passing. As high electric field increases the movement amplitude of the ions it concurrently increases the probability of ion collisions to the separation electrodes, which neutralizes the ions. This phenomenon decreases the signal strength. It is noteworthy that there is similarly a high time-dependent noise in the classification accuracy.

3.2. The effect of signal carry-over on the classification accuracy

The measurements concerning the effect of carry-over on the classification accuracy did not reveal a specific threshold time for unsuccessful classification. We utilized variable delay times and the classification was tested at peak intensities (Fig. 2). For 2, 3, 5, and 11 second intervals, there were no statistically significant differences. Both datasets consisted of 25 points per delay value. Classification accuracies are presented in Table 2. Herein, all ten partially and totally randomized subsets are combined. The results showed no observable trend as a function of delay time. It is worth noting that these delay times were instructed to the knife operator. Due to the manual operation, the actual delay times had some variance. These delay time distributions are presented in the supporting material Fig. S1. The distributions revealed few outliers caused by errors in the manual sampling. In addition, the correlation between the actualized delay times and the classification showed no clear bias (Fig. S2).

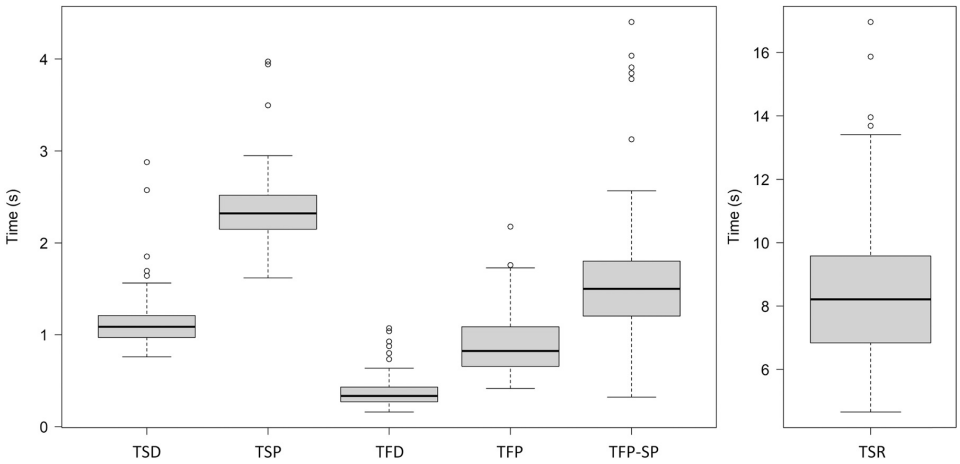

Fig. 4. Distributions of the delay indicator values are illustrated as boxplots. The dataset delay distributions are illustrated for each indicator parameter.

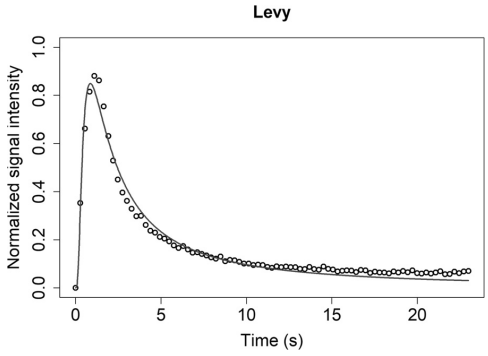

Fig. 5. Curve fitting for the sum of positive ions. The best fit was obtained using the Lévy distribution, a special case of inverse gaussian distribution.

3.3. Tissue type Euclidian distances

The relative differences in the Euclidian distances between malignant and benign breast tissues and the porcine tissues were alike (Fig. 7). Median Euclidian distance of individual malignant tissue samples to benign archetype was 0.59, and for benign tissue samples 0.44. The median Euclidian distance of individual muscle tissue samples to kidney archetype was 0.92, and individual kidney samples to kidney archetype 0.83. This finding suggests that the results of the study are also expected to be generalizable to clinically relevant tissues.

4. Discussion

In this study we shed light on the kinetics of gas detector systems for surgical tissue assessment with a well-controlled mechanistic model. The characteristics of the system are well comparable to those documented with mass spectrometers and further validate the potential of these technologies in surgical use.

Delay in the sample analysis greatly affects the usability and practical applicability of the device. We observed an average delay of 1.12 (SD 0.3) seconds from tissue contact to sensor detection. This is comparable to mass spectrometer-based systems, such as the iKnife system which has a delay from 0.7 to 2.5 s [14] or 1.8 (SD 0.40) seconds [15],

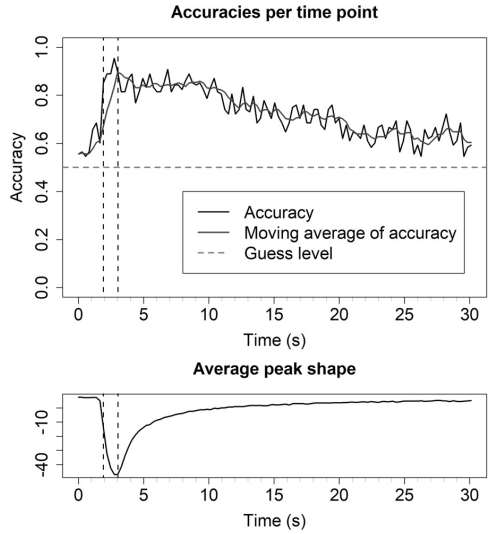

Fig. 6. The classification accuracy for impulse response. A decaying signal weakened the classification accuracy. After 7–8 s from the impulse peak, the classification accuracy decreased significantly. The average peak shape with the separation voltage (Usv) of 200 V and compensation voltage (Ucv) of 0.5 V.

Table 2
The classification accuracies alongside 95% confidence intervals for different delay times. Notably, there are no statistically significant differences in the accuracies.

Delay	Accuracy	95% confidence interval lower limit	95% confidence interval upper limit
1 s	0.74	0.56	0.85
2 s	0.80	0.66	0.90
4 s	0.82	0.69	0.91
10 s	0.71	0.56	0.84

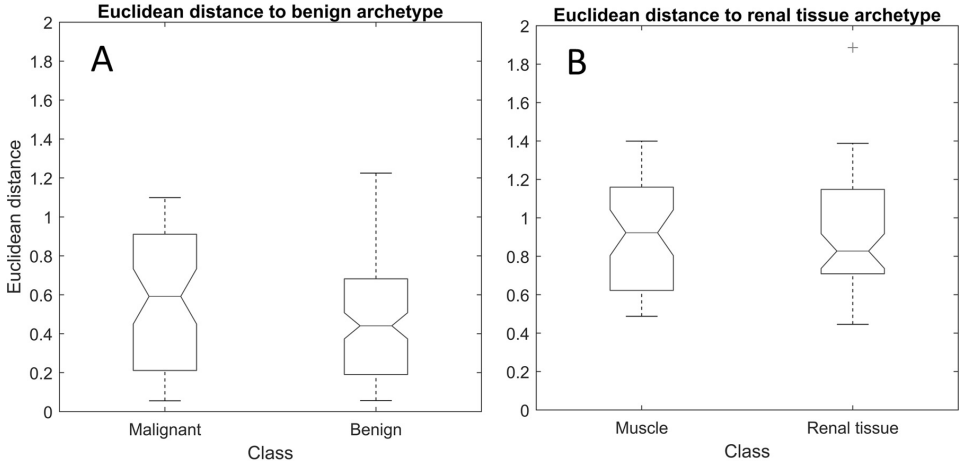

Fig. 7. A) The distributions of the Euclidian distances between malignant and benign breast tissue compared to the benign archetype. B) The distributions of the Euclidian distances between muscle and renal tissue compared to the renal tissue archetype.

but is greater than delays documented for SpiderMass system (0.4 s ± 0.1) [16]. In contrast to our system, which is an add-on to existing smoke evacuators, the iKnife and Spidermass utilize integrated tubing to enable the control of the tube diameter and flow rate. This evidently improves the time to detection. In this study, the TFD was less than half of the TSD implicating that the majority of the delay originated from the pneumatics of the prototype system. In addition to the smoke arrival delay, there is a data acquisition delay of around 200 ms and a data processing delay of around one second in our prototype system. However, these delays can be largely eliminated by increasing computing power and optimizing communication.

Even though the time to detection is rapid and sufficient for clinical use, the residual time of the molecules in the system is long at 8.6 s. This finding is in line with a previous MS study, where increase in the flow rate had a lesser effect on the retention time than on the time to detection [16]. Practical real-time use requires an ability to tolerate signal carry-over to an extent. We assessed this perspective by conducting electrocautery incisions in a random order with randomized delays on two different tissues. Surprisingly, we observed similar classification accuracies across the sampling intervals from 2 to 11 ss with a relatively simple sLDA model despite significant carry-over from the previous measurements. However, we hypothesize that the performance would decay at intervals below 2 s. The achieving of such sub-second intervals with a similar study setup would require computer-controlled sampling which may otherwise not be comparable to a human user. Additionally, impulse type sampling is likely easier to classify than a smooth transition from one tissue to another. The reality during surgery is between these two cases. In a study observing electrocautery activation patterns by consultants and specialists, Meeuwen et al. documented average activation times from 1.4 to 2.3 s [17], resembling more pulsed than continuous smoke production. This is in line with our observations of the system in operation theatre use [18].

As illustrated in Fig. 6, the best classification performance was obtained at the signal peak at 1.1 s after initial detection. This is theoretically the optimal time point for classification due to its high signal-to-noise ratio. Correct classification is therefore possible very shortly after detection, which is ideal for practical use. It is worth noting that the classification accuracy does not decrease along with the decaying signal strength. Rather, there seems to be a minimum requirement for signal strength. In contrary to our expectations, the classification accuracy did not improve with longer recovery delays between cuts. The absolute rate of correct classification remained modest especially for fully randomized delay. This is likely due to the relatively small sample size that does not enable the classifier to reach its full potential. However, the sample size is sufficient to detect the practically meaningful rate of relative classification between delays.

We found no relevant studies related to the effect of surgical margin detection latency on the usability of a surgery assisting device. Literature on latency focuses on telesurgeries, in which the acceptable latency is less than one second [8]. Considering only the time to detection, a latency in this range can be reached whereas taking the retention time into account, we consider a 2–3 s latency realistic for pneumatic systems like DMS and MS. As surgeons typically cut tissues at a pace of 5–15 mm/second [19,20], this latency is acceptable for the intended purpose of alarming of a positive margin during cancer surgery.

The analysis of kinetics in this study was conducted exclusively with benign porcine tissues. In order to assess the generalizability to relevant cancerous tissues, we conducted a similarity analysis of data from cancerous tissues and of porcine tissues in this study. The finding that the difference between grossly malignant and benign tissue is larger than the difference between kidney and muscle tissue is intuitively surprising but is likely explained with heterogeneity of healthy tissue. Additionally, molecular profiling studies have demonstrated pan-cancerous characteristics that exceed the difference between organs. Nevertheless, the findings should be interpreted cautiously and confirmed with more extensive experiments with both benign and malignant human tissues. [21,22].

In order to build a theoretical model for kinetics of surgical smoke analysis systems, we studied the distributions of the signals. Farsad et al., 2013 [23] and Na-Rae et al., 2018 [24] studied chemical pulse transfer under forced flow in ambient air without tubes. Due to diffusion, the impulse response should follow inverse gaussian distribution in forced flow and Lévy distribution when there is no flow [25]. However, in our application and experiment setup, forced flow in a tube was used. These conditions introduced additional effects, namely turbulence and sorption-desorption events to tube walls, into the setting. In sorption-desorption interaction, molecules hit and stick to the tube walls, which delays and stretches the chemical signal. Therefore, we can assume that the signal tail lasts longer than commonly used heavy tailed distributions can estimate. We discovered that the Lévy distribution, which is characterized by a heavy tail, described our system the best, but still lacked heaviness in the tail. We did not try any function combinations to improve the fitting. Another explanation for curve mismatch could be the long nonideal input impulse. In addition to impulse

response, the tube material, size, and temperature affect the overall delay [26]. An accurate model would be beneficial for the simulation of the system behavior.

The sample size was limited, which limits the reliability of the results, since noise and other sporadic system variations may have affected the results. sLDA classifier boundaries are in a linear dimensional space so it can only respond linearly to nonlinear phenomena. Other methods, such as convolutional neural networks (CNNs), could provide different results in terms of the effect of delay on the classification accuracy but require larger data sets to operate sufficiently [6] Therefore, they were not evaluated in the study. In addition, manual sampling has limitations in its accuracy and reliability. However, these accuracy related factors unlikely affected the main conclusions of this study.

The delay comparison between the filter current and the DMS is not straightforward. If a molecule hits the tube wall, it is delayed. In contrast, particulates stick to the wall permanently. Therefore, the particulate signal consists only of non-delayed particulates and the molecular signal is slower than the particulate signal. In other words, the particulate signal does not have a heavy tail. In addition, particulates attached to the tube walls emit molecules. These factors enhance the difference between the filter and the DMS response. The filter responds to both molecules and particulates whereas the DMS responds only to molecules. In addition, in the filter, particulates decrease current caused by ion mobility, and molecules increase the mobility. This causes the two-directional response seen in Fig. 3 filter current.

5. Conclusions

The studied surgical smoke detection system has low latency on signal detection but suffers from long retention times. Surprisingly, the retention time does not have a significant effect on the correct classification rate. The sample impulses produce heavy tailed responses, which are best described by the Lévy distribution, although still lacking heaviness in tailing. The delays exhibited by the smoke analysis system are comparable to MS-based methods and are short enough to enable the surgical application of tissue identification based on surgical smoke. However, to maximize the applicability of the surgical smoke detection systems, a thorough optimization of tubing lengths, flow control, and computational integration are required.

CRediT authorship contribution statement

Markus Karjalainen: Conceptualization, Investigation, Writing – original draft. **Anton Kontunen:** Investigation, Validation, Formal analysis, Writing – review & editing, **Anna Anttalainen:** Software, Validation, Data curation, Visualization, Writing – review & editing. **Meri Mäkelä:** Investigation, Data curation, Writing – review & editing, **Varga Soma:** Investigation, Validation, Writing – review & editing. **Maiju Lepomäki:** Investigation, Formal analysis – review & editing. **Osmo Anttalainen:** Resources, Writing – review & editing. **Pekka Kumpulainen:** Validation, Investigation, Writing – review & editing. **Niku Oksala:** Resources, Supervision, Funding acquisition, Review & editing. **Antti Roine:** Conceptualization, Supervision, Writing – original draft and Review & editing. **Antti Vehkaoja:** Supervision, Project administration, Writing – review & editing.

Declaration of Competing Interest

The authors declare the following financial interests/personal relationships which may be considered as potential competing interests: Markus Karjalainen reports a relationship with Olfactomics Ltd. that includes: employment and equity or stocks. Anton Kontunen reports a relationship with Olfactomics Ltd. that includes: employment and equity or stocks. Anna Anttalainen reports a relationship with Olfactomics Ltd. that includes: employment. Meri Makela reports a relationship with Olfactomics Ltd. that includes: employment. Osmo Anttalainen reports a relationship with Olfactomics Ltd. that includes: employment and equity or stocks. Pekka Kumpulainen reports a relationship with Olfactomics Ltd. that includes: employment and equity or stocks. Niku Oksala reports a relationship with Olfactomics Ltd. that includes: equity or stocks. Antti Roine reports a relationship with Olfactomics Ltd. that includes: employment and equity or stocks.

Acknowledgements

Markus Karjalainen declares funding from The Finnish Cultural Foundation, Pirkanmaa Regional Fund, Finland. Anton Kontunen declares funding from the Doctoral School of the Faculty of Medicine and Health Technology, Tampere University, and Emil Aaltonen Foundation, Finland (Grant number 210073). Maiju Lepomäki declares funding from the Doctoral School of Tampere University, the Finnish Medical Foundation (Grant numbers 2167, 4038), and Cancer Foundation of Finland. Niku Oksala declares funding from Competitive State Research Financing of the Expert Responsibility area of Tampere University Hospital, Finland (Grant numbers 9s045, 9T044, 9U042, 150618, 9V044, 9 ×040, 9AA057, 9AB052 and MK301); from Competitive funding to strengthen university research profiles funded by Academy of Finland, Finland, decision number 292477; and from Tampereen Tuberkuloosisäätiö (Tampere Tuberculosis Foundation). Olfactomics has received funding from the European Union's Horizon 2020 research and innovation programme, EU under grant agreements No 848682.

The study sponsors did not have any involvement in the study design; collection, analysis, and interpretation of data; the writing of the manuscript; or the decision to submit the manuscript for publication.

Appendix A. Supporting information

Supplementary data associated with this article can be found in the online version at doi:10.1016/j.snb.2022.131902.

References

[1] B.W. Maloney, D.M. McClatchy III, B.W. Pogue, K.D. Paulsen, W.A. Wells, R. J. Barth, Review of methods for intraoperative margin detection for breast conserving surgery, J. Biomed. Opt. 23 (10) (2018), 100901.
[2] J. Schwarz, H. Schmidt, Technology for intraoperative margin assessment in breast cancer, Ann. Surg. Oncol. 27 (2020) 2278–2287.
[3] K.-C. Schäfer, et al., In vivo, in situ tissue analysis using rapid evaporative ionization mass spectrometry, Angew. Chem. Int. Ed. 48 (44) (2009) 8240–8242.
[4] M. Sutinen, et al., Identification of breast tumors from diathermy smoke by differential ion mobility spectrometry, Eur. J. Surg. Oncol. 45 (2) (2019) 141–146.
[5] I. Haapala et al., "Identifying brain tumors and healthy brain tissue by direct ion mobility spectrometry analysis of diathermy smoke," 2017.
[6] A. Kontunen, et al., Real time tissue identification from diathermy smoke by differential mobility spectrometry, IEEE Sens. J. 21 (1) (2020) 717–724.
[7] A. Kumcu, et al., Effect of video lag on laparoscopic surgery: correlation between performance and usability at low latencies, Int. J. Med. Robot. Comput. Assist. Surg. vol. 13 (2) (2017), e1758.
[8] F. Richter, Y. Zhang, Y. Zhi, R.K. Orosco, and M.C. Yip, "Augmented reality predictive displays to help mitigate the effects of delayed telesurgery," in 2019 International Conference on Robotics and Automation (ICRA), 2019, pp. 444–450.
[9] M.D. Fabrlzio, et al., Effect of time delay on surgical performance during telesurgical manipulation, J. Endourol. 14 (2) (2000) 133–138.
[10] M. Sutinen et al., "Identifying breast tumors and healthy breast tissue by differential ion mobility (DMS) spectrometry analysis of diathermy smoke (Talk)," 2017, [Online]. Available: http://cofa.uta.fi/admin_cofa/wp-content/uploads/2017/04/BMT-MED-Research-Day-2017_Abstracts3.pdf.
[11] L. Maiju, et al., Laser desorption tissue imaging with Differential Mobility Spectrometry, Exp. Mol. Pathol. (2022), 104759.
[12] J. Virtanen, et al., Differentiation of aspirated nasal air from room air using analysis with a differential mobility spectrometry-based electronic nose: a proof-of-concept study, J. Breath. Res. 16 (2021).
[13] A.V. Chechkin, R. Metzler, J. Klafter, V.Y. Gonchar, Introduction to the theory of Lévy flights (and others), Anomalous Transp. 129 (2008).
[14] J. Balog, et al., "Intraoperative Tissue Identif. Using Rapid Evaporative Ioniz. Mass Spectrom.," vol. 5 (194) (2013) 194ra93, doi: 10.1126/SCITRANSLMED.3005623.
[15] E.R. John St, et al., "Rapid evaporative ionisation mass spectrometry of electrosurgical vapours for the identification of breast pathology: towards an intelligent knife for breast cancer surgery, Breast Cancer Res. 19 (1) (2017) 1–14.
[16] B. Fatou, et al., In vivo real-time mass spectrometry for guided surgery application, Sci. Rep. 6 (1) (2016) 1–14.

[17] F.C. Meeuwsen, A.C.P. Guédon, E.A. Arkenbout, M. van der Elst, J. Dankelman, J. J. Van Den Dobbelsteen, The art of electrosurgery: trainees and experts, Surg. Innov. 24 (4) (2017) 373–378.
[18] A. Kontunen, et al., Tissue identification from surgical smoke by differential mobility spectrometry: an in vivo study, IEEE Access (1) (2021) doi: 10.1109/ACCESS.2021.3136719.
[19] J. Liboon, W. Funkhouser, D.J. Terris, A comparison of mucosal incisions made by scalpel, CO_2 laser, electrocautery, and constant-voltage electrocautery, Otolaryngol. Neck Surg. 116 (3) (1997) 379–385.
[20] S.T. Vedbhushan, M.A. Mulla, D.M. Chandrashekhar, Surgical incision by high frequency cautery (and others), Indian J. Surg. 75 (6) (2013) 440–443.
[21] K.A. Hoadley, et al., Cell-of-origin patterns dominate the molecular classification of 10,000 tumors from 33 types of cancer, Cell 173 (2) (2018) 291–304.
[22] E. Reznik, et al., A landscape of metabolic variation across tumor types, Cell Syst. 6 (3) (2018) 301–313.
[23] N. Farsad, W. Guo, A.W. Eckford, Tabletop molecular communication: Text messages through chemical signals, PLoS One 8 (12) (2013), e82935.
[24] N.-R. Kim, N. Farsad, C. Lee, A.W. Eckford, C.-B. Chae, An experimentally validated channel model for molecular communication systems, IEEE Access 7 (2019) 81849–81858.
[25] Y. Murin, N. Farsad, M. Chowdhury, and A. Goldsmith, "Communication over diffusion-based molecular timing channels," in 2016 IEEE Global Communications Conference (GLOBECOM), 2016, pp. 1–6.
[26] M. Karjalainen, et al., Recovery characteristics of different tube materials in relation to combustion products, Int. J. Ion.-. Mobil. Spectrom. (2020) 1–8.

Markus Karjalainen received the M.Sc. degree in automation engineering from the Tampere university of Technology, Finland, in 2007. He is currently pursuing the D.Sc. degree with the Faculty of Medicine and Health Technology, Tampere University, Finland. From 2006–2017, he was with the Department of Automation Science and Engineering, Tampere University of Technology. He also works as a Hardware Engineer in a university spin-off company, Olfactomics Oy, Tampere, Finland. His research interests include chemical communication and sensor technology.

Anton Kontunen received the B.Sc. and M.Sc. degrees in bioengineering from the Tampere University of Technology, Finland, in 2015 and 2017, respectively. He received the D. Sc. degree from the Faculty of Medicine and Health Technology, Tampere University in 2022. From 2014–2017, he was a Research Assistant with the Department of Automation Science and Engineering, Tampere University of Technology. He also works as a System Engineer in a university spin off company, Olfactomics Oy, Tampere, Finland. His research interests include biomedical engineering, sensor technology, and data science.

Anna Anttalainen received the B.Sc. degree in bioinformation technology (major in computational and cognitive biosciences) and the M.Sc. degree in life science technologies (major in complex systems) from Aalto University, Finland, in 2016 and 2019, respectively. From 2014–2016, she was a Research Assistant with the Department of Neuroscience and Biomedical Engineering. From 2016–2019, she was an Assistant Teacher for a mathematical modeling course with Aalto University. She is currently pursuing a career in data science in Medaffcon Oy, Espoo, Finland. Her research interests include machine learning with a focus on neural networks.

Meri Mäkelä received the M.Sc. degree in bioengineering (major in bio measurements and bioimaging) from Tampere University in 2020. She also works as a usability engineer in a university spin-off company, Olfactomics Oy, Tampere, Finland.

Soma Varga received B.Sc. degree in biochemical engineering and M.Sc. degree in Biotechnology from the Budapest University of Technology and Economics, Hungary, in 2019 and 2021, respectively. He is currently pursuing the PhD. degree in Pázmány P é ter Catholic University, Faculty of Information Technology and Bionics. He was an exchange student as Biomedical Engineer in Tampere University, Finland in 2021. His research interests include spectroscopy, bioinformatics and biotechnology.

Maiju Lepomäki received the M.D. degree from Tampere University in 2018. She is currently pursuing the Ph.D. degree in medicine with the Faculty of Medicine and Health Technology, Tampere University. Since 2020, she has worked as a specializing physician at Fimlab Laboratories in the Department of Pathology. Her research interests are breast pathology, surgical oncology, and novel technologies in surgical margin assessment

Osmo Anttalainen received the M.Sc. degree in energy technology from the Lappeenranta University of Technology, Finland, in 1992. From 1994–2018, he was with Environics Oy, Mikkeli, Finland. He is currently continuing his career in a university spin-off company, Olfactomics Oy, Tampere, Finland. His research interests include ion mobility spectrometry and mixed signal electronics.

Pekka Kumpulainen received the M.Sc. and the D.Sc. (Tech.) degrees from the Tampere University of Technology in 1994 and 2014, respectively. From 1992–2019, he was with the Department of Automation Science and Engineering, Tampere University of Technology. Since 2019 he has been working as an independent consultant in data analytics.

Niku Oksala received the M.D. and Ph.D. degrees in medicine and experimental surgery from the University of Eastern Finland in 2000 and 2003, respectively, and the D.Sc. (Med.) degree in molecular biology from Tampere University, Finland, in 2009. Since 2007, he has been a Consultant Vascular Surgeon and a Clinical Teacher. Since 2014, He is currently a Professor of Vascular Surgery with the Faculty of Medicine and Health Technology, Tampere University, and also a Chief Vascular Surgeon with Tampere University Hospital. He has authored more than 200 international journal articles. His current research interests include biomedical sensor technology, clinical research, and molecular biology. He serves as a Board Member for the Instrumentarium Science Foundation and The Finnish Cardiovascular Research Center, Tampere, Finland. He is the Chairman of the Board and a CMO of Olfactomics Oy, Tampere, Finland.

Antti Roine received the M.D. degree from Tampere University, Finland, in 2014, and the Ph.D. degree from Tampere University, Finland, in 2014. Since 2014, he has been holding various positions as a Physician in surgery, emergency medicine, and family medicine. In this period, he has also acted as a Project Manager in healthcare digitalization in Tampere. He currently acts as the CEO of Olfactomics Oy. He is also an Active Researcher with Tampere University. His research interests include surgical oncology, gas sensors, and the application of artificial intelligence in medical applications.

Antti Vehkaoja received the M.Sc. degree in electrical engineering from the Tampere University of Technology, Finland, in 2004, and the D.Sc. (Tech.) degree in automation science and engineering from the Tampere University of Technology in 2015. He is currently an Associate Professor of Sensor Technology and Biomeasurements with the Faculty of Medicine and Health Technology, Tampere University. He has authored more than 100 international scientific articles. His research interests include sensors and embedded systems for biomedical applications and related signal processing and data analysis methods.